THE UNIVERSITY OF MICHIGAN
INDUSTRY PROGRAM OF THE COLLEGE OF ENGINEERING

LIMIT OF SUPERSATURATION OF NITROGEN VAPOR EXPANDING IN A NOZZLE

Gennaro L. Goglia

A dissertation submitted in partial fulfillment
of the requirements for the degree of
Doctor of Philosophy in the
University of Michigan
1959

August, 1959

IP-379

Doctoral Committee:

Professor Gordon J. Van Wylen, Chairman
Professor Floyd N. Calhoon
Professor Stuart W. Churchill
Professor John A. Calrk
Professor Frank L. Schwartz

ACKNOWLEDGMENTS

It is with pleasure that the author acknowledges the support and guidance of the persons and organizations whose technical and financial assistance made completion of this study possible. In particular the author would like to extend his sincerest thanks to the following:

Professor G. Van Wylen, the committee chairman, for his constant encouragement and indispensable advice, suggestions and criticism.

The author's doctoral committee, who generously provided valuable advice and assistance.

Ward O. Winer, graduate student, for his valuable assistance in compiling the experimental data.

National Science Foundation for their financial support without which this study would have been virtually impossible.

Industry Program of the College of Engineering for their help in the preparation of this report.

The men of the Automotive Laboratory for their aid in the assembling of the apparatus.

TABLE OF CONTENTS

LIST OF TABLES

LIST OF FIGURES

NOMENCLATURE

A	Nozzle cross-sectional area
c	Fractional part of mixture, by mass, which is in the condensed phase
c_p	Specific heat at constant pressure
d	Axial distance downstream measured from throat
h	Specific enthalpy
h_{fg}	Latent heat of vaporization
H_o	Total enthalpy
k	Specific heat ratio
m	Mass rate of flow
M	Mach number
p	Static pressure
p'_o	Measured stagnation pressure as measured by pitot tube
r	Droplet radius
R	Specific gas constant
S	Specific entropy
T	Absolute temperature
v	Specific volume
V	Velocity
w	Pounds mass
ρ	Density
σ	Surface tension

Subscript

c	Refers to condition at onset of condensation
L	Refers to liquid property

Subscript (Cont'd)

o	Refers to stagnation condition
ox	Refers to reservoir condition at nozzle inlet
oy	Refers to stagnation condition downstream of normal shock
s	Refers to saturation condition corresponding to condensation property
v	Refers to vapor property
d	Refers to condition at d section of nozzle
y	Refers to static condition downstream of normal shock
( )*	Refers to condition at which Mach number is unity or throat section
∞	Refers to condition on infinite plane saturation curve

INTRODUCTION

The expansion of a gas or a vapor to high Mach numbers in a supersonic nozzle may lower the temperature of the fluid well below the saturation temperature. When this occurs the fluid may exist for a period of time in a metastable or supersaturated state. In this state the fluid exists at a temperature below the saturation temperature corresponding to the pressure.

This phenomenon has been studied by many investigators. R. Von Helmholtz[1] observed that saturated steam on expanding through an orifice into the atmosphere remained clear for some distance beyond the exit prior to becoming cloudy. His observations also revealed that electrification of the jet greatly increased the condensation process. J. Yellott[2] in his experimental work with steam nozzles substantiated the fact that steam would supersaturate. G. T. Wilson, whose name has been given (by M. H. Martin) to the line marking the limit of supersaturation of steam on the Mollier Chart, has published several papers in the Transactions Royal Society, on this subject. A. Stodola[3] has shown conclusively that supersaturation exists in the flow of steam through nozzles, and demonstrated that the onset and degree of condensation depended upon the amount of impurities, in the form of small particles, contained in the steam.

Similar results were obtained when air, containing water vapor, was expanded in supersonic nozzles. Experimental work by K. Oswatitsch[4] and R. Head[5] showed that the water vapor became greatly supersaturated during such an expansion. In addition R. Head's results indicated that

the onset and degree of condensation were influenced by the amount of impurities present in the humid air. In his work on hypersonic flow J. V. Becker[6] was able to experimentally determine that condensation of the air components occurred in the saturated region. Becker's results were confirmed by investigators at the Guggenheim Aeronautical Laboratories of California Institute of Technology under H. T. Nagamatsu.[7]

At first, theoretical analyses of the condensation of the principal air components were confined to an analysis of the kinetics of condensation of pure nitrogen and pure oxygen. One of the most important and earliest contributions to the condensation theory came when Sir William Thompson and R. Von Helmholtz[9,10] investigated the equilibrium vapor for the coexistence of both the vapor and a liquid drop of a substance. The kinetic theory of condensation was primarily the contribution of Becker and Doring[11] with contributions by Volmer[12] and others. These pure-vapor theories based on the assumption that no foreign nuclei were present were proposed for the prediction of the onset of condensation. Charyk and Lees[13] and Stever and Rathbun[8] also worked on theories predicting the collapse of the supersaturated state in the absence of foreign nuclei. However, none of the theories had been definitely shown to be capable of predicting the onset of condensation for the components of air.

At the Guggenheim Aeronautical Laboratories of the California Institute of Technology[14] calculations were carried out with the assumption of an infinite number of effective condensation nuclei. The calculations assumed that the condensation of air occurred at saturated conditions and that the vapor and condensed phase were always in thermal and dynamic

equilibrium. The assumption of equilibrium was suggested by the experimental work(7,11,15, and 16) which had shown that no condensation shocks occurred when air condensed and that the static pressure of the expanding air increased very gradually. The results of the calculations seemed to check the experimental results available. However, definite verification depended upon more extensive experimental work. Additional experimental work(17,18, and 19) was conducted on supersaturation of gases in hypersonic wind tunnels wherein it was observed that impurities encouraged condensation, and consequently decreased the degree of supersaturation attainable. It was also concluded that for practical purposes the self-nucleation theory for the condensation of bottled gases was not the important one and it was suggested that a new theory be developed based upon the condensation induced by impurities. In the course of the experimental work by Arthur, Nagamatsu, and Willmarth, no limit value of supersaturation was observed.

While the existence of supersaturation has been demonstrated by the work of the authorities heretofore mentioned, no limit line of supersaturation for nitrogen has been established. It was the purpose of this investigation to experimentally determine such a limit line for nitrogen vapor when allowed to expand in a supersonic nozzle.

APPARATUS

The apparatus which was constructed and assembled consisted of a storage tank assembly, a nozzle-diffuser assembly, regulating valves, pressure relief valves, a photomanometer, a pitot tube assembly, a Sanborn recorder, gages, piping, valving and insulation.

Storage Tank Assembly

The storage tank assembly was constructed to be essentially one tank within another. The inner tank was to be used for the storage of the nitrogen necessary for test runs, and the outer tank, which contained liquid nitrogen, was used to maintain a constant temperature in the inner tank. In order to provide sufficient nitrogen vapor for the test runs, a capacity of four cubic foot was required for the inner tank. Since both tanks were to be subjected to -320°F temperatures and pressures as high as 400 psig, 18-8 stainless steel type 304 was used in their construction. The entire tank assembly was enclosed in a five-inch jacket of insulation. A pressure relief valve was connected to each tank.

Nozzle-Diffuser Assembly

The complete nozzle-diffuser assembly, shown in Figure 1, was made of aluminum to prevent corrosion and subsequent contamination of the working fluid. The nozzle-diffuser assembly designed to discharge against a back pressure of one standard atmosphere pressure was one inch wide with a nozzle exit area of approximately 0.5 square inches. The straight divergent section of the nozzle was machined to obtain a high microfinish surface. The sides of the two dimensional source flow nozzle blocks were

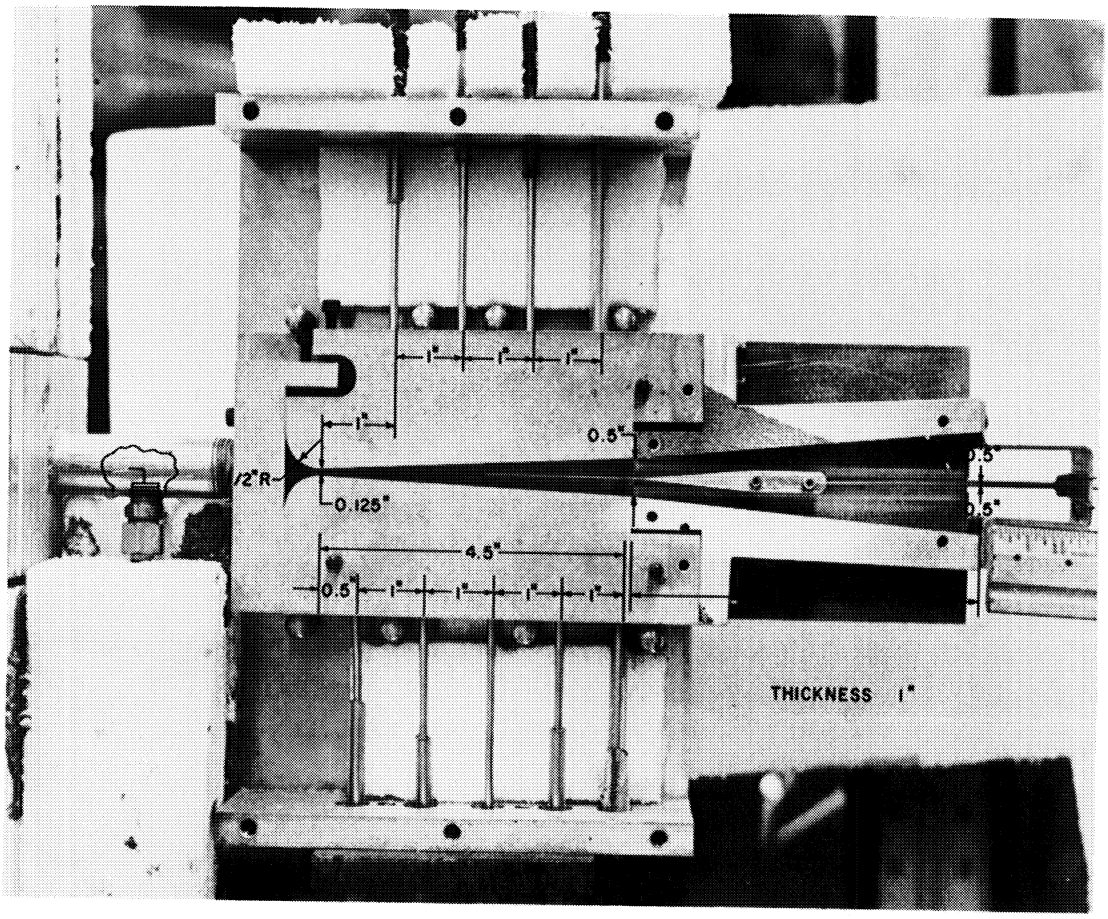

Figure 1. Photograph of Nozzle-Diffuser Assembly.

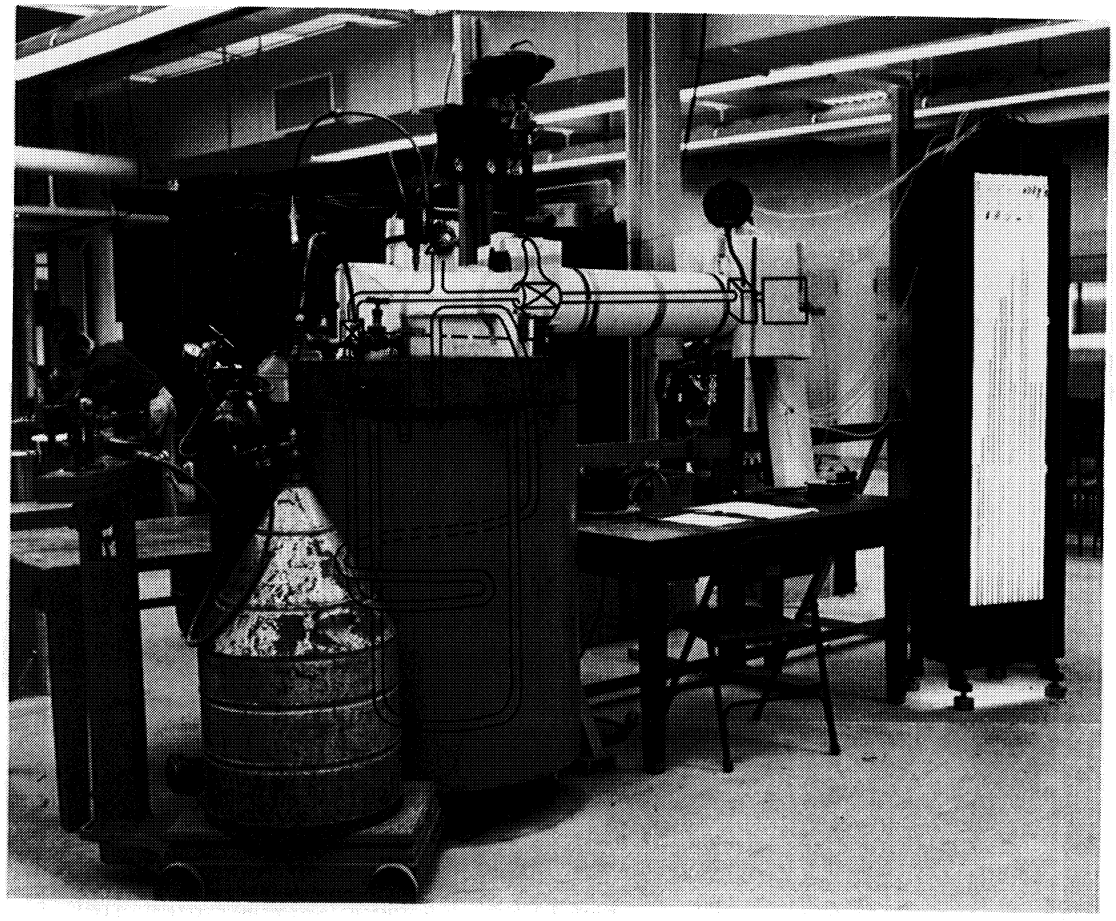

Figure 2. Photograph of Apparatus.

hand-lapped to the wide walls, which were three-eights of an inch in thickness. To enable measurements of the static pressure variations, the divergent sections of the nozzle blocks had pressure taps drilled perpendicular to them at half-inch intervals alternatively on the top and bottom of the blocks. Tygon tubing was used to connect these 0.04-inch diameter pressure taps to the manometer board. The nozzle diffuser assembly was so constructed that the throat height was adjustable from a minimum of 0.0 to a maximum of 0.2 inches. The side walls when assembled were securely clamped into position to eliminate any leaks.

The central body type of diffuser assembly was attached to the exit of the nozzle assembly. Its design was such that the diffuser angle was made to be approximately twice the divergent angle of the nozzle. The diffuser had a two dimensional wedge which could be traversed along the axis of the entire length of the diffuser. The central body type diffuser was selected because the wedge provided a convenient support for the pitot tube in its traverse of the nozzle axis. The wedge angle was designed as to be slightly greater than the divergent angle of the diffuser, and the wedge length was determined by a trial and error method. A throat setting of 0.125 inches was chosen and the nozzle was run on dry bottled nitrogen gas with the wedge in position such that its tip was located at the exit of the nozzle. As the wedge length was decreased, keeping the wedge included angle constant, the separation point, indicated by the static pressure on the nozzle block, was recorded for each wedge length. The optimum wedge length corresponding to a separation point at the greatest distance from the throat was selected. After the selection

of the optimum diffuser wedge size, the stagnation pressure was increased for this setting until separation did not occur. The stagnation pressure at the nozzle inlet was then adjusted to give approximately the same measured stagnation pressure at the exit of the nozzle for other throat settings. This procedure prevented separation from occurring and also gave an almost constant mass flow.

Instrumentation

Stagnation pressure upstream of the nozzle was maintained constant by a Fisher Governor regulating valve placed between the tank and nozzle assemblies. A Minneapolis Honeywell valve positioner was used in conjunction with the Fisher regulator to increase the response of the regulator. A bronze tube Duragauge, just ahead of the nozzle was used to measure stagnation pressures.

The nozzle static pressures were observed on a multiple tube photomanometer panel on which thirteen different pressures could be indicated at one time. With this photomanometer and a photographic technique the pressures were measured. The asymmetry of the static pressure holes (see Figure 1) in the nozzle block allowed a check to see that the flow was the same on the top and bottom of the nozzle. The stagnation pressure probe consisted of a three-inch length of 0.042 inches diameter stainless steel hypodermic tube with an inside diameter of 0.026 inches. By use of this probe which could traverse the nozzle centerline, the stagnation pressure on the nozzle centerline could be measured at any axial station. The probe was designed in accordance with the dimensions recommended in the National Advisory Committee of Aeronautics Technical

Note No. 2223. The station at which the pressure was being measured was indicated by a pointer mounted on the probe and measured by a ruler fixed to the diffuser exit.

The stagnation temperature of the working fluid entering the nozzle was measured by a copper constantan thermocouple mounted in a tee just ahead of the nozzle where the staganation pressure was measured. The junction of the thermocouple extended to the center of the 1/2-inch line which carried the fluid to the nozzle at relatively small velocities. The thermocouple was connected to a Sanborn recorder with which the temperatures were recorded.

All instrumentation was calibrated, the Sanborn recorder being calibrated prior to each day of runs.

TEST PROCEDURE

Fluid

The liquid nitrogen used during this experimental work was obtained from the liquid nitrogen generating machine operated by the Mechanical Engineering Department of the University of Michigan. At both the start and termination of the work, a mass spectrometer analysis of the nitrogen was made. There was little variation. The result of the analysis was as follows:

Purity - 95%

Impurities

Oxygen - 5% .

Later in the program a higher purity nitrogen was purchased at considerable costs. With this higher purity nitrogen several test runs were made to enable a comparison of test results for the two purities. The result of the mass spectrometer analysis of the higher purity nitrogen was as follows:

Purity - 99.995%

Moisture - 2 gr. per 1000 cubic foot maximum

Impurities

Oxygen - less than 20 parts per million

Carbon Burning Gases - less than 5 parts per million

Hydrogen - less than 5 parts per million.

The properties of the nitrogen for analysis at these low temperatures were obtained from References 20 and 21.

Operation

The test runs conducted were for nozzle entrance stagnation pressures of 4.38, 6.09, 7.80, 9.15, 9.84, 10.60, 12.90, and 13.22 atmospheres. Corresponding to each pressure there were at least two test runs conducted and for each pressure the number of degrees of superheat was varied. Runs with higher stagnation pressures at the entrance to the nozzle were attempted but were unsuccessful. The failure to run at these higher pressures was due principally to the fact that the diffuser discharge was to the atmosphere. In order to obtain supersaturation conditions with these higher stagnation pressures, it was necessary to increase the vapor pressures in the tank. With this required increase in pressure, the vapor generation capacity of the tank was exceeded making it impossible to maintain constant stagnation pressures at the inlet to the nozzle. The nozzle throat settings corresponding to the above operating pressures were respectively 0.195, 0.150, 0.125, 0.100, 0.090, 0.090, 0.060, and 0.060 square inches.

In preparation for a test run the nozzle throat area was first adjusted to one of the above settings. The charging of the tanks with liquid nitrogen was then accomplished by pressurizing (with bottled dry nitrogen gas) the containers in which the liquid nitrogen was supplied, thus forcing the liquid into the tanks. A period of time was then allowed for the generation of sufficient pressure necessary for a test run. While equilibrium was being established in the tank liquid nitrogen was forced through the one-inch line connecting the tank with the nozzle-diffuser assembly. This procedure was found necessary in order to maintain the

desired stagnation temperature at the inlet to the nozzle. Without this procedure the thermal capacity of the line would superheat the nitrogen vapor to undesired amounts. With this procedure it was possible to maintain approximately one hundred degrees Fahrenheit of superheat conditions at the inlet to the nozzle. Following the establishment of equilibrium conditions in the tank and the necessary precooling completed a test run was made. In general the duration of test runs did not exceed forty-five seconds. During each test run the following information was recorded: the stagnation temperature, the stagnation pressure at nozzle inlet, the static pressure variation along the nozzle blocks, and the measured stagnation pressure along the axis of the nozzle.

Detection of the Onset of Condensation

In previous experimental work with gases, it was observed that the onset of condensation could be detected by several methods. The methods of locating that section of the nozzle wherein condensation begins falls into either the light scattering or pressure measurement classes. For this particular investigation the pressure measurement method was chosen as it has been proven to be as accurate yet much simpler than the light scattering technique. The pressure measurement method is based upon the fact that condensation during an expansion in a nozzle effects the static pressure.

Buhler[14] showed that when air condensed at the saturation point in a supersonic flow and always remained in dynamic and thermal equilibrium, there was experienced a gradual rise in static pressure to values above those predicted for isentropic flow. Becker[6], Nagamatsu[7], and Wegener[15]

from their results on hypersonic flow revealed non-isentropic effects, principally a gradual increase in static pressure over the isentropic value corresponding to the measured stagnation pressure. This gradual pressure rise was attributed to the condensation that took place. As the vapor condensed, it released its latent heat which in turn was transferred into the stream resulting in the pressure rise. Comparison of light scattering data and pressure data(6,8, and 17) proved this static pressure departure from the isentrope to be due to condensation. When large amounts of vapor condensed, the pressure rise was violent and this phenomenon is called condensation shock. Condensation shocks were not observed with air or nitrogen(6,7, and 8), however, a definite increase in static pressure was observed. Wegener(15), and Nagamatsu and Willmarth(17) in their studies observed no appreciable change in the measured stagnation pressure during condensation. Therefore, a very convenient plot for locating the onset of condensation would be to plot the measured stagnation pressure ratio, p_o'/p_{ox} (the ratio least affected by condensation), against the ratio of static to measured stagnation pressure, p_d/p_o', (the ratio most affected by condensation). The supersaturation limit could then be

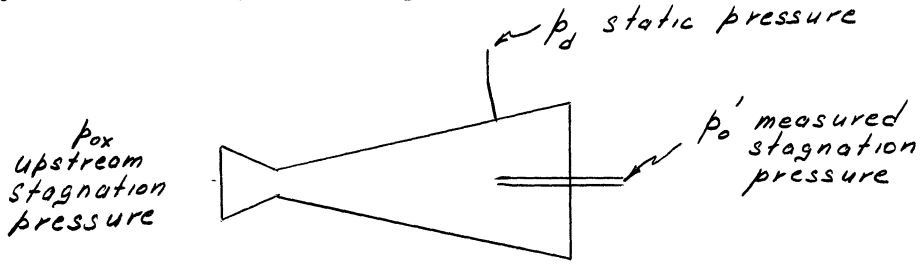

determined by superimposing the plot of the actual expansion in the nozzle on a graph of the isentrope and observing the point of tangential departure of the two curves. This point of deviation of the actual expansion would

mark the onset of condensation. This method was selected as the principal way of locating the supersaturation limit in this investigation.

Since the measured stagnation pressure measurements along the nozzle centerline were found to be nearly the same as those predicted for isentropic flow to the given station, the isentropic perfect gas relations between measured stagnation and static pressure permitted the isentropic static pressures to be calculated from the measured stagnation values. These static pressure values, as determined from p'_o/p_{ox} , when compared with the experimentally measured static pressure, again revealed the departure point. This plot, therefore, provided a method of ascertaining the onset of condensation. A third procedure which was originally suggested by Wegener and Reed[15] was also used to check the location of the collapse of the supersaturated vapor. In this approach the vapor temperatures throughout the expansion were calculated. The tangential point of deviation of the actual expansion from the isentrope, as apparent on a pressure-temperature plot, marked the onset of condensation. The development of the equations necessary for the temperature calculations are given in Appendix A.

THEORY OF SUPERSATURATION

When a fluid undergoes a change of state which involves a change of phase, it is usual to assume that a phase change occurs at the instant. However, if the change of state takes place very rapidly, the phase change may be delayed, and a metastable state may be attained. This is the case when a vapor is expanded in a nozzle from the vapor region to the two-phase region, for at some stage of the expansion the saturation line will be crossed and, at the same instant, condensation should commence. However, it has been shown experimentally that condensation may be delayed until some lower temperature and pressure are attained, and then sudden condensation occurs. Condensation will occur only if the vapor contains condensation nuclei, ions or impurities. In the interval between crossing the saturation line and condensing the vapor is in a metastable state and is said to be supersaturated.

Some insight into this phenomenon can be gained by consideration of the size of droplets and surface tension.

It was shown by early investigation that as far as the order of magnitude of the droplet radius is concerned, its dimension is extremely small, thus the capillary surfaces forces play an important part. If, in each unit of time, there is the same number of molecules given off by the droplet due to its own molecular motion as the number of molecules received by the droplet from the vapor environment, then a state of equilibrium between the droplet and the surrounding atmosphere of vapor is possible. A liquid molecule on a plane liquid surface is subjected to a force of attraction by its neighboring molecules within the hemisphere of action over which the molecular attraction may be assumed to act. The

same liquid molecule when on a convex surface, however, is attracted by fewer molecules. Thus the liquid molecule on the convex surface, is tied to the surface less securely, since the attraction of the vapor can be considered negligible due to its much smaller density. As a result therefore the number of molecules projected from a curved surface will be greater than for the plane surface. The number of molecules falling from the vapor environment on to the droplet surface is proportional to the density of the vapor. If the temperature of the vapor and of the droplet are equal, as is required for thermal equilibrium, the density of the vapor must then be greater than at the plane surface. That is, the vapor must be supersaturated. For if it were a saturated vapor, more molecules would leave the droplet than impinge on it. Hence, in an environment of saturated vapor, small droplets must vaporize. This may be stated in another way by noting that a supersaturated vapor is undercooled relative to the saturation temperature given for its pressure in the vapor tables. This is so because the vapor table saturation temperature is correct only for an equilibrium mixture of a vapor with infinitely large droplets of liquid. When a supersaturated state may change to a stage of normal equilibrium there is a rise in temperature and large drops are present.

Sir William Thompson[9] and R. Von Helmholtz[10] investigated the conditions necessary for equilibrium between the vapor and droplets resulting in the following formulation by Von Helmholtz:

$$\ln p/p_{\infty} = 2\sigma/\rho r\, RT \qquad (T\text{-}1)$$

where p denotes the pressure in equilibrium with the droplet of radius r

at absolute temperature T, p_∞ is the saturation vapor pressure in equilibrium with a liquid surface of infinite radius at T, σ is the surface tension. ρ is the density of the liquid phase, and R is the specific gas constant.

It follows, therefore, for equilibrium between two phases of a pure substance the relation between the temperature and pressure of the vapor is not unique but is different for different curvatures of the surface separating the phases. Equation (T-1) provides the relationship which must exist between the actual pressure and the saturation pressure at the existing temperature if a droplet of radius r is to be in equilibrium with the vapor about it. The significance of an increase in p/p_∞, known as the supersaturation ratio, is that the droplet is bound more securely to the liquid surface and therefore an increase in p/p_∞ enables the droplet to grow. Similarly for a decrease in p/p_∞ the droplet will evaporate. Another observation from Equation (T-1) reveals that the supersaturation ratio for a given size of droplet will increase as the temperature is lowered. This is principally due to the fact that the temperature appears in the denominator. Also in addition to this both the surface tension and density increase with decreasing temperature, however, the surface tension increases at a greater rate than does the density.

Rapidity of Temperature Equalization

In his work with steam Stodola[3] analyzed the problem of heat conduction in the interior of a droplet during an expansion in a nozzle. In this analysis he showed that for a water droplet of radius 3.3×10^{-7} feet that the ratio of temperature at the rim of the droplet to the temperature at the center of the droplet was equal to 0.97. In his study

this radius was considered as the outermost limit, as for droplets of smaller radii it was found that the temperature ratio approached one. He observed, therefore, that the temperature equalization in the interior of the drop for the condensation encountered required an extremely short period of time in comparison with the duration of flow. It was then concluded that the temperature could be regarded as uniformly distributed throughout the droplet. Following this analysis Stodola considered the mass of vapor surrounding the water droplet. He regarded the vapor as being subdivided into spheres, the centers of which were assumed to be at uniform distances apart while the remaining innerspaces were disregarded. With an idea of the relative size of the vapor droplets being obtained from consideration of a ten per cent moisture content in the form of droplets of the same radii size as in the previous analysis, he through a similar analysis concluded that the temperature could also be considered uniformly distributed throughout the vapor.

In considering how rapidly an equalization was taking place between the steam vapor and the water droplet Stodola made use of the kinetic gas theory. The problem was approached in this manner as at the beginning of condensation the free path of the molecule is large in comparison with the diameter of the water droplet and therefore the usual heat conduction equations were no longer valid. In this analysis the simplified assumption was made that all the molecules in a droplet were traveling with a constant velocity and uniformly distributed in all directions. The weight of the molecules impinging on the droplet and held by it was then determined. This was accomplished by encompassing the droplet by a cone of

contact extending in the direction of a space angle to infinity. Under this condition then all molecules at a distance determined by the product of the molecule velocity and time would in that period of time impinge on the droplet. The mass of the molecules impinging on the droplet was then found in terms of the molecule velocity by evaluating the total number of impacts by summing up with respect to the space angle between 0 and 4π. The velocity of the molecule in this expression was then eliminated by making use of the kinetic energy of the motion of the center of gravity of the molecule and of the equation of state for the gas.

The continuity equation was then applied to the droplet and a differential equation for the increase in mass of the droplet was determined. With the use of this continuity equation and the energy balance of the droplet an energy equation was developed. A second energy equation was obtained by use of the energy relationship for the total mass that is the mass consisting of the liquid part and the vapor part. This development involved the understanding that the decrease of internal energy (for adiabatic conditions) supplied the work of expansion. The differential equations developed, however, were in too complicated a form for general integration. An important conclusion, however, was obtained by considering the simplified case of the behavior of a droplet in an infinitely attenuated steam environment. It was shown that, in spite of the rapid change of state, there is nearly thermodynamic equilibrium in the nozzle between the steam and the water droplet.

Instability of the Supersaturated State

As mentioned before, Equation (T-1) shows that for equilibrium between the droplet and the vapor, the temperature and pressure of the

vapor is not unique but is different for different curvatures. This expressed mathematically is:

$$p = f\ (T,\ r)\ .$$

This relation is shown in the sketch below, where the solid curve is the

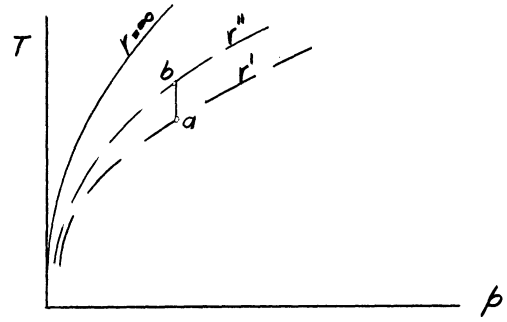

saturation pressure on a plane liquid surface ($r = \infty$) and the dash lines represent the saturation pressures at the surface of the droplets of various radii. Assume for discussion a supersaturated state a, of pressure p and T, in which droplets of radius r' could subsist in thermodynamic equilibrium. Let a drop of radius r'' be formed as a result of collisions, and assume this to be at the same temperature T and pressure p. This drop is larger than that necessary for equilibrium at the given pressure and temperature. The equilibrium point for the droplet of this same pressure and radius is at point b. Hence the vapor in state a is at a temperature lower than the equilibrium temperature corresponding to this new drop of radius r'' and pressure p, and the vapor will condense on the droplet. Thus the droplet will continue to grow until its radius becomes infinite, or until all the vapor is condensed. The radius of the droplet corresponding to state a, is the radius of the smallest droplet of liquid which would grow by condensation if exposed to the vapor in state a.

A physical argument also shows that the equilibrium between the vapor and liquid drop as expressed by Equation (T-1) is an unstable one.

Consider a drop of radius r which is in contact with an infinite extent of vapor at pressure p. If one molecule of the vapor were added to the liquid droplet, the droplet radius would increase while the vapor pressure of the infinite extent of the vapor does not change. However, according to expression (T-1) the slightly enlarged drop has a lower equilibrium vapor pressure, so the existing vapor pressure is greater than the new equilibrium pressure. Hence condensation of the vapor onto the drop will continue. This equation therefore reveals the concept of the critical size drop. For a vapor at a fixed temperature T, if the pressure p is higher than the saturation pressure corresponding to T, there exists a critical radius of liquid drop such that, if a droplet is larger than the critical radius, it will continue to grow by condensation, and if the droplet is smaller than the critical radius, it will continue to shrink by evaporation. The Von Helmholtz supersaturation equation then shows that a requisite for the formation of droplets is nuclei upon which the vapor can condense.

Supersaturation Limit

The supersaturation limit can be best explained by referring to the sketch below. The conventional h-s diagram is modified to include

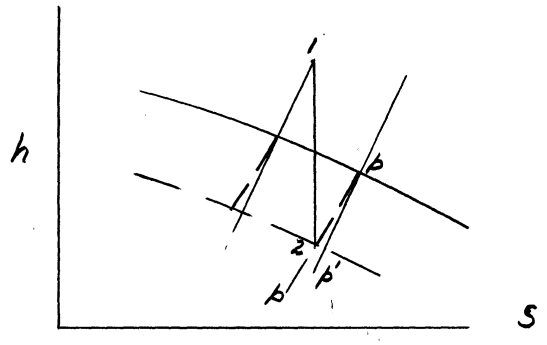

the lines pp which represent the lines of constant pressure for the metastable (supersaturated) states of the vapor. Considering an isentropic

expansion from point (1) through a nozzle with smooth walls, the expansion proceeds without the formation of any liquid until the state (2) is reached. At this state a mist or haze made up of minute liquid particles forms suddenly. This state point could be detected either visually or by pressure measurements. It is this state point at which condensation commences that is defined as the supersaturation limit. The locus of such points (2) defines the supersaturation limit line for expansions along various isentropics.

Kinetics of Condensation

The search for the nucleus upon which condensation occurs motivated many early investigators. At first it was though that dust particles or ions served as nuclei but exhaustive investigations proved this not to be so. From studies of the condensation of water vapor in the absence of foreign nuclei, as observed with the Wilson cloud chamber[22], it was postulated that aggregates of water molecules formed the required condensation nuclei. In the condensation of a pure vapor in the absence of any solid or liquid interface, condensation is assumed to take place on a spontaneously formed liquid nuclei of the substance. This spontaneous generation of nuclei was treated by Volmer and others[11,12, and 23-26]. In an examination of the problem of self-nucleation it is necessary to determine the rate of formation of condensation nuclei, that is, droplets of critical size. For it is only these droplets that are capable of growing rapidly by the addition of vapor and so cause the collapse of the supersaturated state.

Considering the conditions which determine the rate of the further growth of the droplet it is necessary to take into account the fact

that its smallness implies a large ratio of its surface to its volume. Its surface energy and free energy accordingly constitute an important part of the total change of energy or the free energy of the whole system involved in the process of the formation of a nucleus. In a droplet of liquid in a supersaturated state the thermodynamical potential of the system can be expressed as the sum of the surface free energy of the droplet and the free energies of the droplet and vapor. The difference between the thermodynamic potential of this system and that corresponding to the absence of the droplet provides a relationship showing the variation of the free energy with droplet radius. This relationship shows that the free energy increases with droplet size up to a critical value (the stable nucleus size) and then decreases. Droplets larger than critical will tend to increase, decreasing the free energy and becoming centers of condensation nuclei. Droplets smaller than critical size will in general tend to evaporate. Thus the critical droplet size can be reached only by the kinetic process of statistical fluctuations, that is, local and transient deviations from the normal state. The growth of nuclei to the critical drop size, therefore, is the crux of the condensation-rate problem, since it becomes a stable liquid droplet and continues to grow thereafter. Once the droplet has reached critical size it can be considered as condensed. These critical size droplets continue to grow and their growth contributes to the rate of condensation.

The instability of the equilibrium between the supersaturated state and the liquid droplet is expressed in the fact that the free energy change involved in the formation of a droplet of critical size has a maximum rather than a minimum value as in the case of stable equilibrium.

Frenkel[28] shows this maximum value of free energy to be:

$$\Delta \phi^* = \frac{4}{3} \pi \sigma (r^*)^2$$

where σ is the surface tension, and r^* is the critical radius as obtained from Equation (T-1). Since the initial phase is in a state of metastable equilibrium, droplets of critical size of liquid are in a state of unstable equilibrium with the supersaturated vapor, owing to the forces exerted by the surface tension.

In the statistical treatment of a vapor, even when the thermodynamical state of the vapor is such that the vapor is not supersaturated but is a stable unsaturated vapor, there is a distribution of droplets in the system given by the Gibbs formula.

$$N(r) = C e^{-\frac{\Delta \phi(r)}{\gamma T}}$$

where N(r) is the number of droplets of radius r, $\Delta \phi$ (r) is the energy of formation of such a droplet given by the change in thermodynamic potential, γ is the Boltzman's constant, T is the absolute temperature and C is constant which is equal to the sum of the molecules of the system if the total number of droplets is very small compared with the total number of molecules in the system. When this distribution law is applied to a vapor in a state of supersaturation, the number of droplets of given radius decreases with the radius only up to the critical size drop, then it increases rapidly. This increase is due to the fact that $\Delta \phi$ (r) reaches a maximum at the critical size.

The main problem in the theory of nucleation is the question of the appearance of nuclei and thus the rate of transformation. From the previous discussion it is apparent that each droplet has to pass over the energy hump into the range of a stable nuclei. The number of nuclei which

have a high enough thermodynamical potential to do so is given by

$$N(r) = C e^{-\frac{4}{3}\pi\sigma(r^*)^2/\gamma T} \qquad \text{(T-2)}$$

Volmer[12] used these considerations in his analysis of the supersaturated state, as a basis for the determination of the velocity of its condensation.

Since all the droplets which arise in a supersaturated vapor must, in the process of their gradual growth (partially neutralized by the reverse process of re-evaporation), pass through the critical size, the velocity of this process must be proportional to the number of droplets of critical size existing in the vapor, at any given instant, in a state of unstable equilibrium given by Equation (T-2). The velocity of condensation can then be obtained by multiplying the number of such droplets N(r)* by the number of single molecules of the vapor striking their surface in a unit of time. This is so if it is assumed that the droplets do not evaporate, but continue to grow and are eliminated from the system being replaced by an equivalent number of single molecules, so that the vapor remains in a stationary state. The velocity of condensation is thus represented by the formula

$$\frac{dN}{dt} = Ng^* 4\pi(r^*)^2 \frac{p}{\sqrt{2\gamma w \pi T}} e^{-\frac{4}{3}\pi\sigma(r^*)^2/\gamma T}$$

where N is the total number of simple molecules, g* is number of simple molecules constituting liquid droplets of critical size, p is the pressure, and w is the mass of the molecules. Experimental results indicated, however, that the above Volmer theory failed in some cases to predict when the condensation of water vapor or the components of air would occur in the very rapid vapor expansions in a supersonic wind tunnel. As a result Volmer's quasi-equilibrium theory of nucleation was subsequently improved

by Frakas[25], Kaishew[24], and especially by Becker and Doring[11]. In the Becker-Doring theory the velocity of condensation was derived taking into account not only the condensation of the vapor on the surface of the droplets but also the reverse process of their evaporation.

The description of the resulting process is simplified by assuming that all droplets of a certain size slightly exceeding critical are eliminated from the system and replaced by an equivalent number of single molecules. Under such conditions the number of droplets of any size including the individual molecules (which in a purely formal way can be treated as droplets of the smallest possible size) must remain constant.

The number of molecules which are evaporated from the surface of the droplets, consisting of the number of molecules constituting liquid droplets per unit time and area, for a state of stable equilibrium was evaluated. Then the net number of droplets growing from g-1 class to the g class of molecules per second per unit volume was determined assuming that there exists a density, ρ_g, of droplets containing g molecules and that their total surface area is $S_g\rho_g$. Thus the kinetic equation representing the nucleation rate becomes

$$J_g = \rho_{g-1} S_{g-1} \beta - \rho_g S_g \alpha_g$$

where α_g denotes the number of molecules evaporated from the surface of the droplets, ρ_g is the density of droplets containing g molecules, S_g is the total surface area of the droplets, and β is the number of molecules of the vapor impinging each second on unit area. The above difference represents the excess of the number of droplets which, owing to condensation of the vapor on their surface, pass per unit time from the class g-1

to the class g. The rate of change of the number of droplets of a given class is therefore represented by the equation

$$\frac{\partial \rho_g}{\partial t} = J_g - J_{g-1} \quad .$$

The quantities appearing in this equation can be treated as a function of a continuous variable (g) and by the replacement of the finite differences by differential coefficients of the corresponding quantities the nucleation rates can be expressed as

$$J(g) = -D(g) N(g) \frac{\partial}{\partial g}\left(\frac{\rho_g}{N(g)}\right) \quad .$$

By use of these relationships and after a number of approximations, consisting in replacing summations with respect to g by integrations, Becker and Doring found the distribution function f for steady distribution resulting in

$$\frac{\rho_g}{N(g)} = \frac{J}{C D(g^*)} e^{\frac{\Delta\phi(g^*)}{\gamma T}} \sqrt{\frac{2\pi\gamma T}{\lambda}} \quad .$$

The above equation can be shown to be equal to a constant one. Hence solving for J the result becomes

$$J = C D(g^*) e^{\frac{\Delta\phi(g^*)}{\gamma T}} \sqrt{\frac{2\pi\gamma T}{\lambda}} = N(g^*) D(g^*) \sqrt{\frac{\lambda}{2\pi\gamma T}}$$

Then by expressing λ in terms of σ and r and substituting into the above the following final expression for the relative rate or fractional rate of condensation of a supersaturated vapor is obtained

$$\frac{1}{N}\frac{dN}{dt} = \frac{J(g^*)}{C} = \frac{p}{\gamma T}\frac{4(r^*)^3}{3}\sqrt{\frac{2\pi\sigma}{w}} e^{-\frac{4}{3}\pi\sigma(r^*)^2/\gamma T}$$

With the condensation rate equation above a family of constant rate lines can be determined for a given pressure and temperature which in turn could

be plotted on a pressure-temperature plot for a vapor. Such a calculation was made by Head[5] for water vapor in calculating the expected condensation rate of steam in steam nozzles and also for water vapor in wind tunnels. Charyk, Less, and Bogdonoff did the same for nitrogen and oxygen. Inaccuracies are involved in the prediction of condensation rates due to the inaccuracies in the values of the fluid properties, especially of the surface tension. In addition to the error introduced by the extrapolation of the properties to low temperature, there is another inaccuracy due to the fact that at times supersaturated vapor can condense into the liquid phase and sometimes into the solid phase.

The experimental results of Wegener and Smelt[29] showed that the degree of (water vapor) supersaturation which is reached in the expansion of moist air in small nozzles is much greater than that predicted by the Becker-Doring theory. It was also found that the supersaturation increases rapidly with the time rate of expansion. The time required for the growth of droplets of appreciable size from nuclei has been calculated by Oswatitsch.[4] Since this time may be comparable with the other times involved in the problem, the droplet growth time will play a role in rapid expansions. However, from the Becker-Doring theory the rate of nucleation varies extremely rapidly with the degree of supersaturation. Thus it would be expected that in a situation where the supersaturation is increasing rapidly with the time, the formation and growth of new nuclei will condense more vapor than the continued growth of nuclei.

In the early stages of condensation, the highly variable nucleation rate will therefore dominate the process and, after condensation has reduced the supersaturation to a point where nucleation disappears, the

droplet growth process will govern the return to equilbrium. Therefore, the initial appearance of condensation is determined by nucleation. The dependence of the degree of supersaturation on the rate of expansion from the experiments of Wegener and Smelt indicates that the nucleation process requires an appreciable time.

In an effort to resolve the apparent contradictions between theory and experimental work, Lees[16] modified the Volmer theory by proposing that when the condensation nuclei become very small, they can no longer be considered as continuous liquid states. From this idea he concluded that there was a cut-off in the values of the nucleus formation frequency as given by Volmer.

Kantrowitz[27] however, suggested that the predicted values of nucleus formation frequency were too high because of a time lag associated with reaching the quasi-equilibrium distribution given by Becker and Doring. He pointed out that these investigators neglected the following considerations associated with time lag: the build up to an equilbrium distribution of droplets smaller than critical size; the heating of the nucleus due to bombardment by molecules of the condensing phase; and the inability of the liquid nuclei to absorb all the molecules hitting their surface. Kantrowitz then modified the Becker-Doring theory to take account of the time delay in the nucleation rate due to a statistical random walk phenomenon in the growth of the nuclei. That is, molecules may attach or detach themselves from a growing nuclei, and the process of their growth must take into account both of these occurrences, with the net growth being the desired quantity.

In the calculations carried out by Kantrowitz, wherein he neglected the work required to form the droplets of the condensing phase, an attempt was made to determine whether the time lag associated with the approach to steady state rate of formation of condensation nuclei could account for the discrepancies between the theory and the experiments. A similar calculation was carried out by Probstein(30) in which he took into account the work required to form the droplets of the condensing phase. He also considered the time lag arising from the heating of the nuclei due to bombardment by molecules of the condensing phase. The results indicated that the build up time was not appreciably lengthened by the inclusion of the work term. The results of both showed that the time lag alone would not account for the existing discrepancies between the theory and the experimental work.

The condensation rate theories, in particular the Becker-Doring theory, predicated negligible condensation rates of points where experimental determinations by light-scattering and static pressure measurements revealed that condensation was evidently present. The general interpretation was made that the condensation detected was not the condensation of the pure substance on spontaneously formed nuclei but rather that it was the condensation on nuclei of impurities. As an illustration, condensation of air appeared to start at only slight degrees of supersaturation whereas the pure vapor theories predicted fairly substantial degrees of supersaturation before condensation was to start. Since the resulting predictions of condensation rates did not fit well the observed experimental results, Stever and Rathbun(8) proceeded to modify the usually employed condensation nucleation theory. They modified the nucleation theory of

condensation to take account of a postulated variation of surface tension with decrease in size of the spontaneously formed drops which act as nuclei of condensation.

In the experimental work on condensation of steam in steam nozzles and water vapor in wind tunnels, the point at which the degree of supersaturation reached its maximum and condensation began was known to be at a point where the critical size drops were very small, containing a few molecules. Stever and Rathbun as well as others recognized the manner in which the small critical droplet size effected the value of surface tension. By consideration of a number of molecular bonds holding a molecule to the surface of a small droplet compared with the number holding it to the surface of a large droplet, it was observed that the surface tension of a droplet was dependent on the radius of the droplet. Stever and Rathbun demonstrated the smallness of the size of the critical droplets for nitrogen, by plotting the condensation rate lines based on the Becker-Doring theory. They showed that the number of molecules in a critical droplet was less then about a dozen by the time the fractional condensation rate reached one per second, at a Mach number slightly greater than five.

In their modification of the Becker-Doring theory they first developed a modification of the expression for the vapor pressure in equilbrium with a droplet and also obtained a modified expression for the critical droplet size. They accomplished this by starting with an assumption that the surface energy for unit surface was a function of the radius r, and then proceeded as in the unmodified theory. Their modified expression for the vapor pressure in equilbrium with a droplet became the

following:

$$\frac{p}{p_\infty} = e^{\frac{2\sigma_\infty v_l}{rT r^2}\frac{d}{dr}(r^2 f(r))} \qquad \text{(T-3)}$$

which reduces to Equation (T-1) when f(r) equals 1 for the case of constant surface energy per unit surface.

The derivation of the expression for the condensation rate was also altered to take into account, the original assumption. The following expression resulted:

$$\frac{1}{N}\frac{dN}{dt} = \frac{4}{3} r^3 \frac{p}{rT}\sqrt{\frac{\pi\sigma_\infty}{w}}\sqrt{\frac{2}{r}\frac{d}{dr}(r^2 f(r)) - \frac{d^2}{dr^2}(r^2 f(r))}\; e^{-\frac{4\pi\sigma_\infty}{rT} r\left\{r f(r) - \frac{1}{3}\frac{d}{dr}(r^2 f(r))\right\}} \qquad \text{(T-4)}$$

which again reduces to the Becker-Doring condensation rate for f(r) equal 1. Equations (T-3) and (T-4) were then rewritten in terms of the surface tension σ, which is also a function of the radius of curvature of the surface. It was then observed that in terms of the radius - dependent surface tension that Equation (T-1) remained unchanged in form. The expression for the fractional condensation rate however yielded

$$\frac{1}{N}\frac{dN}{dt} = \frac{4}{3} r^3 \frac{p}{rT}\sqrt{\frac{2\pi}{w}}\sqrt{\sigma - r\frac{d\sigma}{dr}}\; e^{-\frac{8\pi}{rT}\left\{\int_0^r r\sigma\, dr - \frac{1}{3}r^2\sigma\right\}}$$

In the application of their modified theory Stever and Rathbun used a quasi-thermodynamic form of the variation of surface tension with radius as developed by Tolman.(31) This form was qualitatively verified by a statistical mechanical treatment by Kirkwood and Buff.(32) Tolman's simplified expression for the surface tension was

$$\sigma = \sigma_\infty\left(\frac{1}{1 + \frac{2\delta}{r}}\right)$$

where δ was almost a constant for a given substance and ranged from about 0.25 to 0.6, the intermolecular distance in the liquid state. The value δ used in the application was δ equal 1/2D where D was the intermolecular distance. They applied their modified theory to pure oxygen and pure nitrogen and plotted the condensation rate lines on a pressure-temperature plot. A comparison was made with the unmodified Becker-Doring theory and it was clearly shown that the modification of the theory due to surface tension variation with curvature changes the predicted condensation rates so that they become much higher for a given degree of supersaturation. Condensation was also observed to take place much closer to the saturation line than in the unmodified theory.

It was also observed that there was fairly close crowding of the lines of high condensation rates to the saturation lines and therefore one would not expect to obtain very high degrees of supersaturation of either pure oxygen or pure nitrogen. It was also noticed from these plots that high rates of condensation were reached before the critical radius had dropped below a value of 1.5D, that is, before the droplets got below 10 or 12 molecules.

The resulting predictions of condensation rates by Stever and Rathbun agreed well with the observed experimental results on the assumption that the condensation was initiated by the formation of nuclei of oxygen or nitrogen. Neither their theory nor their experimental work had precluded the possibility that the observed condensation took place on nuclei of impurities and therefore further experimental work was deemed necessary. Their modification of the theory with its predictions of

higher condensation rates, however, indicated that such condensation onto nuclei of impurities was not necessarily the explanation of the relatively low supersaturation ratios reached before condensation started. Their investigations also revealed that the time lags in the initiation of condensation were negligible once the fluid had reached a supersaturated state sufficient to start condensation according to the modified nucleation theory. The results of Stever and Rathbun were significant, but did not indicate the amount of supersaturation obtainable nor the effect of foreign nuclei on the condensation process. None of the theories advanced were definitely shown to be capable of predicting the onset of condensation.

There has been some experimental evidence which was interpreted as showing that gases condense on nuclei of impurities rather than on the self-generated nuclei postulated in the pure-vapor theories.

Arthur and Nagamatsu[18] conducted an experimental investigation to determine the effects of impurities on the supersaturation of commercial bottled nitrogen as it was expanded in a hypersonic nozzle. For their reservoir conditions of 8-1/3 atmospheres pressure and stagnation temperature of 70°F with no additives, they found the gas supersaturated approximately 32.4 °R. They also observed that the degree of supersaturation decreased with the addition of impurities. Their results indicated that both carbon dioxide and water vapor were extremely powerful nuclei for condensation as only a fractional percentage of either was required to completely eliminate the supersaturation. It was concluded that for impurity concentrations slightly greater than those in commerically bottled nitrogen gas the condensation was caused by foreign impurities and not by

self-nucleation of the gas, however, it was recommended that the effects of impurities on supersaturation should be investigated further. Their observations during the condensation process revealed that there was no condensation shock but that the condensation was gradual.

SUMMARY OF PREVIOUS INVESTIGATIONS

The Von Helmholtz equation, the result of an investigation of the equilibrium vapor pressure for coexistence of both a vapor and a liquid drop of a substance, led to the concept of the critical size drop. For a vapor at a fixed temperature, if the pressure is higher than the saturation pressure corresponding to its temperature there exists a critical radius of liquid droplet such that, if a drop is larger than the critical radius it will continue to grow by condensation.

In the kinetic theory of condensation, condensation is assumed to take place on spontaneously formed liquid nuclei of the substance. Volmer developed a theory of self-nucleation, wherein he determined the rates of formation of condensation nuclei, that is, droplets of critical size. Becker and Doring improved this theory by their development of an expression for the velocity of condensation taking into account not only the condensation of the vapor on the surface of the droplet but also its evaporation.

In an effort to resolve the apparent contradictions between the theory and experimental results consideration was given to the time delay in the nucleation rate. It was shown, however, that the time lags would not account for the discrepancies.

Stever and Rathbun modified the Becker-Doring theory taking into account the dependence of surface tension on drop radius and its effect on the condensation theory. Their modification resulted in predicted condensation rates being much higher than in the Becker-Doring theory for a given number of degrees of supersaturation.

None of the theories advanced were definitely shown to be capable of predicting the onset of condensation.

While the existence of supersaturation has been demonstrated, no limit line of supersaturation for nitrogen has previously been established. It was the purpose of this investigation to experimentally determine such a limit line for superheated nitrogen vapor and to compare these experimentally determined results with the theoretical analysis which has been made.

EXPERIMENTAL RESULTS

The experimental data and results obtained from the investigation are given in Table I through VI and plotted in Figures 3 through 15.

A tabulation of the stagnation properties at the inlet to the nozzle with the throat settings for these operating conditions is presented in Table I.

The sketch below illustrates the nomenclature of the pressures measured.

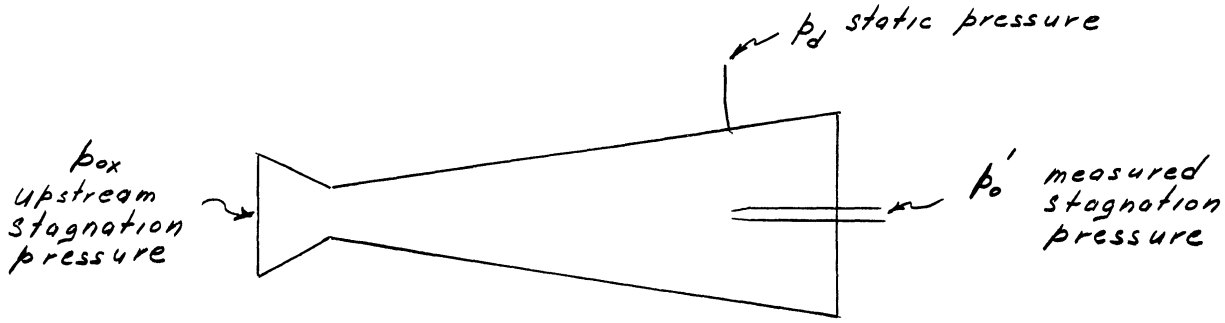

The measured pressure ratios as determined for each one-half inch internal downstream of the throat are shown in Table II. The first of these ratios, the measured stagnation pressure ratio, is the stagnation pressure as measured by a pitot tube on the centerline of the nozzle (p_o') divided by the stagnation pressure upstream of the nozzle (p_{ox}). The pressure ratio p_d/p_{ox} is the ratio of the static pressure p_d as measured on the divergent section of the nozzle blocks, in the vertical plane of symmetry, to the measured stagnation pressure on the centerline of the nozzle p_o'. The measured stagnation pressure used in these ratios is the stagnation pressure downstream of the normal shock which stands in front of the pitot tube. The measurements on the nozzle centerline were made at the same axial station as the static pressure holes on the wall.

Actually, the centerline measurements should have been made slightly downstream of the static pressure holes on the nozzle walls so that the static pressures measured were those upstream of the shock wave. However, it was found that there was no measurable difference in pressure between the two locations. Hence, the small position correction of the probe was neglected for all measured stagnation pressures on the nozzle centerline.

The experimental data were evaluated by a number of methods. The results of the evaluations are shown in graphical form.

Two methods were used to compare the static and measured stagnation pressure data as tabulated in Table II. The first method required a plot of the measured stagnation pressure ratio p_o'/p_{ox} against the pressure ratio p_d/p_o'. With these parameters a comparison of the experimentally measured ratios with those calculated theoretically for the isentropic-perfect gas flow was possible. The theoretically calculated pressure ratio p_x/p_{oy} is based upon the assumption that the shock wave which stands ahead of the mouth of the pitot tube is normal to the stagnation streamline at the point where the latter crosses it. In addition the particles following the stagnation streamline are assumed to be brought to rest isentropically after the shock. It is therefore permissible to express p_x/p_{oy} as follows:

$$\frac{p_x}{p_{oy}} = \left(\frac{p_y}{p_{oy}}\right)\left(\frac{p_x}{p_y}\right) \qquad \text{(R-1)}$$

where p_{oy}/p_y is the stagnation pressure ratio downstream of the normal shock and p_y/p_x is the static pressure ratio across the normal shock. By the definition of the stagnation pressure ratio

$$\frac{p_{oy}}{p_y} = \left(1 + \left(\frac{\kappa-1}{2}\right) M_y^2\right)^{\frac{\kappa}{\kappa-1}} \qquad \text{(R-2)}$$

and the developed expressions for the relation between the Mach numbers across the normal shock(33)

$$M_y^2 = \frac{M_x^2 + \frac{2}{k-1}}{\left(\frac{2k}{k-1}\right)M_x^2 - 1} \tag{R-3}$$

as well as that for the static pressure ratio across the normal shock(33)

$$\frac{p_y}{p_x} = \left(\frac{2k}{k+1}\right)M_x^2 - \frac{k-1}{k+1} \tag{R-4}$$

the resulting formula

$$\frac{p_{oy}}{p_x} = \left\{\left(\frac{k+1}{2}\right)M_x^2\right\}^{\frac{k}{k-1}} \Bigg/ \left\{\left(\frac{2k}{k+1}\right)M_x^2 - \frac{k-1}{k+1}\right\}^{\frac{1}{k-1}} \tag{R-5}$$

is obtained. Similarly the theoretically calculated pressure ratio p_{oy}/p_{ox} may be found by observing that

$$\frac{p_{oy}}{p_{ox}} = \left(\frac{p_{oy}}{p_y}\right)\left(\frac{p_y}{p_x}\right)\left(\frac{p_x}{p_{ox}}\right) \tag{R-6}$$

where p_{oy}/p_y is the stagnation pressure ratio downstream of the normal shock, p_y/p_x is the static pressure ratio across the normal shock, and p_{ox}/p_x is the stagnation pressure ratio upstream of the normal shock. With the relations mentioned above the theoretically calculated pressure ratio p_{oy}/p_{ox} becomes

$$\frac{p_{oy}}{p_{ox}} = \left\{\frac{\left(\frac{k+1}{2}\right)M_x^2}{1+\left(\frac{k-1}{2}\right)M_x^2}\right\}^{\frac{k}{k-1}} \Bigg/ \left\{\left(\frac{2k}{k+1}\right)M_x^2 - \frac{k-1}{k+1}\right\}^{\frac{1}{k-1}} \tag{R-7}$$

In these expressions the value of k for nitrogen used was 1.4 and the subscripts x and y denoted the conditions upstream and downstream of the

normal shock respectively. From the expressions for p_x/p_{oy} and p_{oy}/p_{ox} the isentrope was then plotted. The experimentally measured values were then superimposed on this plot as shown in Figure 3. As observed from the plots with the exception of Figure 6 the experimentally measured pressure ratios lie on the isentrope for some distance along the nozzle and then deviate from the isentrope. Since isentropic flows from all reservoirs conditions lie on the one isentrope the rise observed is due to the increase in static pressure associated with the heat released by the condensing vapor. The tangential point of departure, therefore, clearly defines the onset of condensation. Figure 6 represents those runs wherein there was experienced no condensation.

The second method of comparing the static and impact pressure data can be seen in Figure 4. In this set of curves the variation of the experimentally measured stagnation pressure ratio p_o'/p_{ox} against the nozzle length is shown. In addition a comparison of this value is made to the theoretically calculated stagnation pressure ratio which would be expected for a perfect gas isentropic flow. These plots reveal that the experimentally measured stagnation pressure ratio is very nearly that for isentropic flow. Therefore, the isentropic perfect gas relations between the measured stagnation and static pressures allow the isentropic static pressure to be calculated from the measured stagnation pressure. In the method of obtaining the isentropic static pressure the Mach number was first found by use of Equation (R-7), having measured the stagnation pressure ratio p_o'/p_{ox}. With this Mach number and the definition of the stagnation pressure ratio the isentropic static pressure was determined.

Then the isentropic static pressure ratios (p_x/p_{ox}) obtained were compared to the experimentally measured static pressure ratio values. This comparison is shown in Figure 4. As can be seen there results a departure of the measured static pressure ratios from the calculated isentropic static pressure ratio values. The tangential departure points as measured on this plot compare within experimental accuracy to those as observed from Figure 3.

The properties at the onset of condensation were determined from the observed tangential points of departure in Figure 3. The product of the noted stagnation pressure ratios p'_o/p_{ox} and the pressure ratios p_c/p'_o gave the static pressure ratios. The static pressures at the onset of condensation were then known. From the static pressure ratios p_c/p_{ox} and with the definition of the stagnation pressure ratio it was possible to calculate the Mach number at condensation. The definition of the stagnation temperature

$$\frac{T_{ox}}{T_c} = 1 + \left(\frac{\kappa-1}{2}\right) M_c^2$$

was then used to determine the temperature at condensation. The number of degrees of supersaturation defined as the difference between the saturation temperature for an infinite plane surface at the condensation pressure and the condensation temperature was then readily obtained. The supersaturation pressure ratios were computed as the ratios of the condensation pressures to the saturation pressures for an infinite plane surface at the condensation temperatures. The droplet radii were calculated from these supersaturation pressure ratios with the use of the Von Helmholtz's equation. The existing properties at the onset of condensation are tabulated in Table IV.

A third method of checking the location of the onset of condensation used here was first suggested by Wegener[15] and later by Nagamatsu and Willmarth.[17] This method is dependent upon the fact that in a condensing flow the equation of momentum and continuity are unchanged if it is assumed that the droplets of the condensed phase are in dynamic equilibrium with the vapor phase. This assumption seems reasonable since the droplets are formed from the vapor and in all probability retain the gross velocity of the vapor. As can be seen in Appendix A where the equations for this method are given the integrated forms require the use of the experimentally determined area and static pressure ratios. The effective area ratio following the onset of condensation was determined from the isentropic perfect gas theory using Equation (R-7) and the experimentally measured stagnation pressure ratio. Determination of the Mach number in this manner permitted the calculation of the area ratio from the area ratio equation as developed in Reference 33.

$$\frac{A}{A^*} = \frac{1}{M}\left\{\left(\frac{2}{K+1}\right)\left(1+\left(\frac{K-1}{2}\right)M^2\right)\right\}^{\frac{K+1}{2(K-1)}} \qquad \text{(R-8)}$$

The justification for the use of the isentropic perfect gas theory as a means of obtaining the effective area ratio after condensation was based upon the previously mentioned result, as shown in Figure 4. It was shown there that the experimentally measured stagnation pressure ratio was nearly the same as that for isentropic flow. The static pressure ratio variation expressed as a function of d inches downstream of the onset of condensation was also needed for the evaluation of the properties of the two phase fluid. This expression was obtained by determining the equation

of the curve that best fitted the experimentally measured static pressure ratios downstream of condensation as shown in Figure 4. With the effective area ratio and this static pressure ratio equation the properties of the two phase fluid downstream of the point of condensation were calculated and the results tabulated in Table V.

The calculated temperature values as recorded in Table V were then plotted against the measured static pressures as shown by Figure 5. These curves reveal the existence of the supersaturated state in that the expansion continued beyond the saturation curve. The actual expansion finally deviated from the isentropic and this point of the departure again marked the onset of condensation.

A correlation between the results of this investigation and those of previous experimentors is shown in Figure 7. The supersaturation pressure ratios there plotted are for the condensation points where the droplet radii were all approximately of the same magnitude as shown in Table IV.

The supersaturated state could not be correctly represented on the conventional Mollier chart since its construction is based upon equilibrium conditions. Thus a modified Mollier chart was constructed to include the supersaturated pressure lines pp. In addition the Mollier diagram had to be extrapolated to pressures below the 10 psia value. The method of extrapolation is discussed in Appendix B. The isentropic part of the expansions for the various test runs were then plotted on this modified Mollier chart and the limits of the isentropic expansions noted. The limit of supersaturation was designated as the intersection of the isentropic expansion and the supersaturation pressure line for the

condensation pressure. The locus of these points representing the supersaturation limits for the expansion along various isentropes fitted to a curve defined the supersaturation limit line. As observed from these results the limit line of supersaturation almost parallels the saturation line and lies between the two and four per cent condensate lines. A different plot of the supersaturation limit line is shown in Figure 9 wherein the condensation temperature and pressures were used as parameters.

TABLE I

ORIGINAL TEST DATA

Run No.	Temperature m.v. °F	Pressure atm. psia	Superheat °F	Throat Setting in^2	Static Pressures Inches Mercury Measured Stagnation Pressures psia Inches from Throat 1/2	1	1-1/2	2	2-1/2	3	3-1/2	4	4-1/2	Manometer Reference Inches Mercury
	4.45	4.38			25.8	35.4	43.1	44.2	47.5	47.9	50.8	52.1	52.9	
50-S-2	-226	64.23	67.24	0.195	59.23	53.23	48.23	44.23	40.23	38.23	35.23	33.23	31.23	31.9
	4.4	4.38			22.7	33	41	42.3	45.6	47.9	48.8	49.5	50.9	
50-5	-222	64.36	71.24	0.195	59.36	54.36	48.36	45.36	41.36	37.36	35.36	33.36	30.36	29.4
	4.0	7.8			13.8	28.8	38.6	43.5	45.7	47.4	49.5	50.6	51.5	
100-5	-192	114.29	87.35	0.125	96.29	84.29	71.29	61.29	54.29	49.29	43.29	39.29	36.29	29.7
	4.2	9.15			11.8	29.2	39.1	44	46.2	48.1	50.2	51.3	52.1	
120-2	-206.67	134.21	68.37	0.10	108.21	89.21	72.21	61.21	53.21	48.21	42.21	38.21	34.21	29.2
	3.85	9.15			11.1	28.6	38.9	43.8	46.2	48.3	49.6	50.6	52.8	
120-1	-181.33	134.3	93.71	0.10	109.3	90.3	74.4	64.3	56.3	49.3	44.3	38.4	34.4	29.6
	3.8	9.15			15.3	30.5	38.8	44.8	46.6	48.2	50.3	51.3	51.4	
120-3	-178	134.2	97.04	0.10	106.21	87.2	73.2	61.2	54.2	49.2	41.2	37.2	34.2	28.8
	4.0	9.84			20.6	31.5	41.5	46.1	48.8	50.45	51.7	52.7	53.7	
130-5	-192	144.28	81.11	0.09	109.28	91.3	75.3	62.3	54.3	48.3	43.3	38.3	34.3	31.3
	3.90	9.84			14	31.5	41	45.5	47.8	49.4	50.7	52.2	52.4	
130-1	-185	144.42	88.11	0.09	111.4	90.4	74.4	62.4	55.4	49.4	44.4	38.4	34.4	29.5
	3.8	9.84			20.2	31.7	41.3	47.0	49.5	50.6	52.0	53.7	54.4	
130-6	-178	144.3	95.11	0.09	110.3	89.3	74.3	61.3	54.3	50.3	43.3	38.3	35.3	32.3
	3.71	10.6			26.2	30.8	40.5	47.0	49.0	51.3	52.2	53.5	54.0	
140-5	-172	154.3	99.2	0.09	114.3	96.3	80.3	65.3	57.3	50.3	46.3	40.3	37.3	31.5
	3.70	10.6			11.7	29.8	39.5	42.3	44.7	47.7	50.4	50.6	51.2	
140-1	-171.67	154.4	99.53	0.09	118.4	98.4	79.4	66.4	56.4	51.4	45.4	41.4	38.4	29.2
	3.60	10.6			25.7	29.9	38.7	46.3	49.1	50.9	51.9	52.4	52.4	
140-6	-164.67	154.3	106.53	0.09	114.3	96.3	82.3	66.3	56.8	50.3	45.3	41.3	38.3	30.9
	3.53	13.22			17.9	33.54	43.5	48.0	50.2	51.2	53.0	53.6	55.0	
180-8	-160	194.3	104.43	0.06	131.3	105.3	81.8	66.3	55.3	50.3	41.3	38.3	34.3	31.5
	3.40	13.22			18.4	34.3	42.5	48.4	50.8	52.0	53.2	53.9	55.1	
180-5	-151.33	194.4	113.11	0.06	129.4	102.4	83.4	66.4	54.4	49.4	42.4	38.4	34.4	31.0
	3.25	12.9			18.2	33.7	43.4	48.5	51.0	52.2	53.8	54.2	54.7	
180-7	-142	189.3	123.19	0.06	129.3	103.3	82.3	67.3	56.3	49.3	41.3	38.3	35.3	31.4
	2.9	13.22			19.2	33.5	43.6	48.8	51.5	53.0	53.8	54.7	55.2	
180-2	-120	194.4	144.43	0.06	129.4	102.4	82.4	67.4	58.4	52.4	48.4	42.4	37.4	31.5
	2.9	13.22			19.5	33.6	43.3	48.4	51.0	52.6	53.7	54.4	55.5	
180-6	-120	194.3	144.43	0.06	131.3	103.3	82.3	67.3	59.3	53.3	47.3	42.3	36.3	31.3
	3.91	9.15			15.8	31.1	41.3	46.4	48.5	50.4	52.2	52.7	54.7	
120P-1	-186	134.3	89.0	0.10	108.3	90.3	74.3	62.3	57.3	49.3	43.3	40.3	36.3	31.5
	3.38	13.22			17.8	34.0	44.3	48.9	50.6	52.5	54.3	55.2	56.0	
180P-1	-150	194.15	114.43	0.06	129.2	103.2	81.2	65.2	56.2	51.2	42.2	38.2	34.2	31.8
	2.6	4.38			28.0	35.7	43.5	44.7	48.0	49.5	51.5	52.2	52.8	
50-6	-102.3	64.36	190.94	0.195	58.36	54.36	47.36	45.36	41.36	38.36	35.36	34.36	32.36	31.4
	3.4	7.8			13.8	29.0	38.6	43.6	44.8	47.6	49.8	51.0	51.4	
100-4	-151.33	114.27	128.02	0.125	97.27	82.27	69.27	60.27	55.27	49.27	44.27	40.27	38.27	29.0
	2.9	9.15			20.8	31.2	41.4	46.0	48.2	51.8	52.4	54.0	54.9	
120-6	-120	134.3	155.04	0.10	105.3	90.3	74.3	64.3	58.3	49.3	47.3	41.3	38.3	31.7
	2.5	10.5			14.7	30.2	40.0	46.1	47.5	50.4	51.5	52.9	53.9	
140-2	- 96.5	154.1	174.7	0.09	118.4	97.4	80.4	66.4	62.4	54.4	50.4	45.4	40.4	31.1
	4.2	4.38			24.5	34.4	42.0	43.0	46.0	48.5	49.5	50.2	51.2	
50-4	-206.5	64.36	85.7	0.195	59.36	53.36	47.36	45.36	41.36	37.36	35.36	33.36	31.36	29.6
	4.08	6.09			22.3	32.9	41.4	44.0	47.5	50.5	51.7	52.2	53.0	
75-5	-198	89.37	87.9	0.15	78.37	68.37	59.37	55.37	49.37	44.37	40.37	37.37	34.37	31.3
	4.0	6.09			24.3	33.0	41.7	44.8	46.9	49.85	51.6	52.5	52.7	
75-8	-192	89.38	93.9	0.15	78.38	68.38	58.38	54.38	49.38	43.38	38.38	36.38	34.38	31.0
	3.5	13.22			17.1	33.2	43.5	46.3	48.8	49.3	50.3	51.3	52.9	
180-13a	-158	194.4	106.4	0.06	131.4	103.4	82.4	68.4	57.4	53.4	44.4	42.4	34.4	29.6

TABLE II

EXPERIMENTALLY MEASURED PRESSURE RATIOS

Run No.		Inches from Throat 1/2	1	1-1/2	2	2-1/2	3	3-1/2	4	4-1/2
	p'_o/p_{ox}	0.923	0.845	0.736	0.705	0.642	0.595	0.534	0.502	0.471
50-S-2	p_a/p'_o	0.286	0.227	0.179	0.174	0.153	0.144	0.135	0.128	0.123
	p_a/p_{ox}	0.264	0.192	0.132	0.123	0.098	0.086	0.072	0.0644	0.0578
	p'_o/p_{ox}	0.922	0.845	0.751	0.705	0.644	0.58	0.558	0.518	0.473
50-5	p_a/p'_o	0.298	0.232	0.186	0.175	0.155	0.141	0.138	0.135	0.129
	p_a/p_{ox}	0.275	0.1969	0.140	0.123	0.099	0.082	0.076	0.0696	0.068
	p'_o/p_{ox}	0.84	0.736	0.62	0.536	0.474	0.43	0.379	0.344	0.317
100-5	p_a/p'_o	0.229	0.176	0.145	0.123	0.119	0.113	0.105	0.103	0.102
	p_a/p_{ox}	0.193	0.129	0.09	0.066	0.0564	0.0486	0.0398	0.0353	0.0323
	p'_o/p_{ox}	0.807	0.665	0.537	0.456	0.395	0.359	0.314	0.284	0.255
120-2	p_a/p'_o	0.209	0.159	0.129	0.114	0.1103	0.102	0.0925	0.088	0.0872
	p_a/p_{ox}	0.169	0.106	0.696	0.0517	0.0438	0.0367	0.0291	0.025	0.0223
	p'_o/p_{ox}	0.812	0.67	0.553	0.478	0.419	0.366	0.329	0.285	0.258
120-1	p_a/p'_o	0.213	0.163	0.132	0.113	0.108	0.103	0.10	0.103	0.0845
	p_a/p_{ox}	0.174	0.1099	0.072	0.0541	0.0454	0.0377	0.033	0.0294	0.0218
	p'_o/p_{ox}	0.792	0.650	0.545	0.456	0.404	0.366	0.307	0.277	0.255
120-3	p_a/p'_o	0.197	0.153	0.127	0.104	0.101	0.0962	0.088	0.0863	0.091
	p_a/p_{ox}	0.155	0.0995	0.0692	0.0473	0.0406	0.0352	0.0222	0.0239	0.0282
	p'_o/p_{ox}	0.757	0.633	0.522	0.431	0.376	0.348	0.30	0.265	0.238
130-5	p_a/p'_o	0.179	0.155	0.123	0.112	0.1045	0.101	0.0988	0.0987	0.0957
	p_a/p_{ox}	0.1352	0.0981	0.0643	0.0484	0.0394	0.0338	0.0296	0.0262	0.0227
	p'_o/p_{ox}	0.772	0.626	0.515	0.432	0.383	0.342	0.307	0.267	0.239
130-1	p_a/p'_o	0.198	0.149	0.12	0.106	0.0983	0.0927	0.0906	0.0825	0.091
	p_a/p_{ox}	0.153	0.0933	0.0607	0.0456	0.0376	0.0318	0.0278	0.022	0.022
	p'_o/p_{ox}	0.765	0.618	0.515	0.424	0.376	0.348	0.30	0.265	0.245
130-6	p_a/p'_o	0.184	0.163	0.133	0.124	0.1072	0.105	0.106	0.0987	0.0981
	p_a/p_{ox}	0.141	0.101	0.0685	0.0526	0.0404	0.0365	0.0318	0.0262	0.0240
	p'_o/p_{ox}	0.741	0.624	0.52	0.423	0.372	0.325	0.30	0.261	0.242
140-5	p_a/p_o	0.148	0.152	0.121	0.102	0.093	0.091	0.0895	0.087	0.0876
	p_a/p_{ox}	0.1091	0.0948	0.0628	0.0432	0.0353	0.0296	0.0279	0.0227	0.0212
	p'_o/p_{ox}	0.766	0.63	0.514	0.43	0.367	0.33	0.294	0.268	0.248
140-1	p_a/p'_o	0.194	0.145	0.1175	0.103	0.0976	0.103	0.088	0.0942	0.0938
	p_a/p_{ox}	0.149	0.0913	0.0604	0.0443	0.0357	0.034	0.0259	0.0253	0.0233

TABLE II (CONT'D)

EXPERIMENTALLY MEASURED PRESSURE RATIOS

Run No.		Inches from Throat 1/2	1	1-1/2	2	2-1/2	3	3-1/2	4	4-1/2
140-6	p'_o/p_{ox}	0.741	0.630	0.533	0.43	0.368	0.326	0.293	0.267	0.249
	p_d/p'_o	0.147	0.150	0.127	0.102	0.0945	0.089	0.0883	0.091	0.0979
	p_d/p_{ox}	0.109	0.0945	0.0678	0.0436	0.0348	0.029	0.0259	0.0243	0.0243
180-8	p'_o/p_{ox}	0.676	0.542	0.42	0.341	0.284	0.258	0.212	0.197	0.171
	p_d/p'_o	0.159	0.126	0.103	0.0937	0.0927	0.0917	0.091	0.09	0.0815
	p_d/p_{ox}	0.1075	0.0685	0.0432	0.0319	0.0264	0.0238	0.0194	0.0178	0.0143
180-5	p'_o/p_{ox}	0.666	0.527	0.428	0.341	0.279	0.254	0.218	0.197	0.177
	p_d/p'_o	0.159	0.124	0.104	0.0875	0.085	0.082	0.081	0.0808	0.0728
	p_d/p_{ox}	0.1055	0.0652	0.0446	0.0298	0.0238	0.0208	0.0178	0.0160	0.0129
180-7	p'_o/p_{ox}	0.684	0.546	0.435	0.355	0.297	0.260	0.218	0.20	0.186
	p_d/p'_o	0.160	0.129	0.102	0.0918	0.0846	0.084	0.08	0.08	0.082
	p_d/p_{ox}	0.1095	0.0703	0.0445	0.0312	0.0248	0.0216	0.0175	0.0160	0.0154
180-2	p'_o/p_{ox}	0.666	0.527	0.424	0.346	0.30	0.27	0.248	0.218	0.192
	p_d/p'_o	0.158	0.13	0.102	0.0869	0.0774	0.0715	0.0704	0.0695	0.0724
	p_d/p_{ox}	0.105	0.0686	0.0433	0.0301	0.0232	0.0196	0.0175	0.0152	0.0139
180-6	p'_o/p_{ox}	0.677	0.532	0.423	0.351	0.305	0.274	0.243	0.218	0.187
	p_d/p'_o	0.153	0.127	0.103	0.088	0.078	0.0722	0.0698	0.0705	0.0662
	p_d/p_{ox}	0.104	0.0675	0.0432	0.0304	0.0238	0.0198	0.0170	0.0153	0.0124
50-4	p'_o/p_{ox}	0.925	0.83	0.736	0.706	0.644	0.583	0.549	0.518	0.487
	p_d/p'_o	0.286	0.226	0.176	0.1725	0.154	0.137	0.130	0.127	0.123
	p_d/p_{ox}	0.265	0.188	0.1295	0.122	0.0993	0.080	0.0714	0.0658	0.060
75-5	p'_o/p_{ox}	0.878	0.766	0.665	0.62	0.553	0.497	0.452	0.418	0.384
	p_d/p'_o	0.242	0.193	0.159	0.146	0.13	0.115	0.108	0.11	0.1085
	p_d/p_{ox}	0.212	0.148	0.106	0.0906	0.072	0.0573	0.049	0.046	0.0416
75-8	p'_o/p_{ox}	0.878	0.764	0.654	0.608	0.553	0.486	0.429	0.407	0.384
	p_d/p'_o	0.226	0.196	0.156	0.139	0.132	0.118	0.109	0.105	0.109
	p_d/p_{ox}	0.198	0.150	0.102	0.0845	0.073	0.0574	0.0468	0.0432	0.0418
180-13a	p'_o/p_{ox}	0.677	0.532	0.423	0.351	0.305	0.274	0.245	0.218	0.187
	p_d/p'_o	0.156	0.122	0.104	0.0905	0.0865	0.0886	0.088	0.0884	0.0855
	p_d/p_{ox}	0.106	0.0650	0.044	0.0318	0.0264	0.0243	0.0216	0.0193	0.0160

TABLE III

ISENTROPIC VALUES CALCULATED FROM p_o'/p_{ox}

Run No.		Inches from Throat 1/2	1	1-1/2	2	2-1/2	3	3-1/2	4	4-1/2
	p_o'/p_{ox}	0.923	0.845	0.736	0.705	0.642	0.595	0.534	0.502	0.471
50-S-2	A/A*	1.18	1.36	1.64	1.73	1.96	2.15	2.45	2.62	2.82
	p_d/p_{ox}	0.28	0.195	0.131	0.119	0.098	0.084	0.068	0.059	0.052
	p_o'/p_{ox}	0.925	0.83	0.736	0.706	0.644	0.583	0.549	0.518	0.487
50-4	A/A*	1.19	1.39	1.64	1.73	1.95	2.21	2.39	2.55	2.72
	p_d/p_{ox}	0.272	0.19	0.131	0.119	0.097	0.079	0.070	0.061	0.055
	p_o'/p_{ox}	0.922	0.845	0.751	0.705	0.644	0.58	0.558	0.518	0.473
50-5	A/A*	1.18	1.36	1.60	1.73	1.95	2.20	2.35	2.58	2.82
	p_d/p_{ox}	0.28	0.195	0.140	0.119	0.099	0.081	0.071	0.061	0.052
	p_o'/p_{ox}	0.84	0.736	0.62	0.536	0.474	0.430	0.379	0.344	0.317
100-5	A/A*	1.37	1.65	2.05	2.44	2.81	3.15	3.70	4.06	4.45
	p_d/p_{ox}	0.189	0.130	0.090	0.066	0.052	0.044	0.0338	0.029	0.0252
	p_o'/p_{ox}	0.807	0.665	0.537	0.456	0.395	0.359	0.314	0.284	0.255
120-2	A/A*	1.46	1.87	2.42	2.95	3.50	3.89	4.47	5.22	5.65
	p_d/p_{ox}	0.168	0.103	0.067	0.048	0.037	0.031	0.025	0.0195	0.0172
	p_o'/p_{ox}	0.812	0.67	0.553	0.478	0.419	0.366	0.329	0.285	0.258
120-1	A/A*	1.44	1.86	2.35	2.8	3.26	3.78	4.28	5.01	5.6
	p_d/p_{ox}	0.169	0.105	0.072	0.053	0.042	0.033	0.0265	0.0209	0.0175
	p_o'/p_{ox}	0.792	0.650	0.545	0.456	0.404	0.366	0.307	0.277	0.255
120-3	A/A*	1.49	1.93	2.40	2.95	3.41	3.81	4.61	5.2	5.65
	p_d/p_{ox}	0.159	0.10	0.069	0.049	0.038	0.032	0.0238	0.198	0.0175
	p_o'/p_{ox}	0.757	0.633	0.522	0.431	0.376	0.348	0.30	0.265	0.238
130-5	A/A*	1.58	1.97	2.51	3.07	3.66	4.02	4.70	5.41	6.12
	p_d/p_{ox}	0.148	0.097	0.063	0.045	0.0345	0.0295	0.023	0.0182	0.0151
	p_o'/p_{ox}	0.772	0.626	0.515	0.432	0.383	0.342	0.307	0.267	0.239
130-1	A/A*	1.54	2.02	2.58	3.12	3.6	4.08	4.61	5.38	6.1
	p_d/p_{ox}	0.152	0.092	0.061	0.044	0.0352	0.029	0.0238	0.0188	0.0153
	p_o'/p_{ox}	0.741	0.624	0.52	0.423	0.372	0.325	0.30	0.261	0.242
140-5	A/A*	1.63	2.03	2.54	3.20	3.70	4.33	4.76	5.5	5.95
	p_d/p_{ox}	0.130	0.092	0.062	0.043	0.0335	0.026	0.023	0.0179	0.016
	p_o'/p_{ox}	0.766	0.63	0.514	0.43	0.367	0.33	0.294	0.268	0.248
140-1	A/A*	1.57	2.01	2.57	3.15	3.78	4.25	4.81	5.38	5.81
	p_d/p_{ox}	0.143	0.093	0.062	0.044	0.0332	0.0265	0.0218	0.0188	0.0165
	p_o'/p_{ox}	0.741	0.630	0.533	0.43	0.368	0.326	0.293	0.267	0.249
140-6	A/A*	1.63	2.01	2.47	3.15	3.78	4.32	4.81	5.38	5.81
	p_d/p_{ox}	0.130	0.093	0.066	0.044	0.0332	0.026	0.0218	0.0188	0.0163
	p_o'/p_{ox}	0.676	0.542	0.42	0.341	0.284	0.258	0.212	0.197	0.171
180-8	A/A*	1.83	2.41	3.24	4.08	5.02	5.58	6.85	7.42	8.65
	p_d/p_{ox}	0.105	0.068	0.0415	0.0285	0.0210	0.0178	0.0128	0.0113	0.0091
	p_o'/p_{ox}	0.666	0.527	0.433	0.341	0.279	0.254	0.218	0.197	0.177
180-5	A/A*	1.87	2.5	3.13	4.10	5.10	5.68	6.69	7.45	8.35
	p_d/p_{ox}	0.107	0.064	0.0435	0.0285	0.0205	0.0172	0.0135	0.0115	0.0096
	p_o'/p_{ox}	0.684	0.546	0.435	0.355	0.297	0.260	0.218	0.202	0.186
180-7	A/A*	1.80	2.37	3.10	3.89	4.79	5.53	6.7	7.25	7.85
	p_d/p_{ox}	0.115	0.072	0.045	0.0315	0.0225	0.0178	0.0135	0.0119	0.0105
	p_o'/p_{ox}	0.666	0.527	0.424	0.346	0.30	0.27	0.241	0.218	0.192
180-2	A/A*	1.87	2.5	3.20	4.04	4.72	5.32	6.00	6.69	7.68
	p_d/p_{ox}	0.106	0.064	0.422	0.0291	0.023	0.0188	0.0158	0.0135	0.011
	p_o'/p_{ox}	0.677	0.532	0.423	0.351	0.305	0.274	0.243	0.218	0.187
180-6	A/A*	1.83	2.46	3.20	3.92	4.61	5.23	5.91	6.69	7.80
	p_d/p_{ox}	0.106	0.066	0.0422	0.0305	0.0237	0.0195	0.016	0.0135	0.0107

TABLE IV

PROPERTIES AT ONSET OF CONDENSATION

Run No.	Condensation Temperature °R	Condensation Pressure atm	Degrees Supersaturation $T_s - T_c$ °R	Condensation Mach No. M_c	Supersaturation Ratio p_c/p_∞	Droplet Radius at Condensation r ft x 10^9
50-S-2	126	0.497	3.42	2.07	1.315	13.5
50-5	122.5	0.42	4.67	2.17	1.50	9.75
100-5	123	0.513	6.79	2.43	1.73	7.15
120-2	129.2	0.855	7.69	2.19	1.745	6.26
120-1	121.1	0.492	8.14	2.55	1.95	6.08
120-3	117.9	0.427	9.49	2.64	2.27	5.27
130-5	124.9	0.669	8.43	2.40	1.92	5.8
130-1	123.2	0.59	8.38	2.48	1.955	5.84
130-6	123.7	0.605	8.25	2.53	1.92	5.94
140-5	121.0	0.503	8.54	2.63	2.01	5.79
140-1	120.9	0.492	8.34	2.64	1.982	5.96
140-6	117.5	0.413	9.48	2.75	2.27	5.28
180-8	123.8	0.59	7.78	2.67	1.85	6.26
180-5	119.45	0.478	9.41	2.81	2.203	5.22
180-7	115.2	0.363	10.45	2.96	2.565	4.76
180-2	109.0	0.256	12.26	3.25	3.56	3.62
180-6	110.0	0.264	11.67	3.23	3.24	4.2
120P-1	118.5	0.474	10.5	2.57	2.4	4.84
180P-1	124.0	0.555	6.8	2.71	1.72	7.1
180-13a	121	0.534	9.8	2.74	2.17	5.26
75-5	112.5	0.317	10.5	2.58	3.02	4.3
75-8	116.0	0.328	7.3	2.55	2.05	6.2

TABLE V

PROPERTIES DOWNSTREAM OF CONDENSATION

Run No.	Distance Downstream from Throat Inches	Pressure p_d atm	Area Ratio $A/A^*)_d$	Velocity Ratio $V/V^*)_d$	Density Ratio $\rho/\rho^*)_d$	Temperature Ratio $T/T^*)_d$	Temperature T_d °R	Fraction of Condensation C_d
50-S-2	2-1/2	0.422	1.98	1.703	0.287	0.642	125	0.0095
	3	0.369	2.18	1.734	0.265	0.606	118.2	0.0035
	3-1/2	0.321	2.37	1.777	0.238	0.589	114.9	0.009
	4	0.282	2.56	1.802	0.217	0.601	117.2	0.0235
	4-1/2	0.253	2.76	1.825	0.198	0.594	116.0	0.027
100-5	2-1/2	0.423	2.79	1.838	0.195	0.528	118.0	0.002
	3	0.359	3.15	1.868	0.170	0.516	115.3	0.0055
	3-1/2	0.311	3.51	1.907	0.149	0.517	115.4	0.021
	4	0.275	3.88	1.93	0.134	0.511	114.0	0.0268
	4-1/2	0.252	4.23	1.943	0.122	0.522	116.2	0.038
120-1	2-1/2	0.402	3.25	1.878	0.164	0.512	119	0.008
	3	0.345	3.70	1.913	0.141	0.521	121	0.028
	3-1/2	0.302	4.15	1.94	0.124	0.524	121.8	0.0395
	4	0.265	4.61	1.961	0.1104	0.522	121	0.047
	4-1/2	0.240	5.06	1.965	0.101	0.518	120.2	0.049
120-3	2-1/2	0.354	3.39	1.91	0.154	0.478	112.2	0.004
	3	0.298	3.85	1.934	0.134	0.464	109	0.006
	3-1/2	0.258	4.32	1.98	0.117	0.473	111	0.0315
	4	0.229	4.80	1.998	0.105	0.467	109.9	0.0345
	4-1/2	0.206	5.28	2.003	0.0947	0.469	110	0.037
130-5	2	0.476	3.08	1.869	0.174	0.535	124	0.016
	2-1/2	0.387	3.59	1.91	0.146	0.522	120.8	0.0275
	3	0.332	4.11	1.939	0.126	0.527	122	0.04
	3-1/2	0.285	4.63	1.964	0.1098	0.524	121	0.049
	4	0.251	5.15	1.986	0.0978	0.524	121	0.057
	4-1/2	0.219	5.68	2.01	0.0876	0.513	118	0.063
130-1	2	0.449	3.08	1.874	0.173	0.502	115	0.006
	2-1/2	0.369	3.59	1.912	0.146	0.492	112.7	0.0125
	3	0.313	4.11	1.942	0.125	0.496	113.5	0.026
	3-1/2	0.273	4.63	1.966	0.1098	0.496	113.5	0.0345
	4	0.2405	5.15	1.988	0.0976	0.494	113.1	0.0430
	4-1/2	0.216	5.68	2.01	0.0876	0.499	114.0	0.0545
140-5	2	0.458	3.19	1.886	0.166	0.493	118.1	0.002
	2-1/2	0.374	3.74	1.915	0.139	0.485	117.5	0.0095
	3	0.314	4.28	1.955	0.1196	0.480	115.2	0.0245
	3-1/2	0.271	4.83	1.965	0.1035	0.480	115.5	0.0275
	4	0.241	5.39	2.00	0.093	0.484	116.0	0.0445
	4-1/2	0.222	5.93	2.01	0.0839	0.495	118.5	0.0505
140-1	2	0.47	3.17	1.88	0.168	0.50	120	0.003
	2-1/2	0.379	3.70	1.92	0.1408	0.488	117.2	0.0135
	3	0.323	4.23	1.948	0.1213	0.486	116.9	0.0235
	3-1/2	0.282	4.78	1.975	0.106	0.494	118.9	0.0395
	4	0.250	5.32	1.992	0.0945	0.496	119.0	0.048
	4-1/2	0.223	5.87	2.017	0.0847	0.499	120.0	0.0575
140-6	2-1/2	0.369	3.70	1.923	0.140	0.475	117	0.0085
	3	0.308	4.23	1.955	0.121	0.462	113.9	0.0135
	3-1/2	0.275	4.78	1.973	0.106	0.480	118.2	0.032
	4	0.250	5.32	1.983	0.0946	0.491	120.0	0.0435
	4-1/2	0.222	5.85	1.99	0.0855	0.486	119.2	0.0453
180-3	1-1/2	0.573	3.32	1.887	0.1597	0.50	125.0	0.005
	2	0.422	4.09	1.944	0.122	0.487	122.0	0.0235
	2-1/2	0.347	4.80	1.981	0.105	0.491	122.2	0.0355
	3	0.294	5.55	1.985	0.0910	0.482	120.5	0.0385
	3-1/2	0.246	6.31	2.02	0.0785	0.470	118.0	0.0475
	4	0.210	7.09	2.064	0.0682	0.475	118.2	0.070
	4-1/2	0.180	7.83	2.083	0.061	0.455	113.5	0.07
180-5	2	0.395	4.07	1.947	0.126	0.4535	116.5	0.0065
	2-1/2	0.315	4.82	1.998	0.104	0.446	114.5	0.024
	3	0.270	5.59	2.005	0.0895	0.455	117.0	0.0315
	3-1/2	0.236	6.37	2.028	0.0773	0.457	117.5	0.045
	4	0.2065	7.15	2.045	0.0682	0.457	117.0	0.052
	4-1/2	0.181	7.91	2.076	0.061	0.455	117.0	0.0655
180-7	2-1/2	0.313	4.72	1.979	0.107	0.431	114.1	0.009
	3	0.266	5.46	2.009	0.0914	0.441	116.6	0.03
	3-1/2	0.232	6.2	2.033	0.0794	0.447	118.3	0.044
	4	0.206	6.96	2.043	0.0701	0.453	119.0	0.0455
	4-1/2	0.187	7.71	2.052	0.0631	0.452	118.0	0.053
180-2	3-1/2	0.2218	6.31	2.078	0.0764	0.369	104.5	0.0165
	4	0.2012	7.08	2.103	0.0705	0.371	105.0	0.0335
	4-1/2	0.184	7.84	2.118	0.0605	0.405	114.5	0.0585
180-6	3-1/2	0.221	6.16	2.037	0.0797	0.464	114.5	0.0185
	4	0.196	6.9	2.062	0.0701	0.416	117.9	0.0375
	4-1/2	0.172	7.65	2.081	0.0626	0.411	116	0.045

TABLE VI

COMPUTED TEMPERATURES RUN NO. 140-2

Run No.	Distance Downstream from Throat Inches	Pressure p_d atm	Area Ratio $A/A^*)_d$	Velocity Ratio $V/V^*)_d$	Temperature Ratio T/T^*	Temperature T_d °R
140-2	1-1/2	0.66	2.5	1.804	0.536	162.5
	2	0.488	3.0	1.861	0.490	148.5
	2-1/2	0.391	3.5	1.902	0.469	142.0
	3	0.326	4.0	1.934	0.451	137.0
	3-1/2	0.273	4.5	1.962	0.433	131.0
	4	0.233	5.0	1.989	0.417	126.0
	4-1/2	0.20	5.5	2.012	0.398	120.0

TABLE VII

SURFACE TENSION AND DROPLET RADII

Run No.	Condensation Temperature T_c °R	Surface Tension σ Independent of r lbs/ft $\sigma \times 10^4$	Droplet Radius Based on σ Independent of r r ft $\times 10^9$	Droplet Radius Based on σ Dependent Upon r r ft $\times 10^9$	Surface Tension σ Dependent on r lbs/ft $\sigma \times 10^4$
50-5	122.5	7.13	9.75	8.7	6.4
100-5	123.0	7.09	7.15	6.04	6.1
120-1	121.1	7.28	6.08	5.05	6.08
130-1	123.2	7.08	5.84	4.80	5.71
140-5	121.0	7.24	5.79	4.8	5.99
180-6	110	8.32	4.2	3.2	6.34
75-8	116	7.75	6.2	5.2	6.5

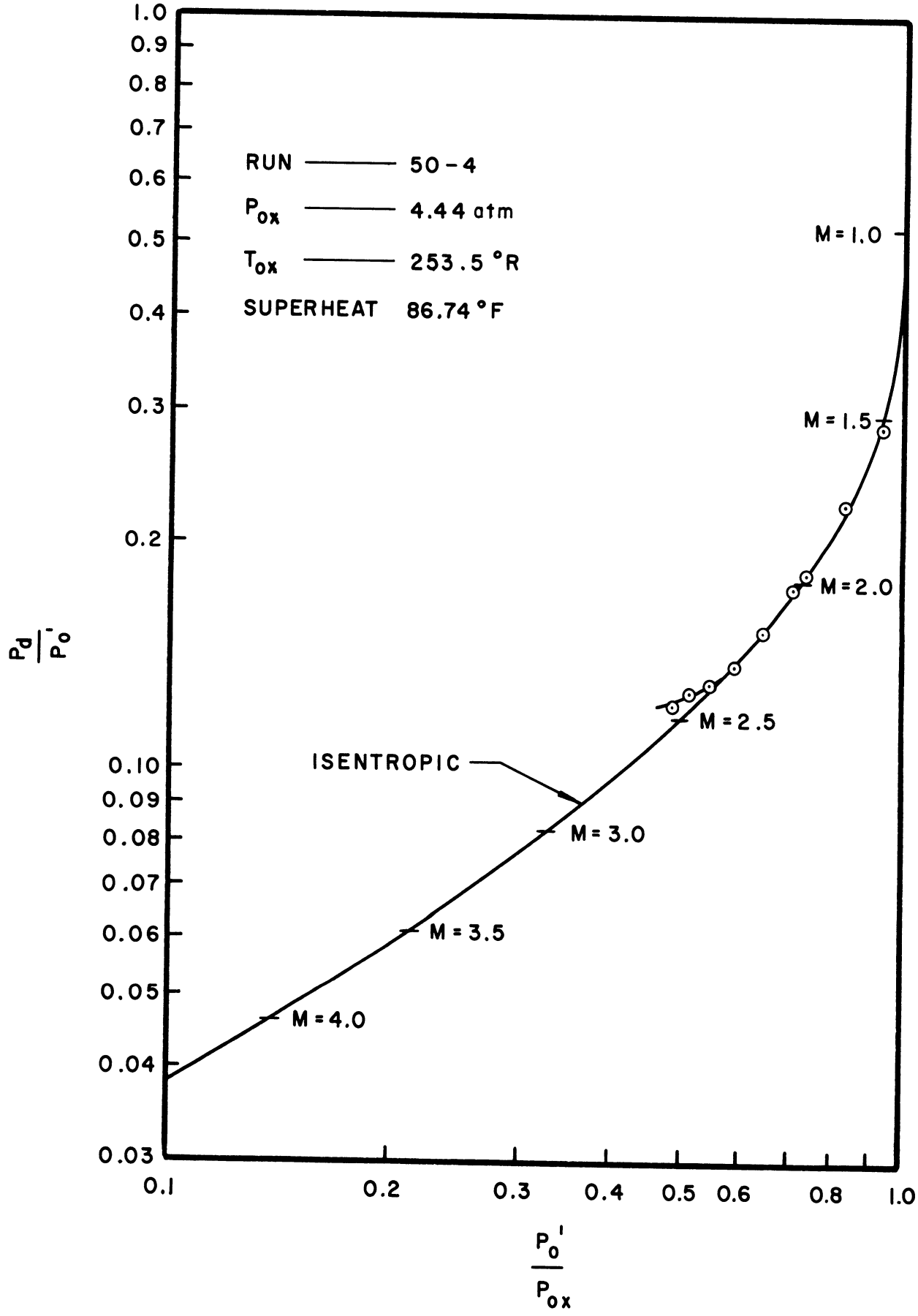

Figure 3-1. Comparison of Actual Expansion with Isentropic p_o'/p_{ox} vs. p_d/p_o'.

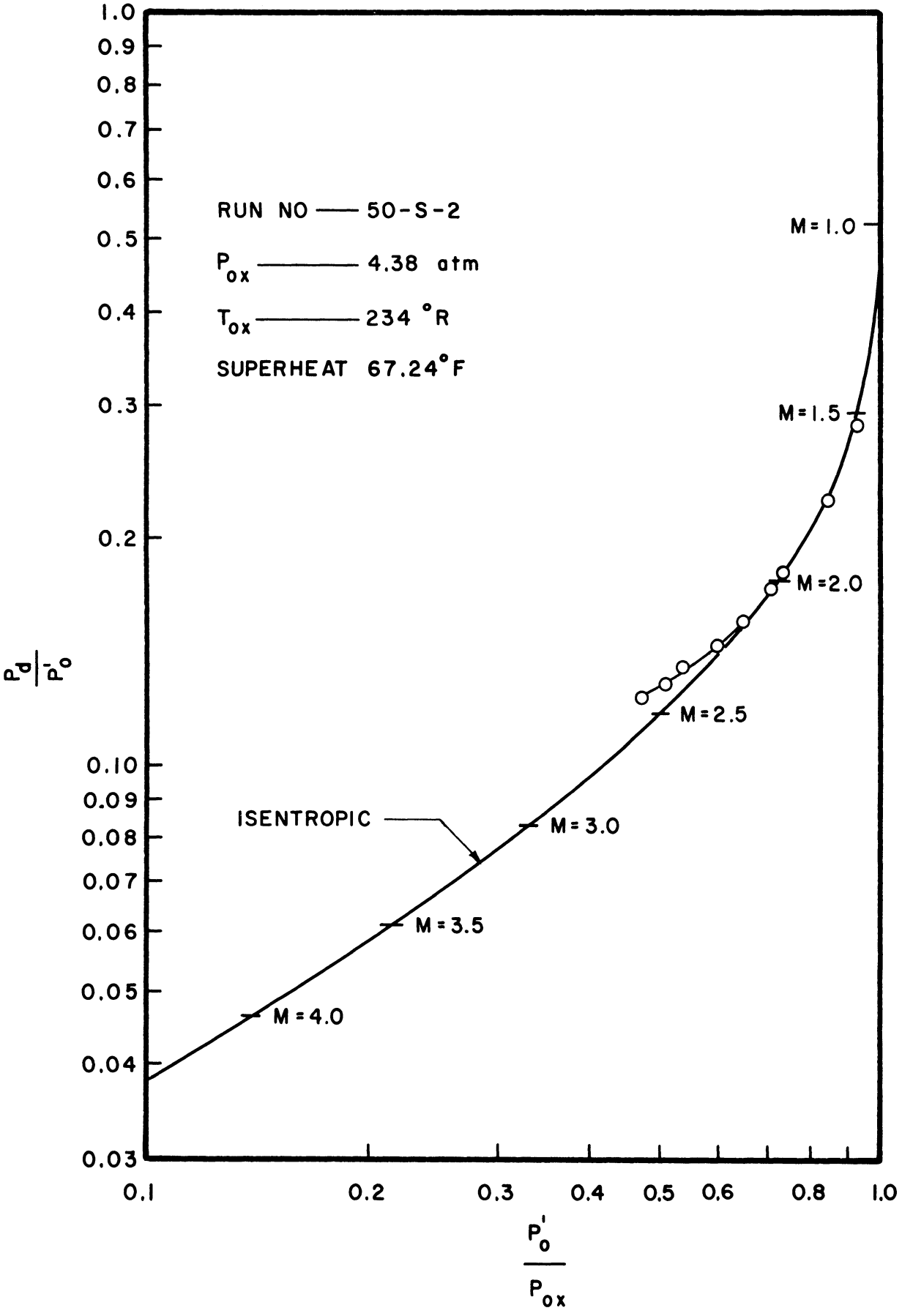

Figure 3-2. Comparison of Actual Expansion with Isentropic p_o'/p_{ox} vs. p_d/p_o' .

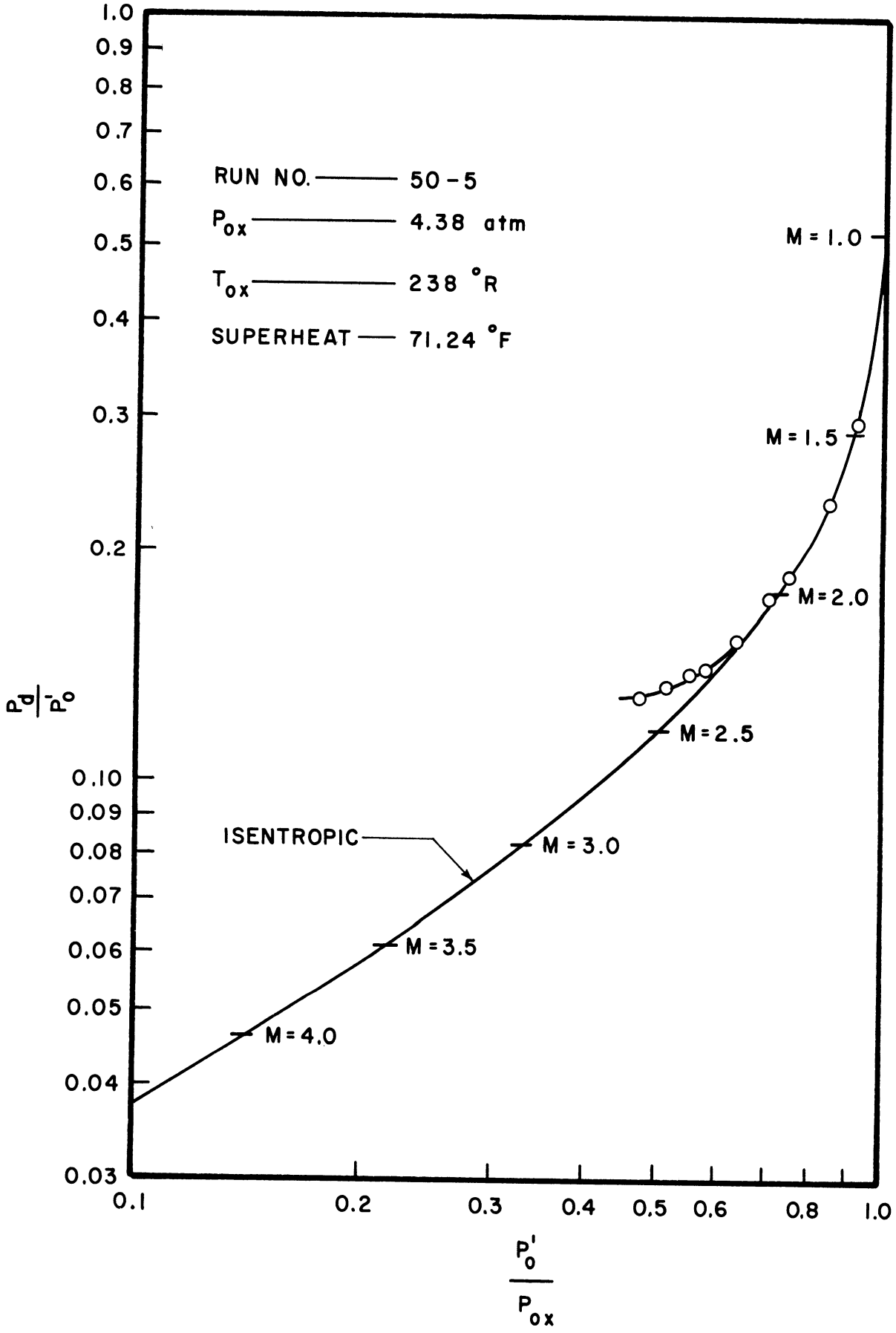

Figure 3-3. Comparison of Actual Expansion with Isentropic p_o'/p_{ox} vs. p_d/p_o' .

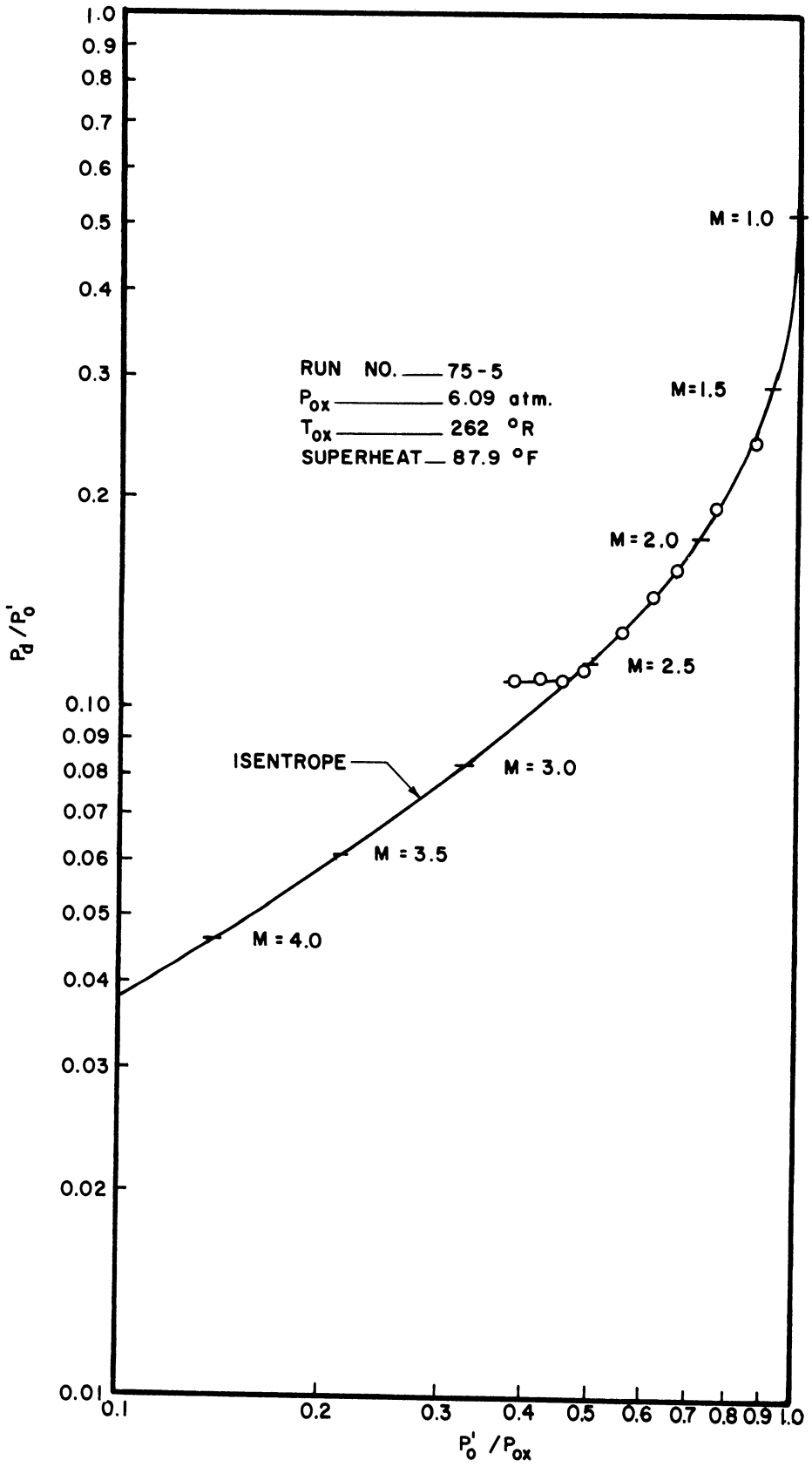

Figure 3-4. Comparison of Actual Expansion with Isentropic p_o'/p_{ox} vs. p_d/p_o' .

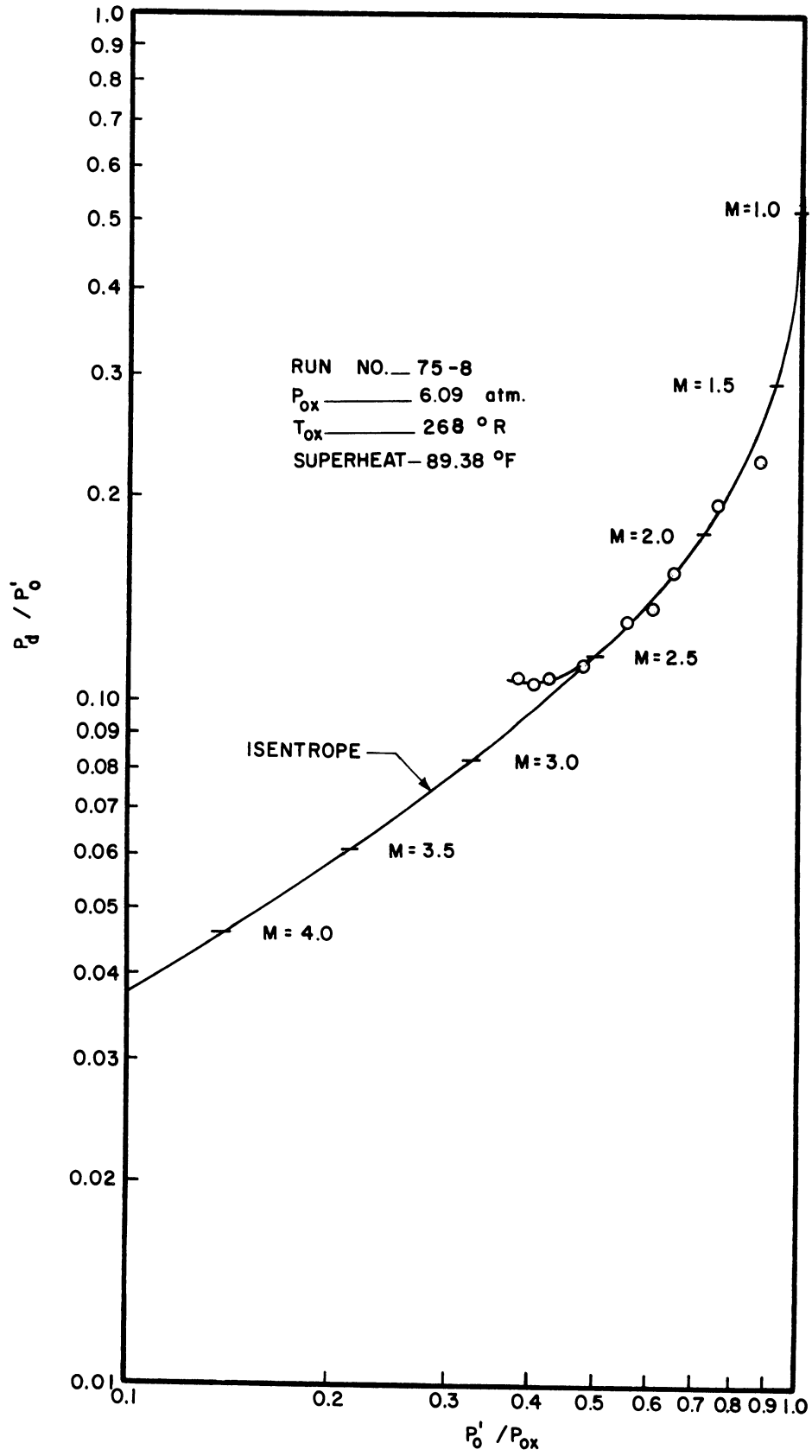

Figure 3-5. Comparison of Actual Expansion with Isentropic p_o'/p_{ox} vs. p_d/p_o' .

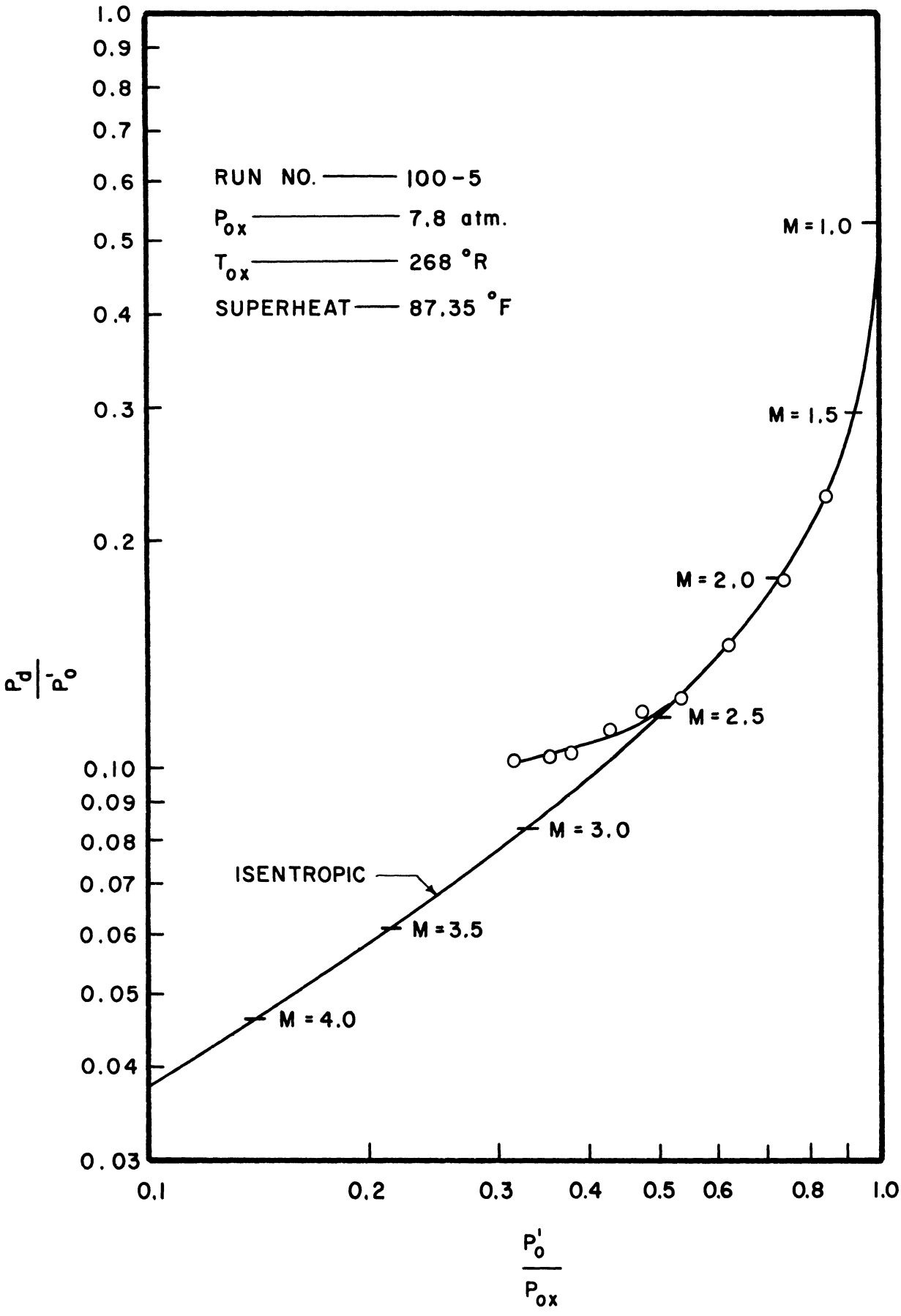

Figure 3-6. Comparison of Actual Expansion with Isentropic p_o'/p_{ox} vs. p_d/p_o' .

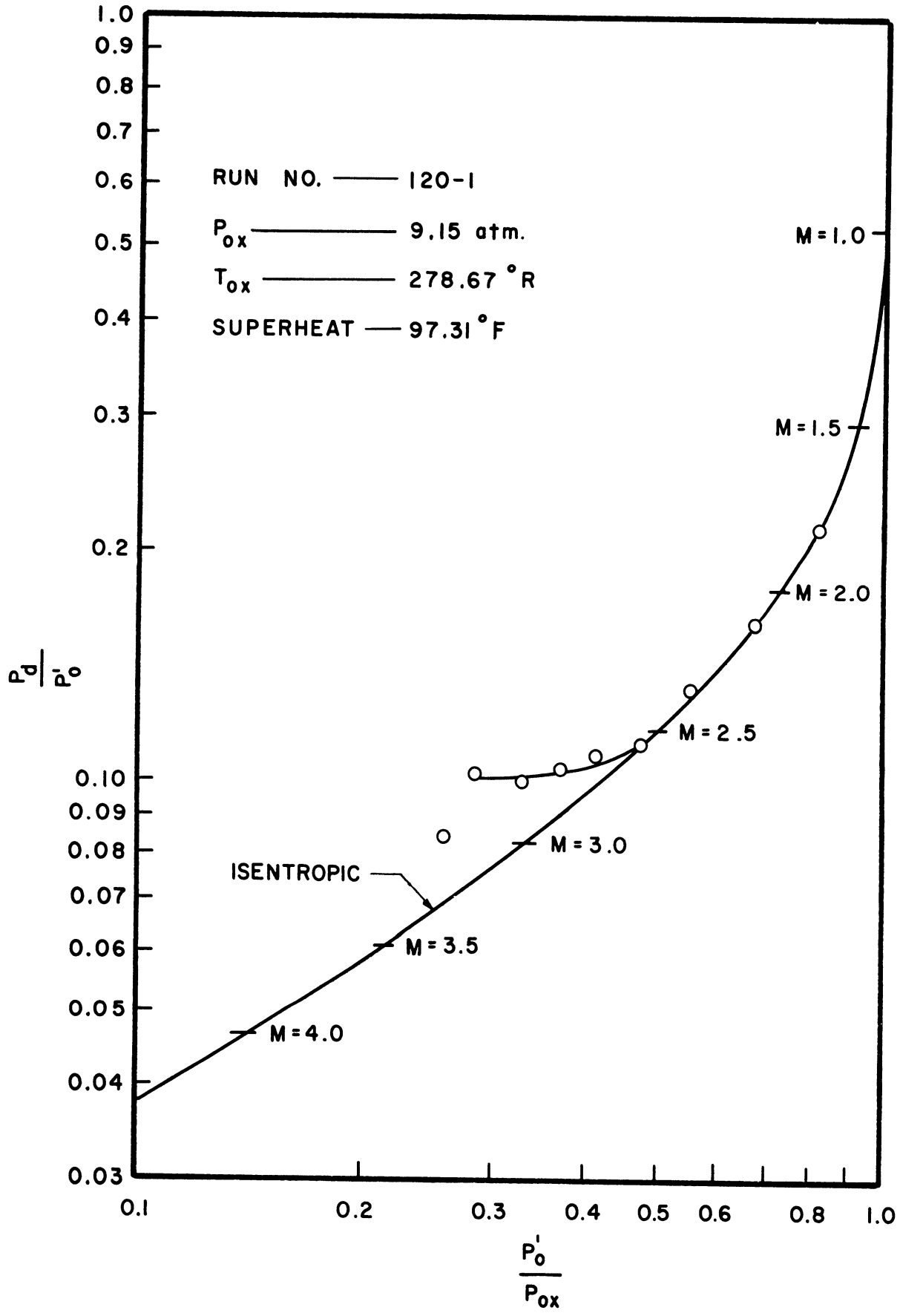

Figure 3-7. Comparison of Actual Expansion with Isentropic p_o'/p_{ox} vs. p_d/p_o' .

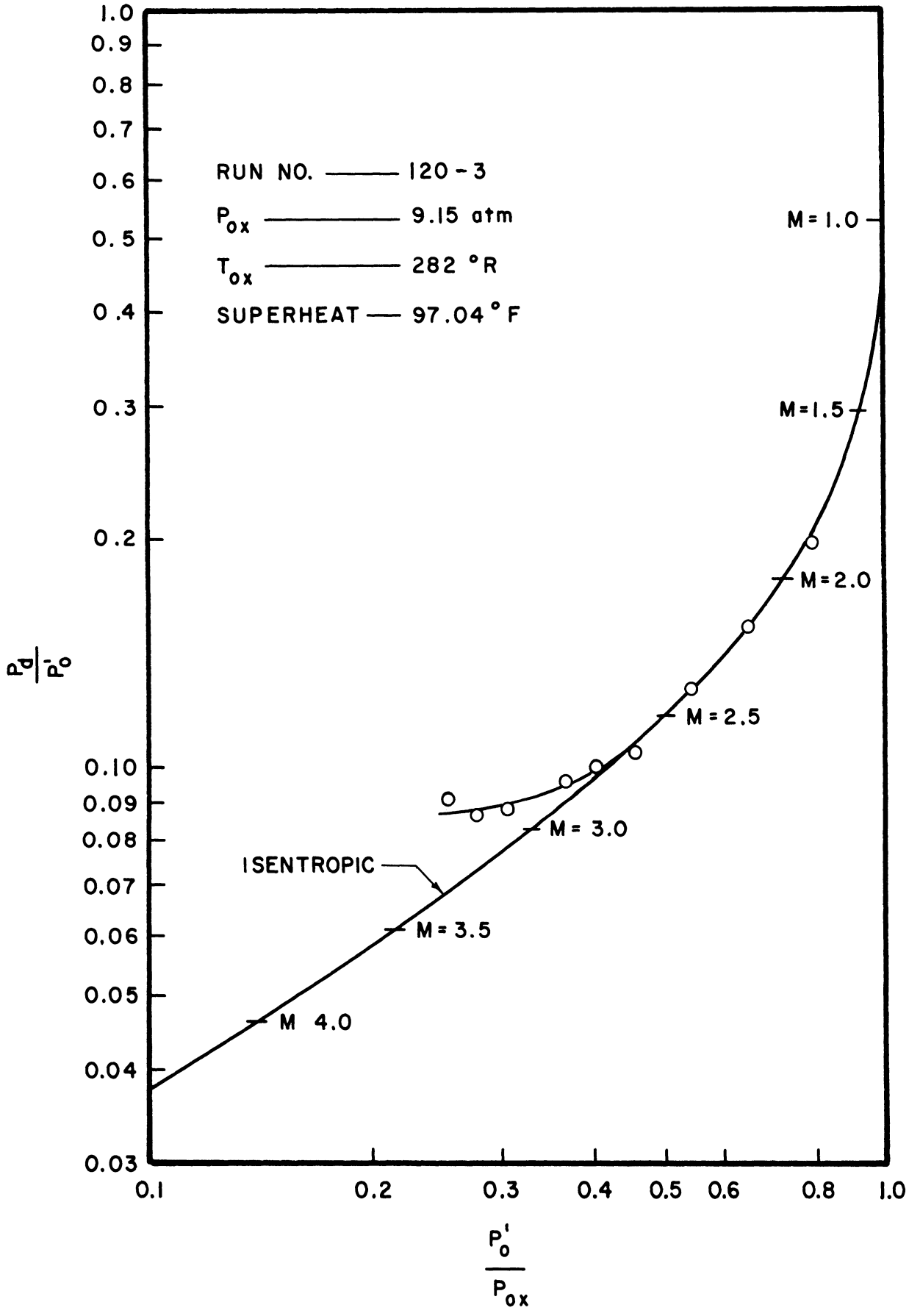

Figure 3-8. Comparison of Actual Expansion with Isentropic p_o'/p_{ox} vs. p_d/p_o' .

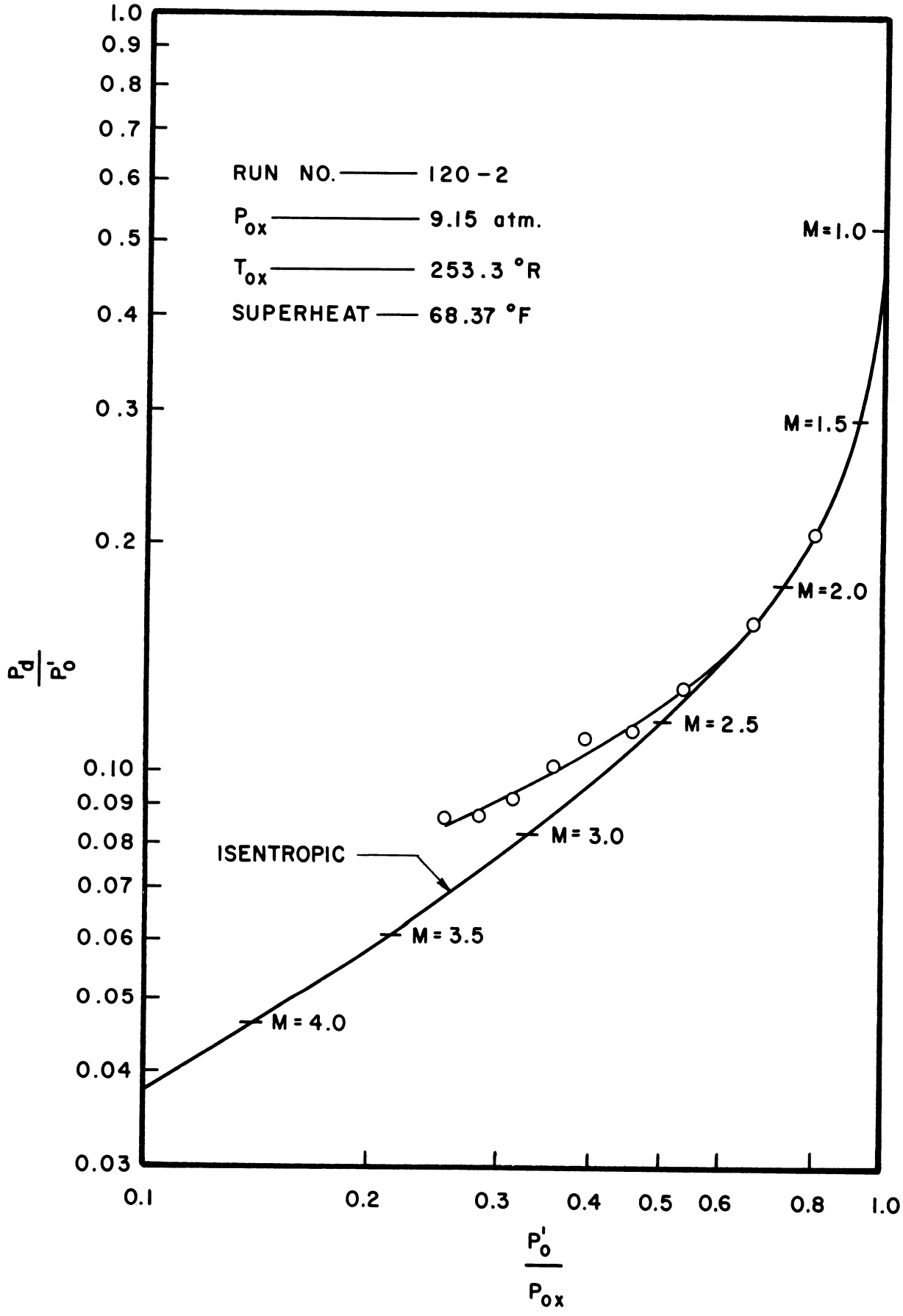

Figure 3-9. Comparison of Actual Expansion with Isentropic p_o'/p_{ox} vs. p_d/p_o' .

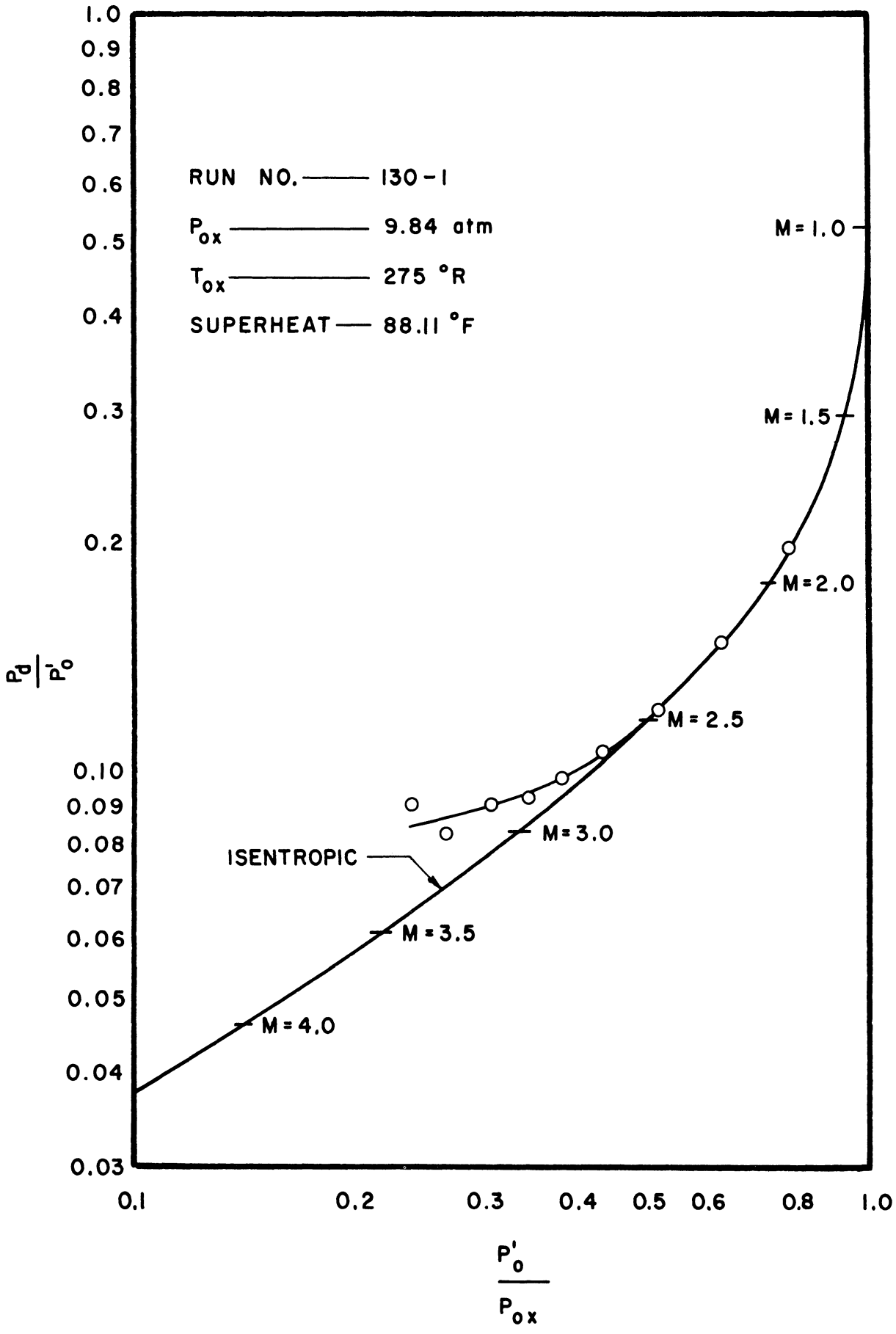

Figure 3-10. Comparison of Actual Expansion with Isentropic p'_o/p_{ox} vs. p_d/p'_o .

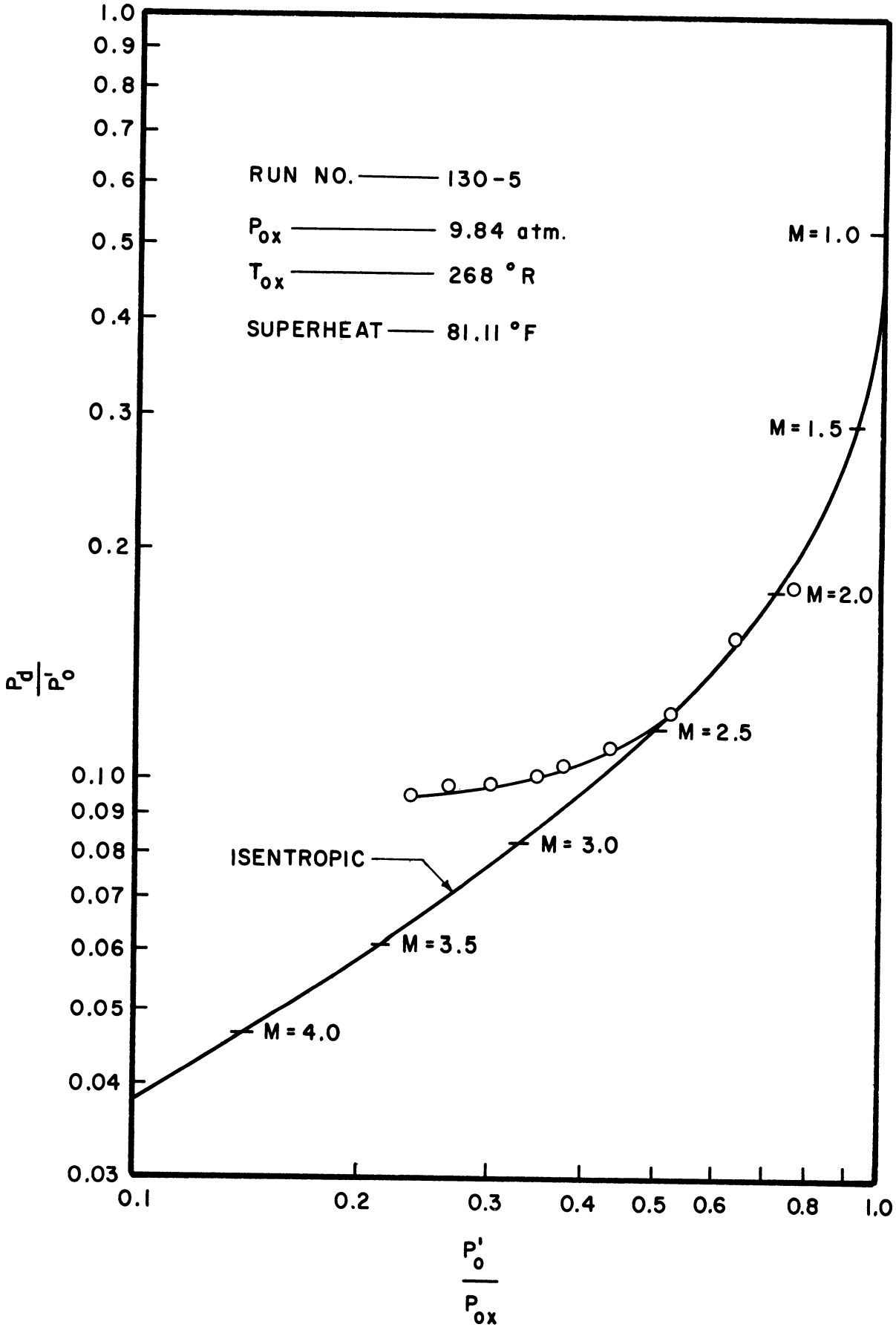

Figure 3-11. Comparison of Actual Expansion with Isentropic p_o'/p_{ox} vos. p_d/p_o' .

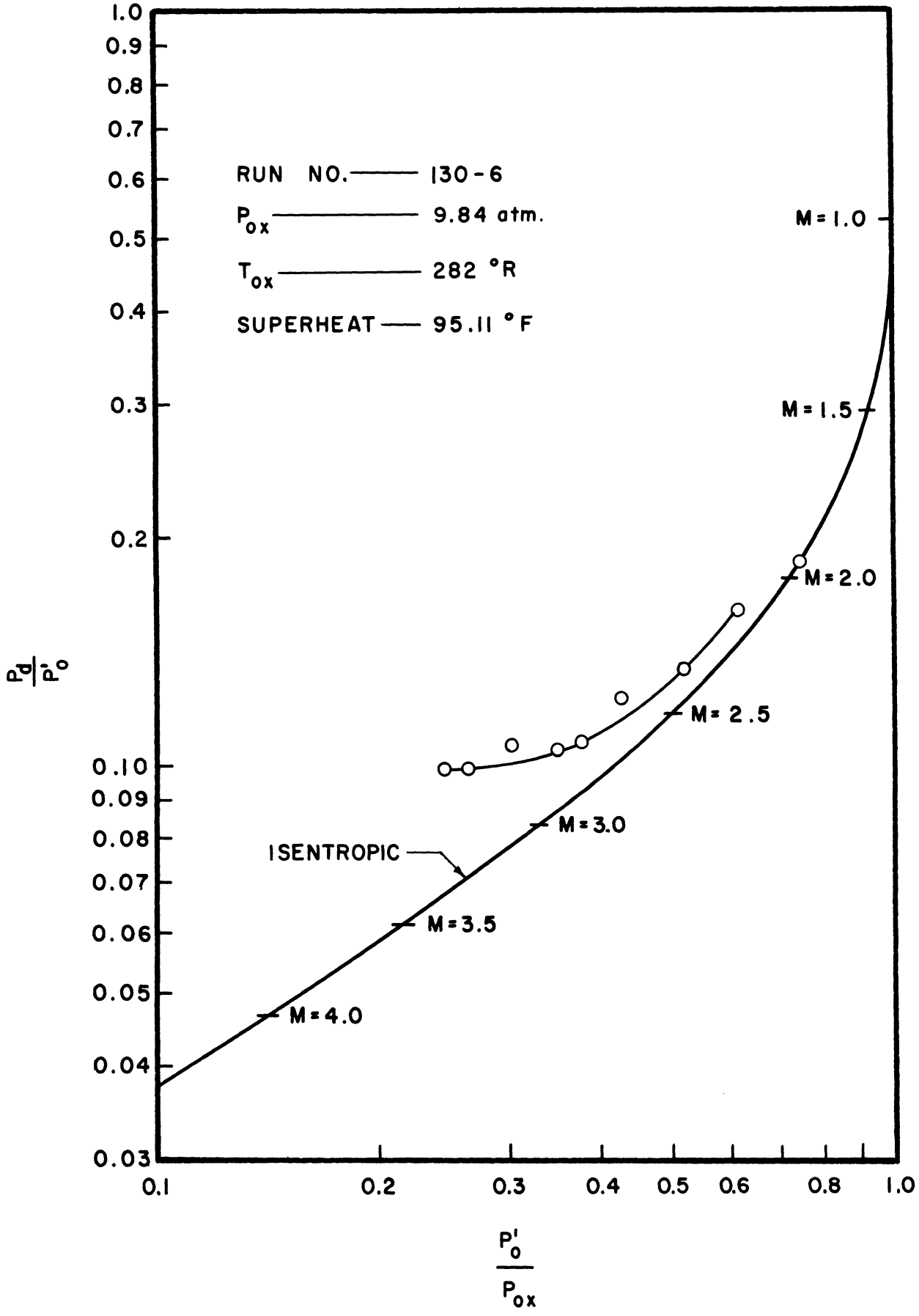

Figure 3-12. Comparison of Actual Expansion with Isentropic p'_o/p_{ox} vs. p_d/p'_o .

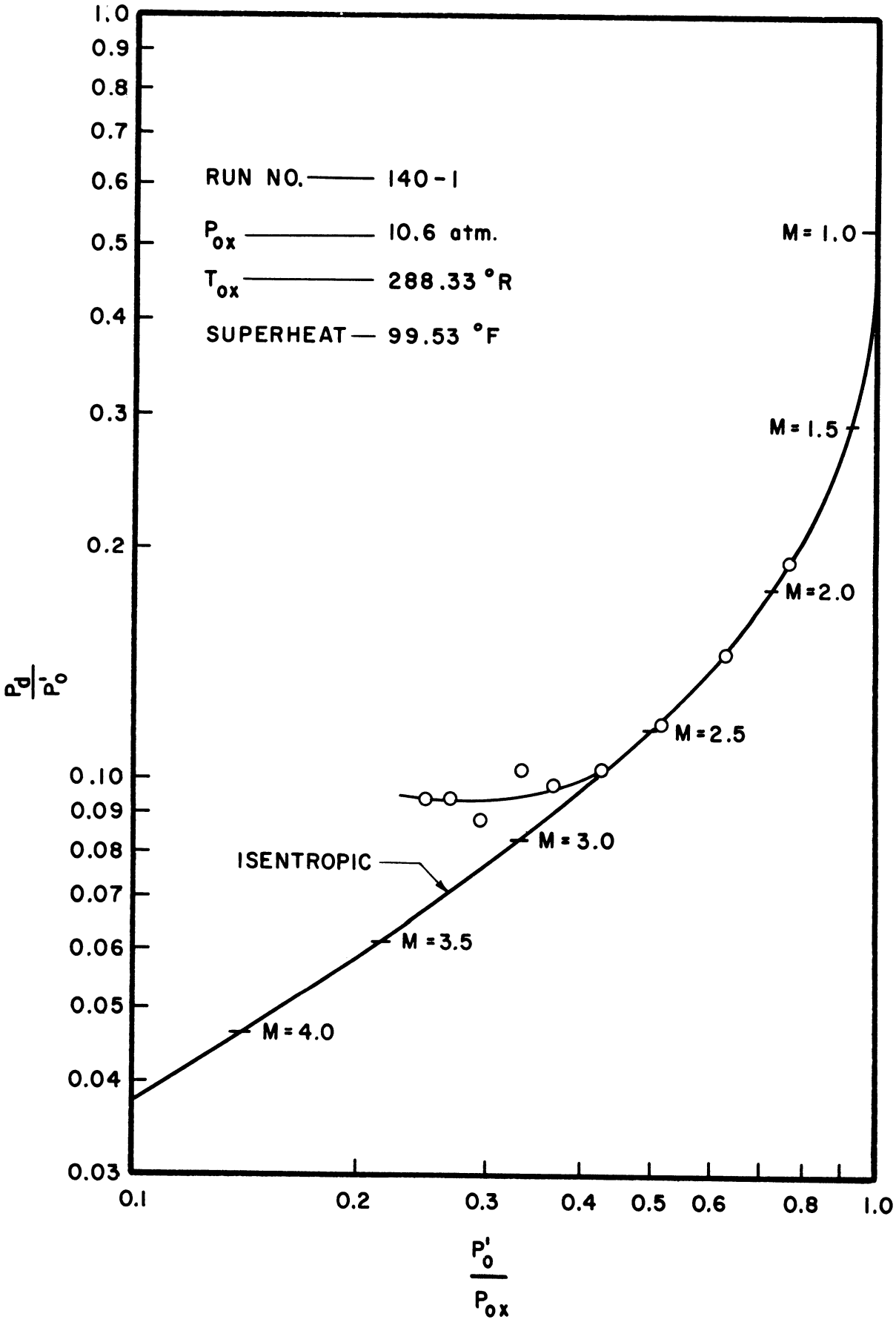

Figure 3-13. Comparison of Actual Expansion with Isentropic p_o'/p_{ox} vs. p_d/p_o' .

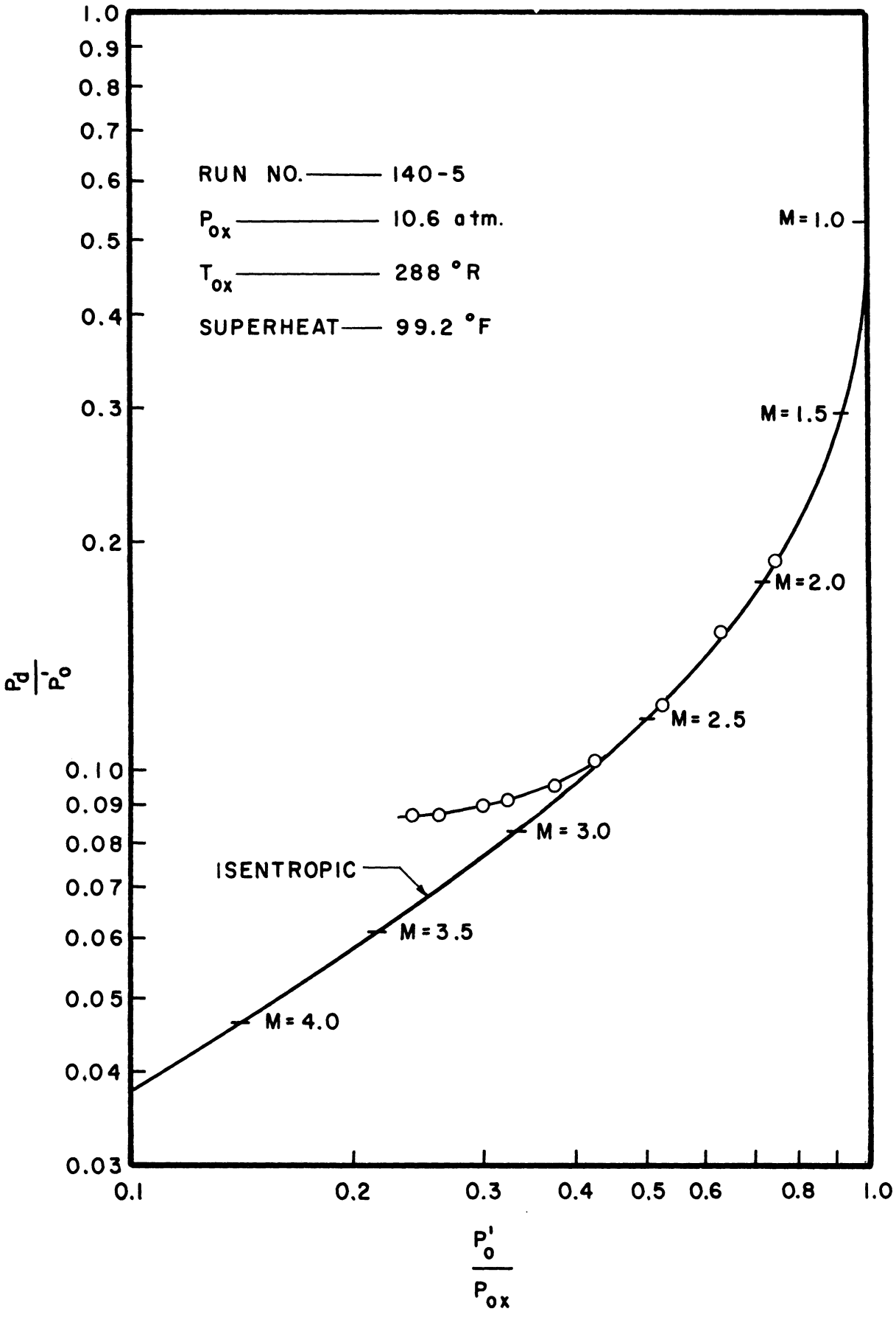

Figure 3-14. Comparison of Actual Expansion with Isentropic p_o'/p_{ox} vs. p_d/p_o' .

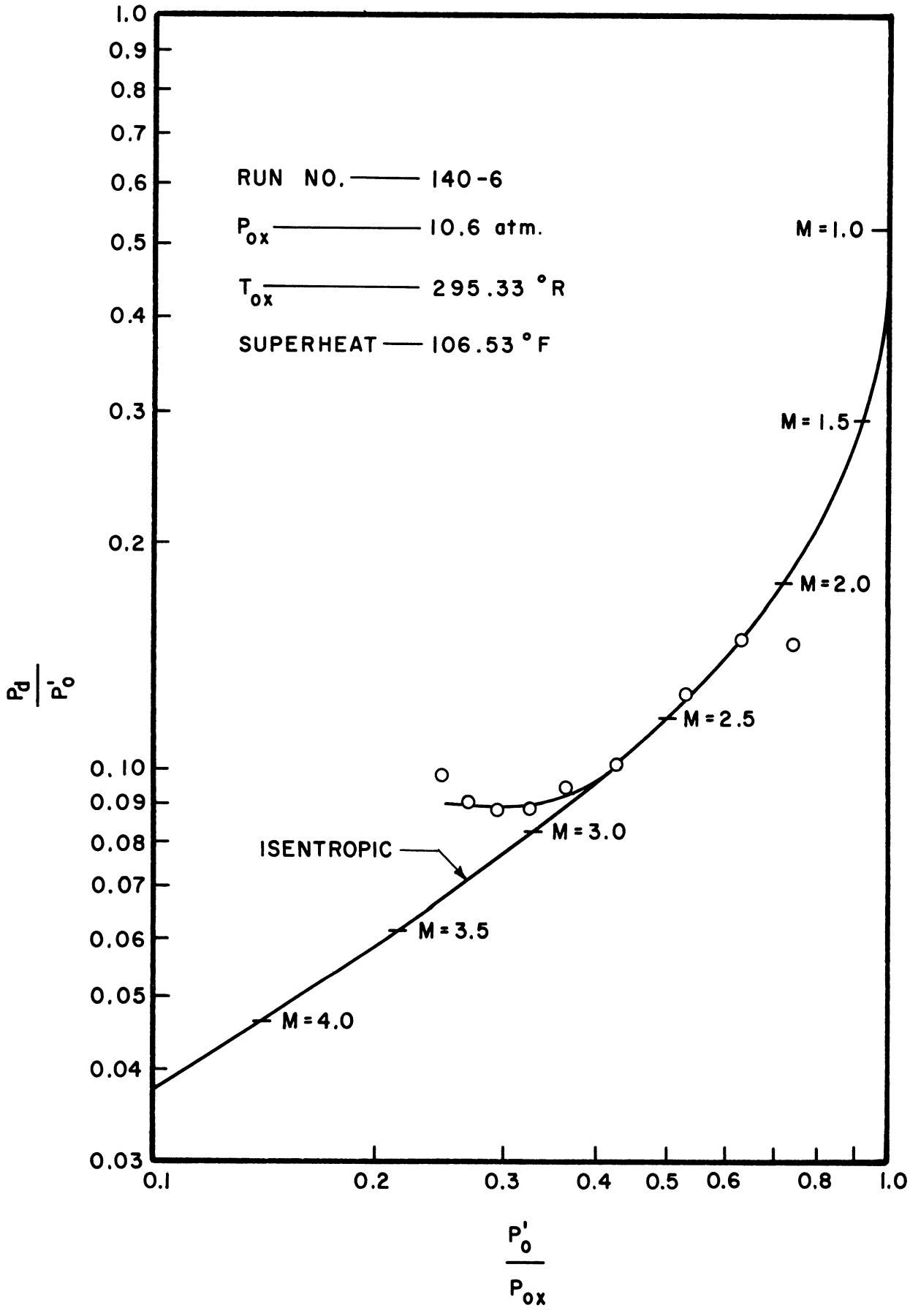

Figure 3-15. Comparison of Actual Expansion with Isentropic p'_o/p_{ox} vs. p_d/p'_o .

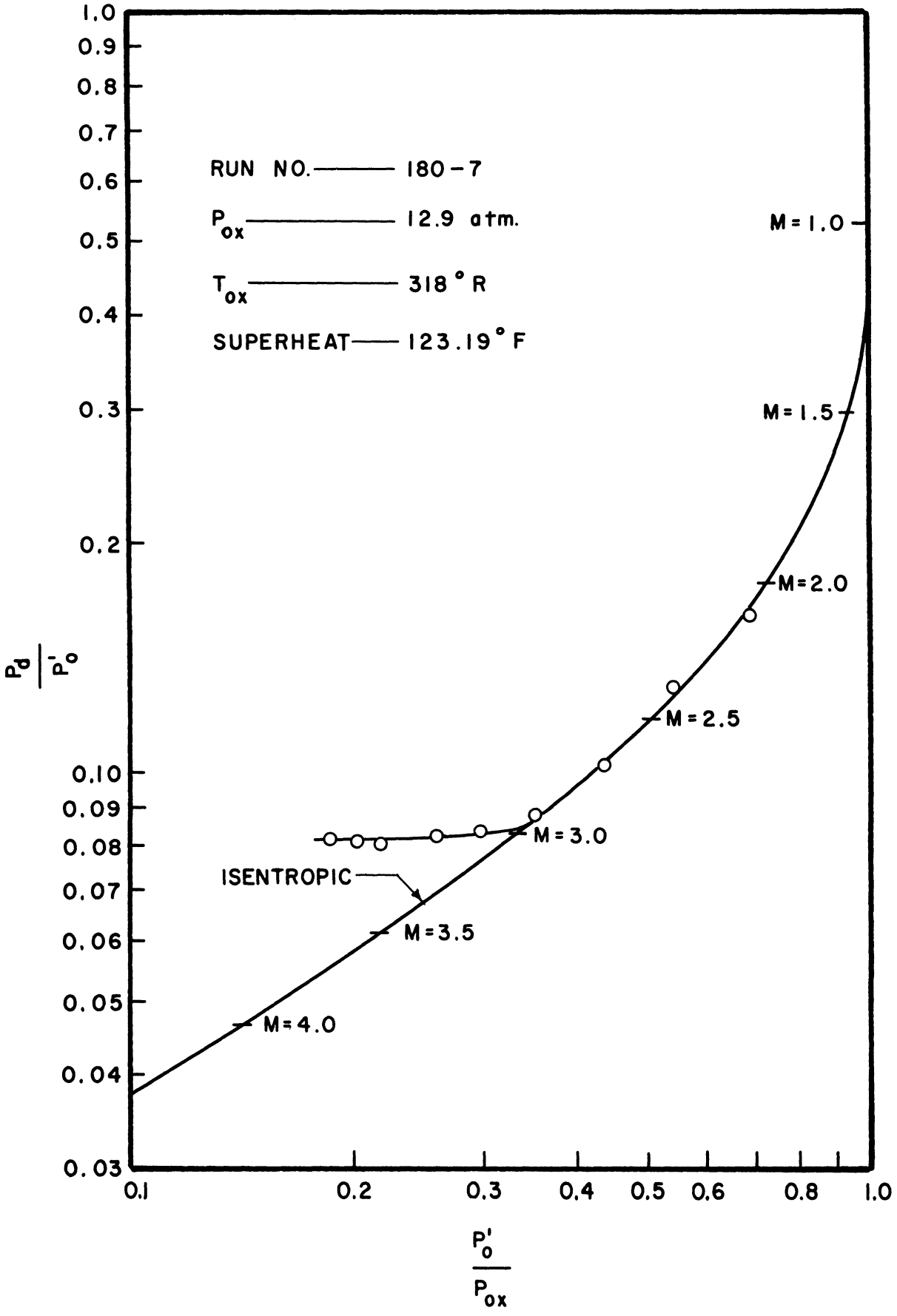

Figure 3-16. Comparison of Actual Expansion with Isentropic p'_o/p_{ox} vs. p_d/p'_o .

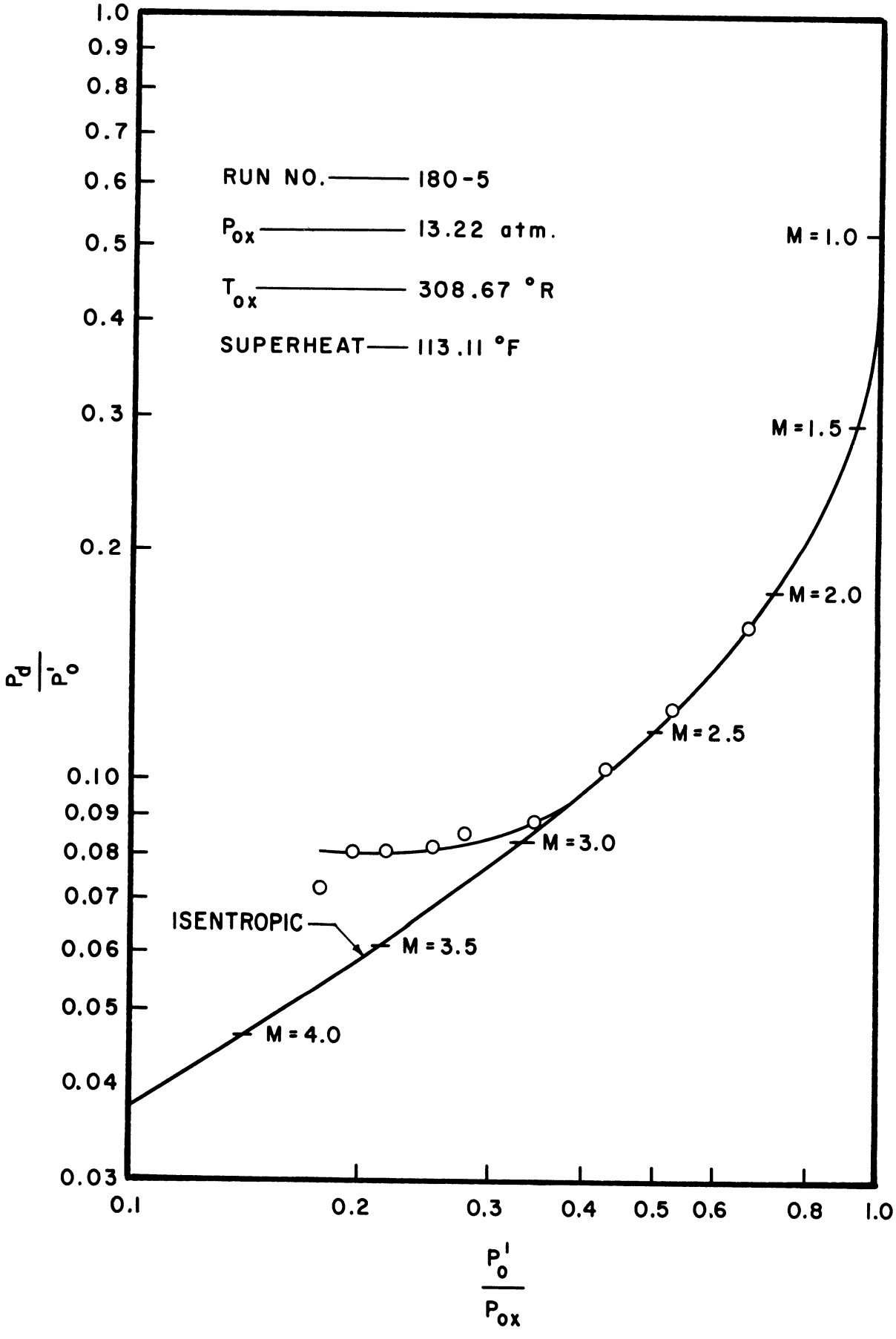

Figure 3-17. Comparison of Actual Expansion with Isentropic p_o'/p_{ox} vs. p_d/p_o' .

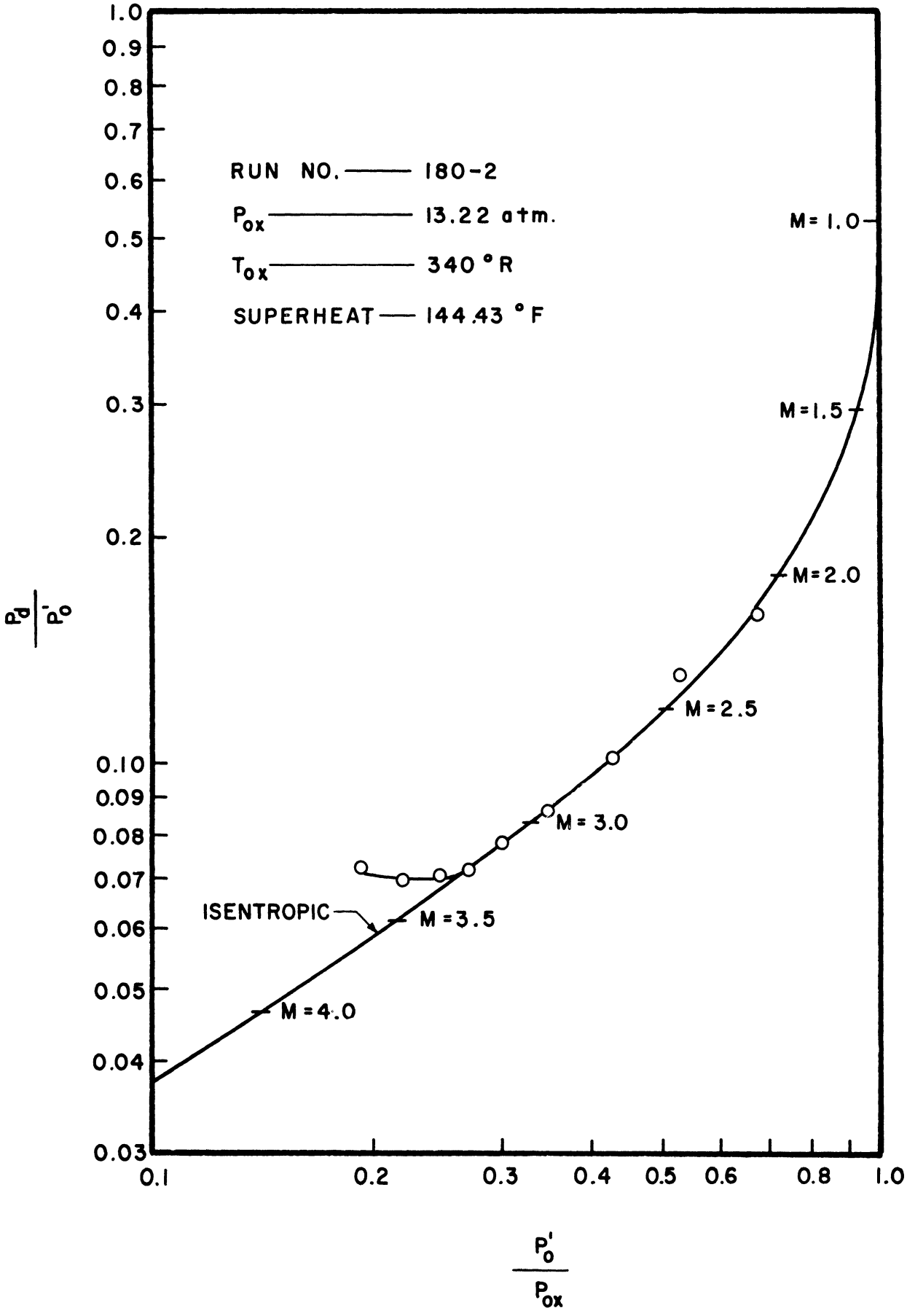

Figure 3-18. Comparison of Actual Expansion with Isentropic p_o'/p_{ox} vs. p_d/p_o' .

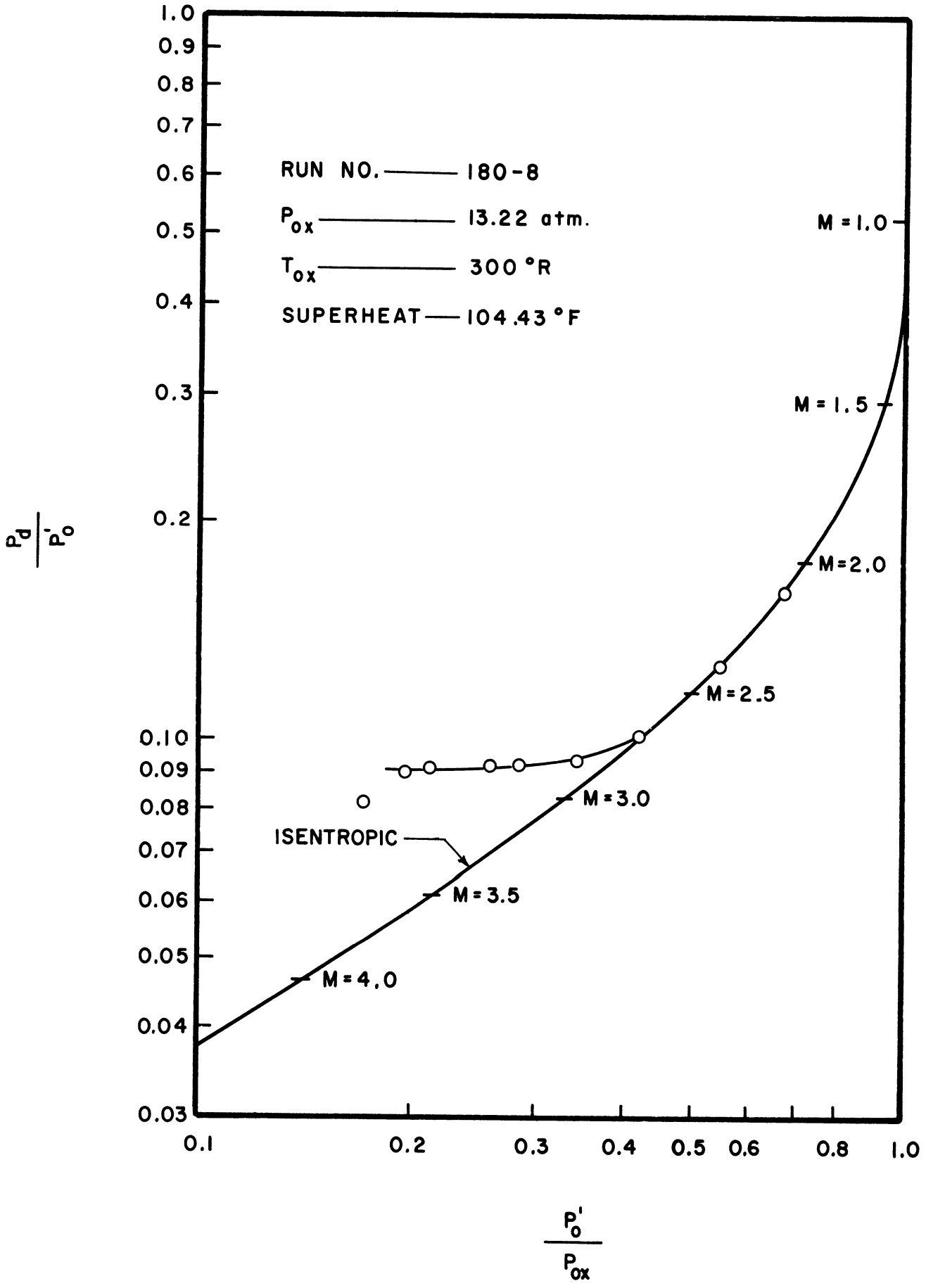

Figure 3-19. Comparison of Actual Expansion with Isentropic p_o'/p_{ox} vs. p_d/p_o' .

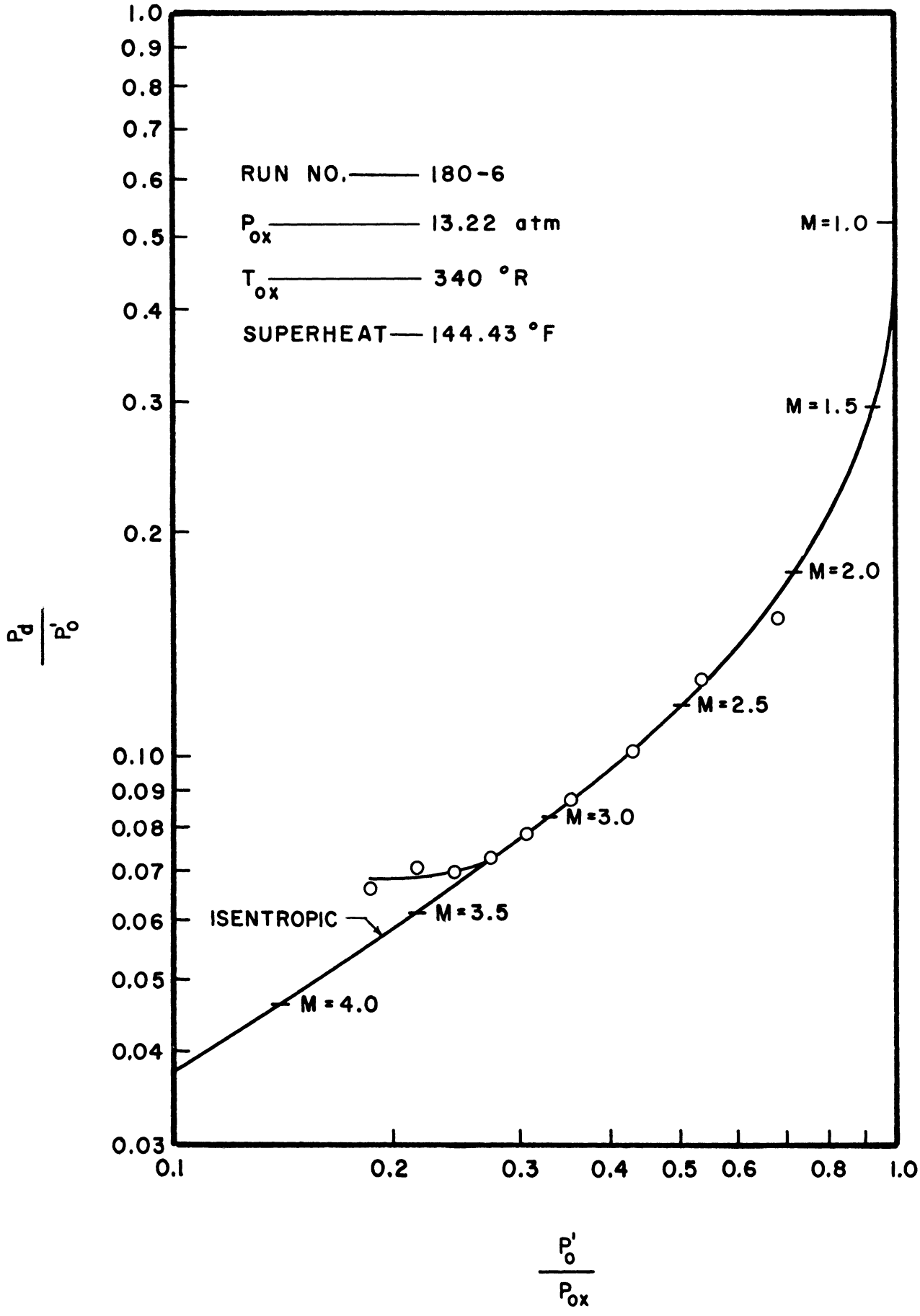

Figure 3-20. Comparison of Actual Expansion with Isentropic p_o'/p_{ox} vs. p_d/p_o' .

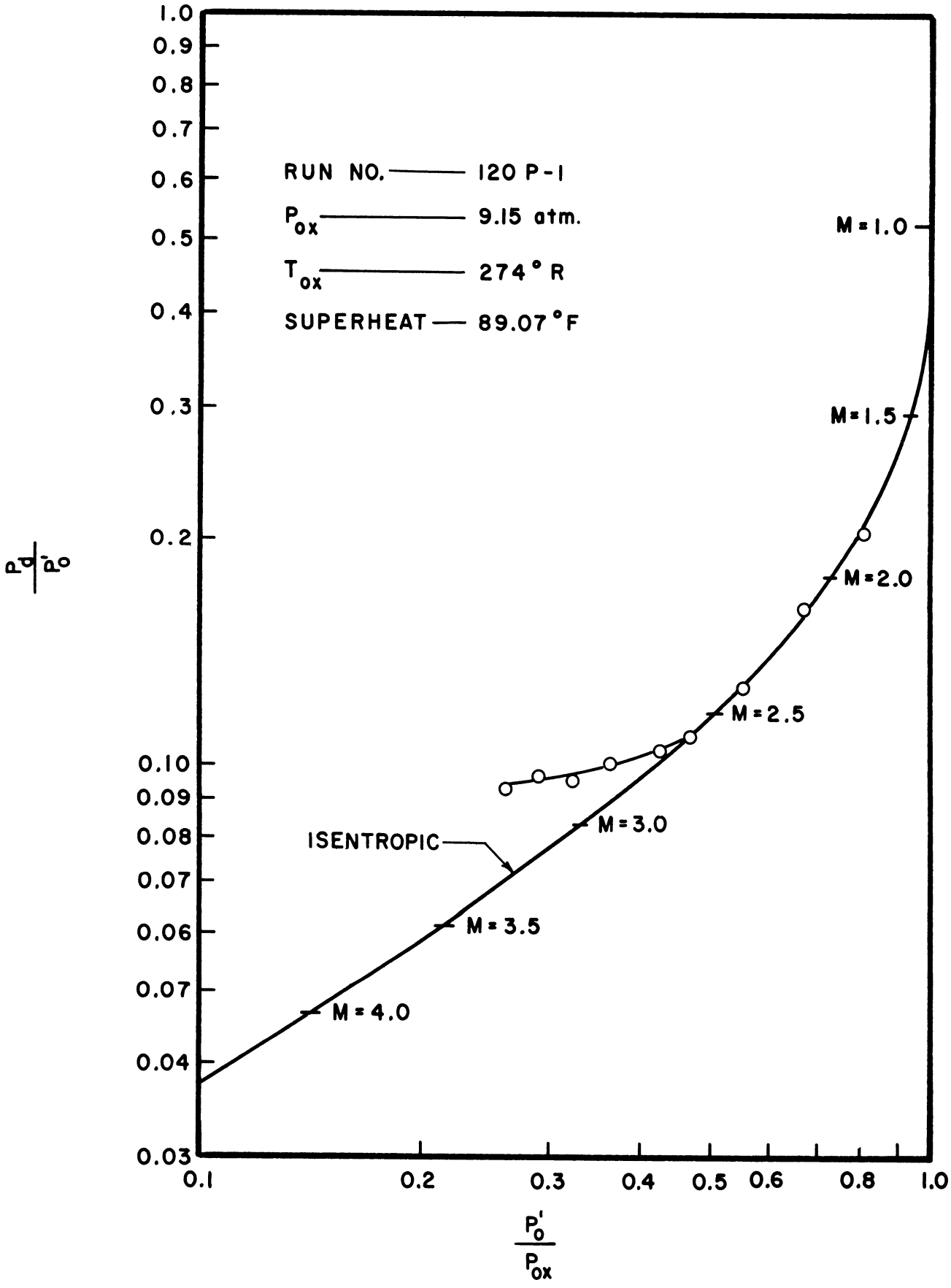

Figure 3-21. Comparison of Actual Expansion with Isentropic p_o'/p_{ox} vs. p_d/p_o' .

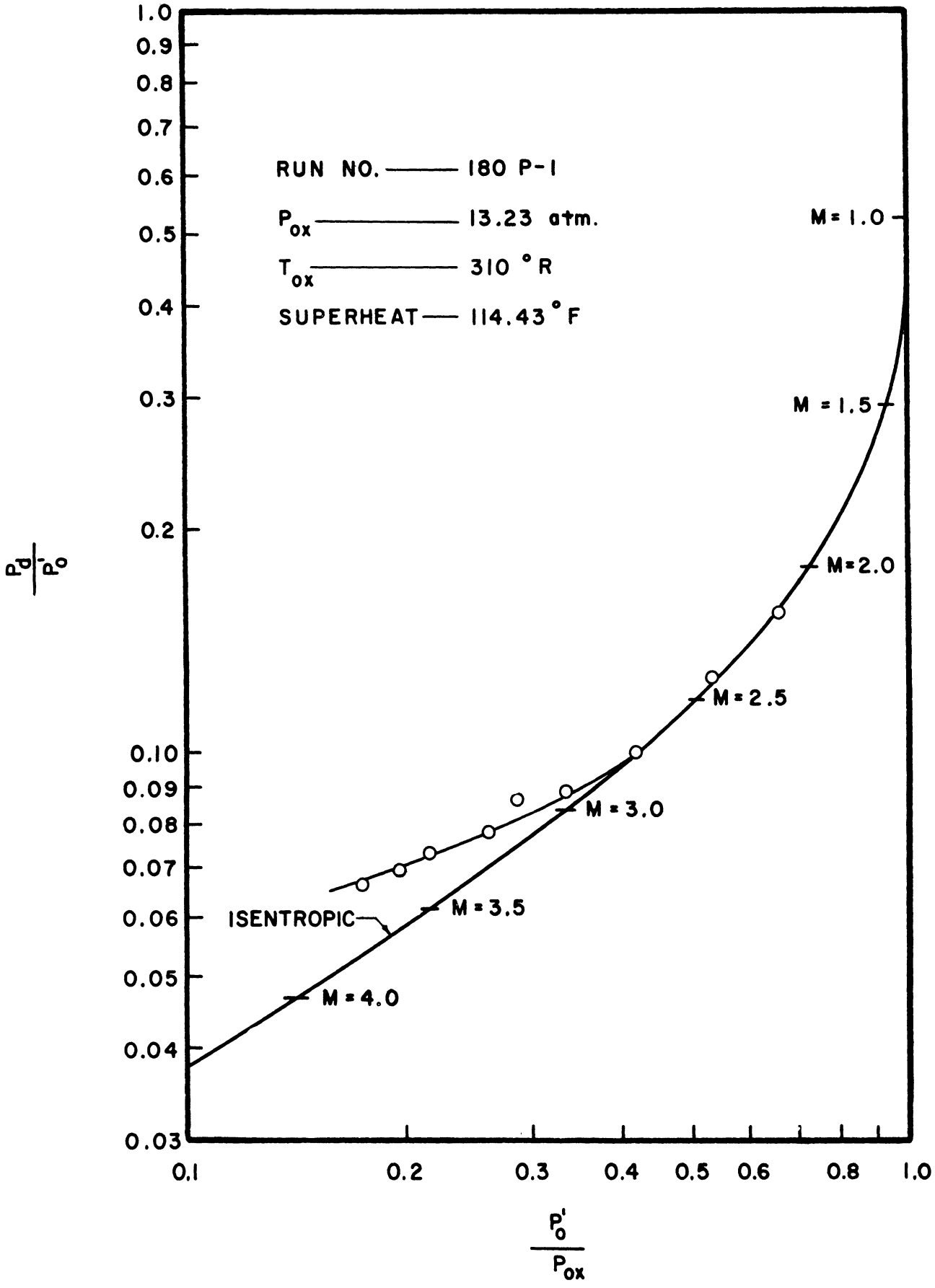

Figure 3-22. Comparison of Actual Expansion with Isentropic p_o'/p_{ox} vs. p_d/p_o' .

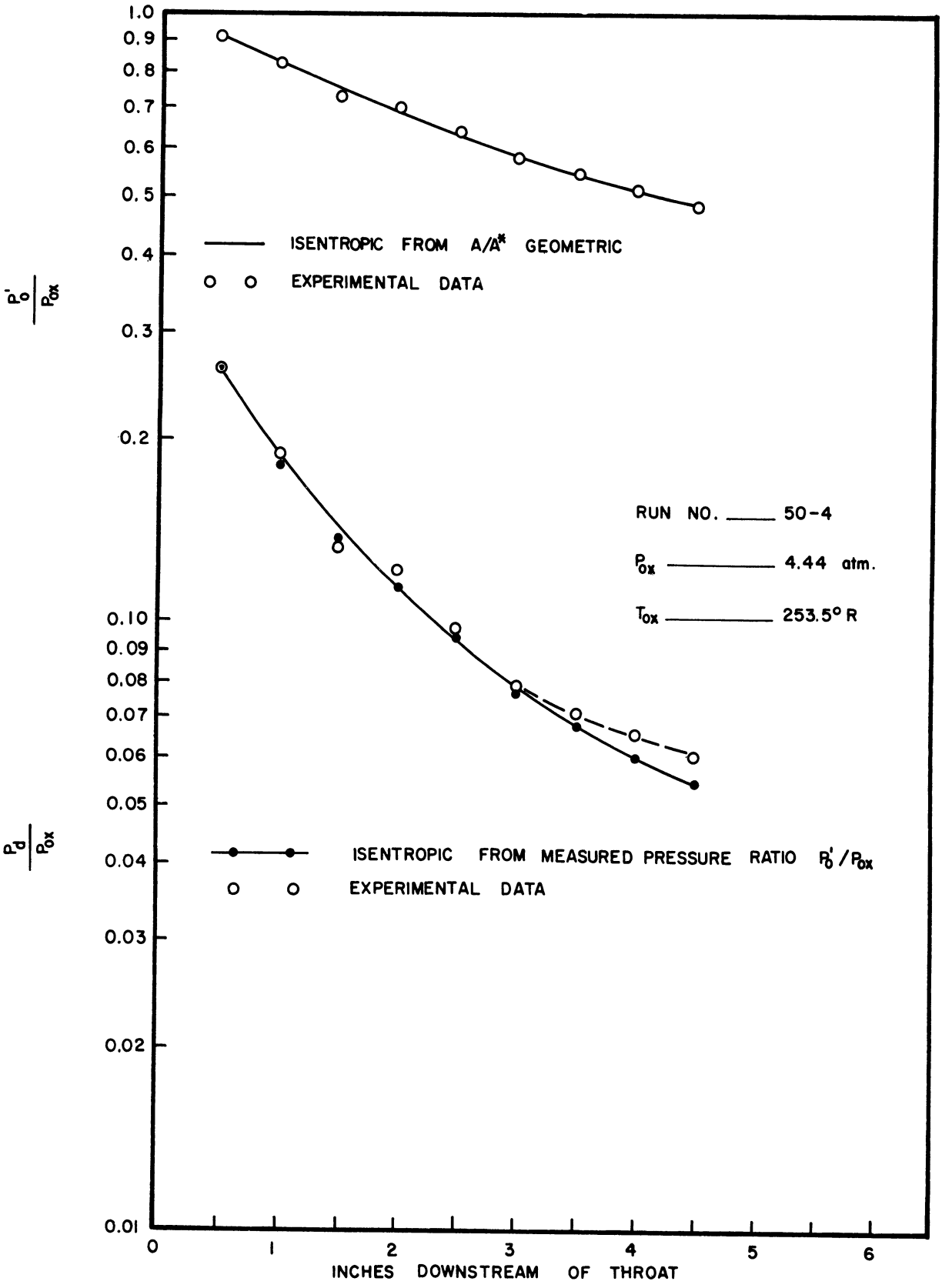

Figure 4-1. Comparison of Experimentally Measured Pressure Ratios Along Nozzle with Isentropic.

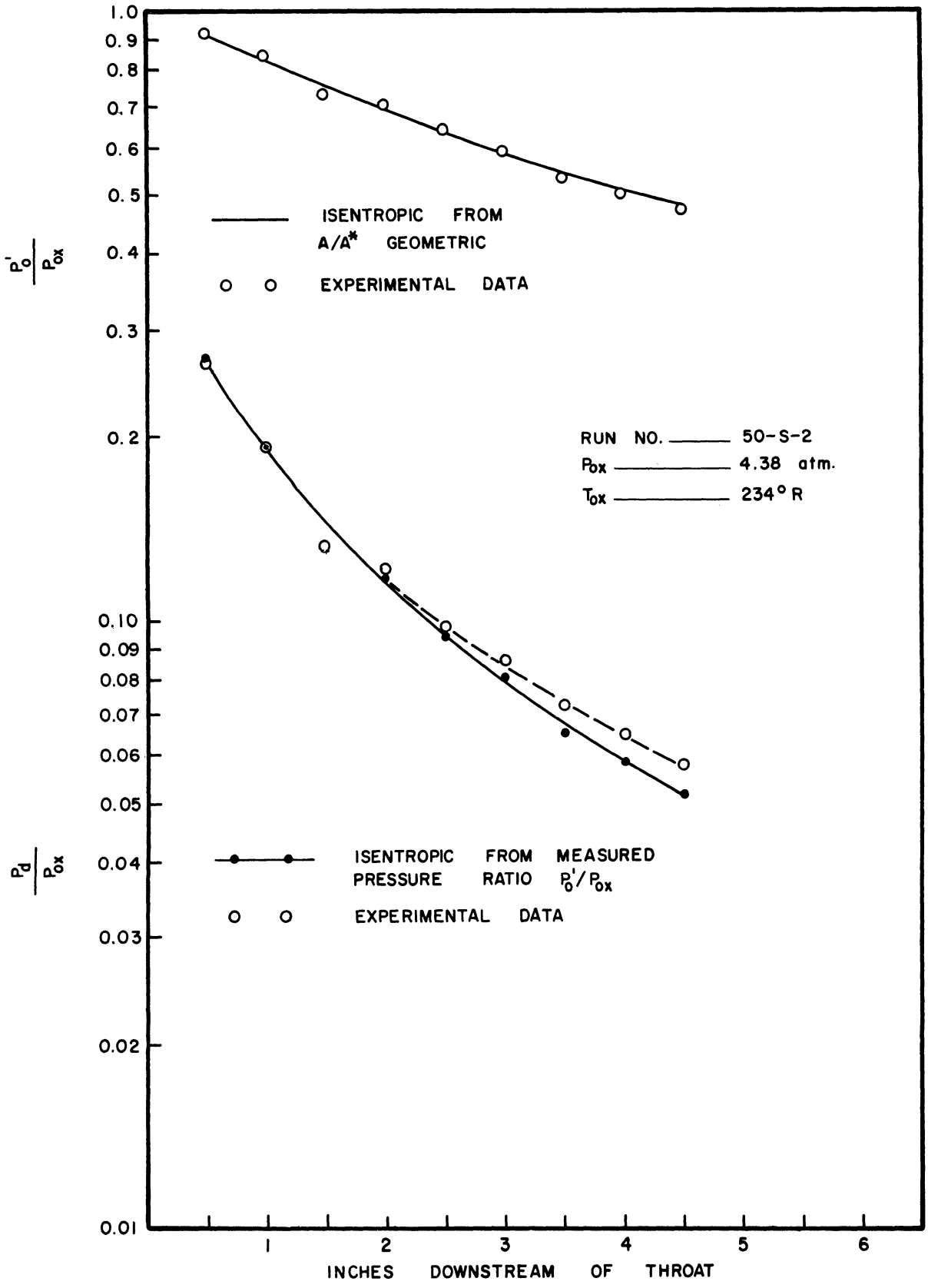

Figure 4-2. Comparison of Experimentally Measured Pressure Ratios Along Nozzle with Isentropic.

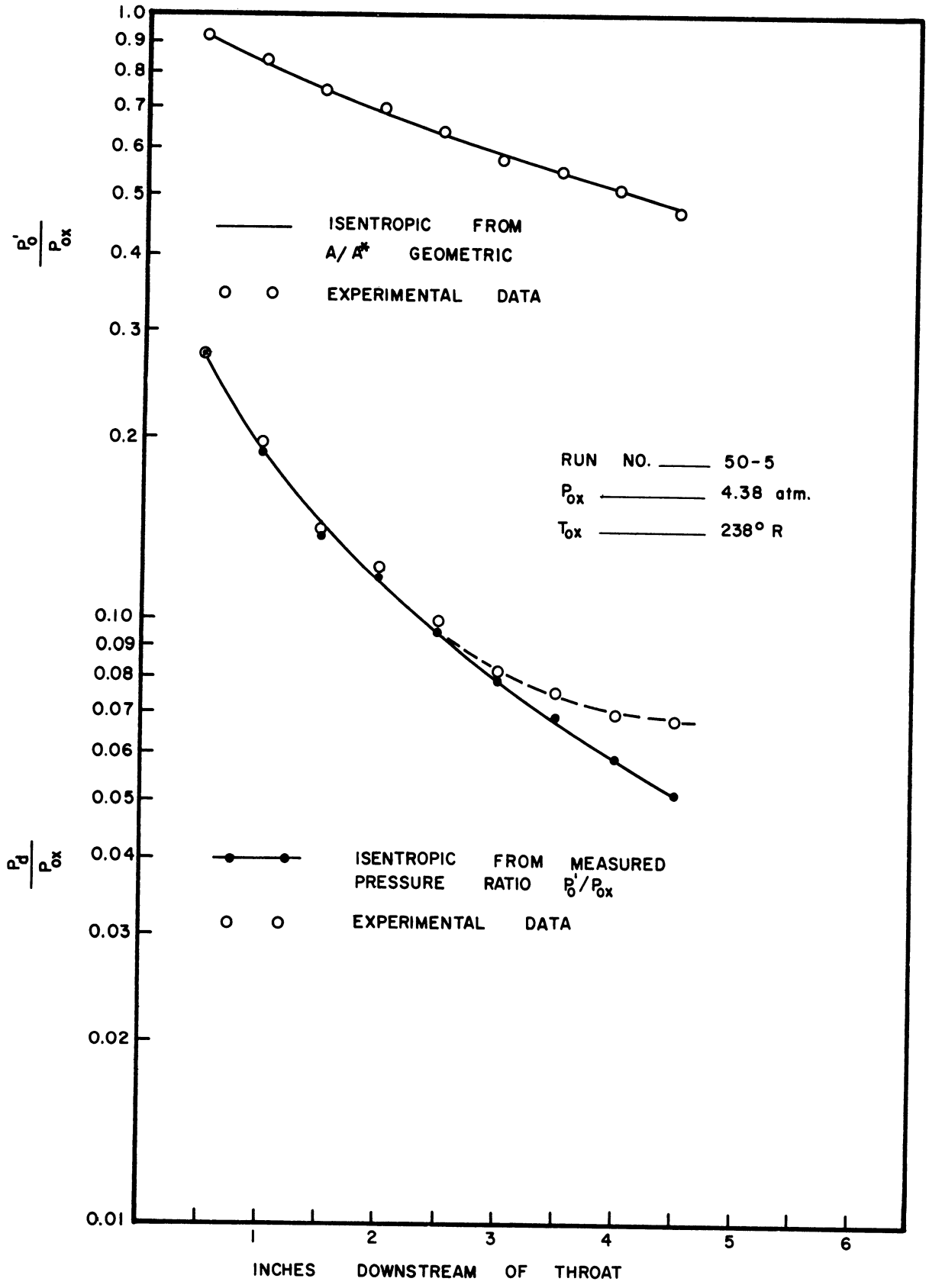

Figure 4-3. Comparison of Experimentally Measured Pressure Ratios Along Nozzle with Isentropic.

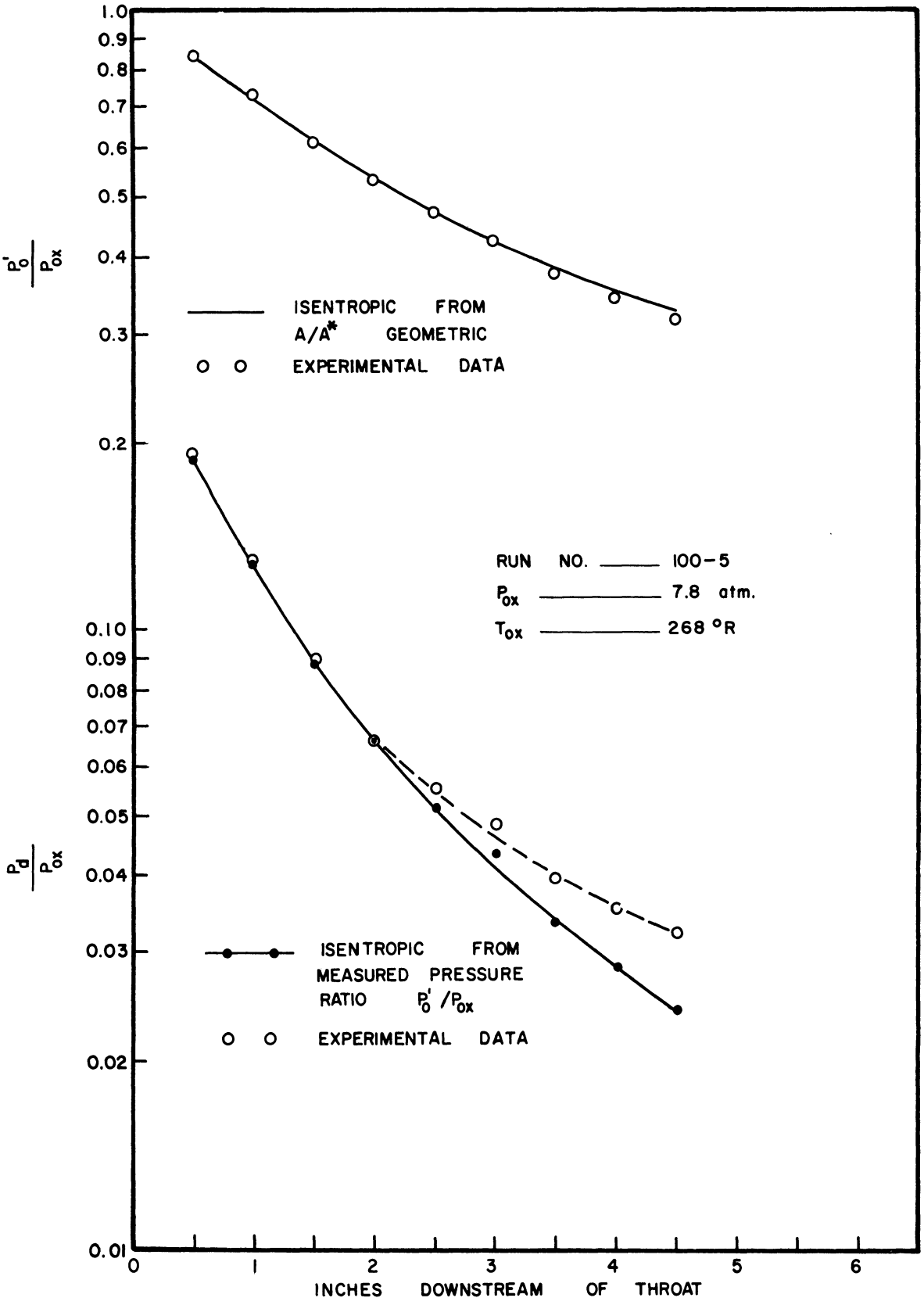

Figure 4-4. Comparison of Experimentally Measured Pressure Ratios Along Nozzle with Isentropic.

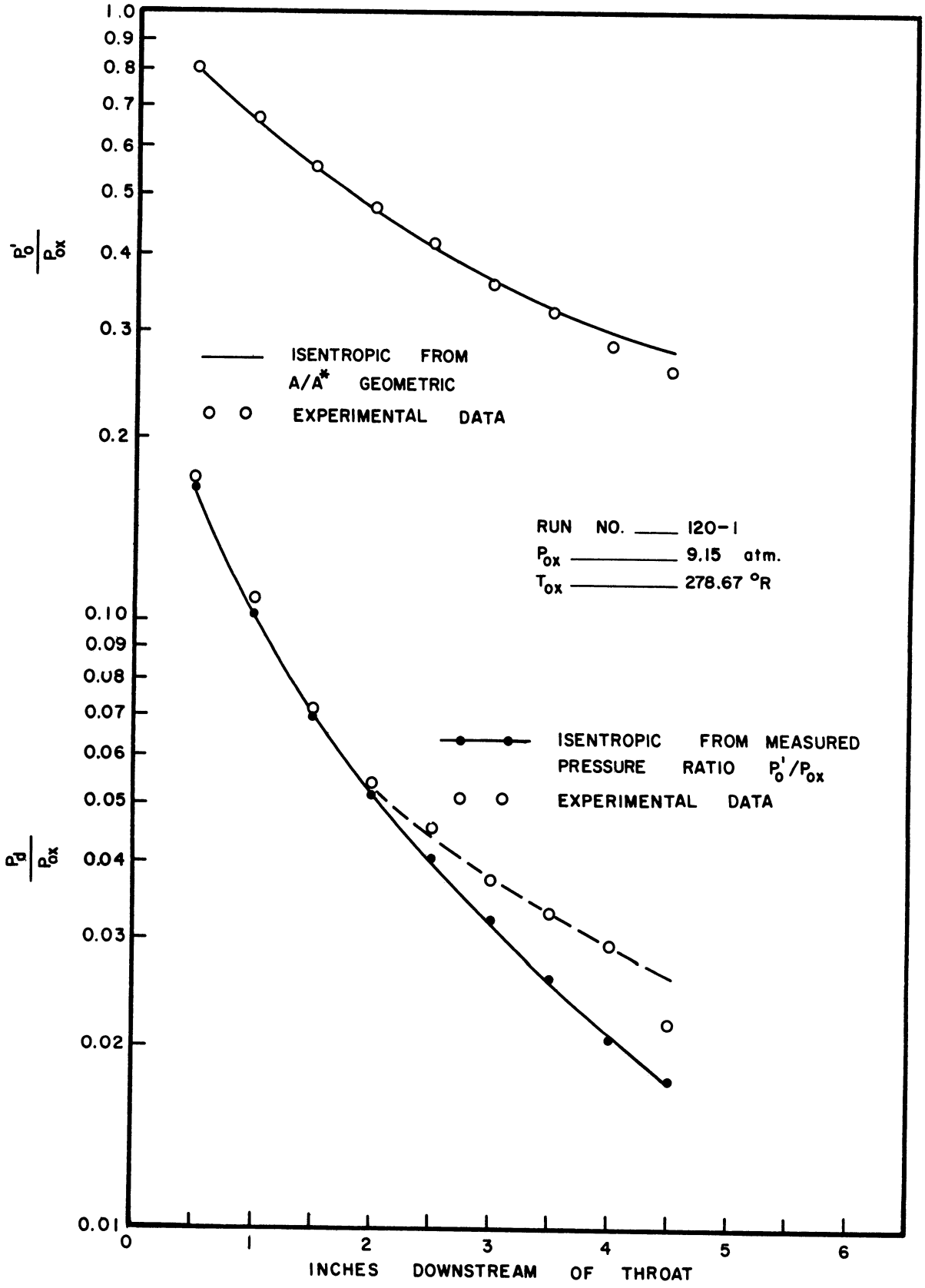

Figure 4-5. Comparison of Experimentally Measured Pressure Ratios Along Nozzle with Isentropic.

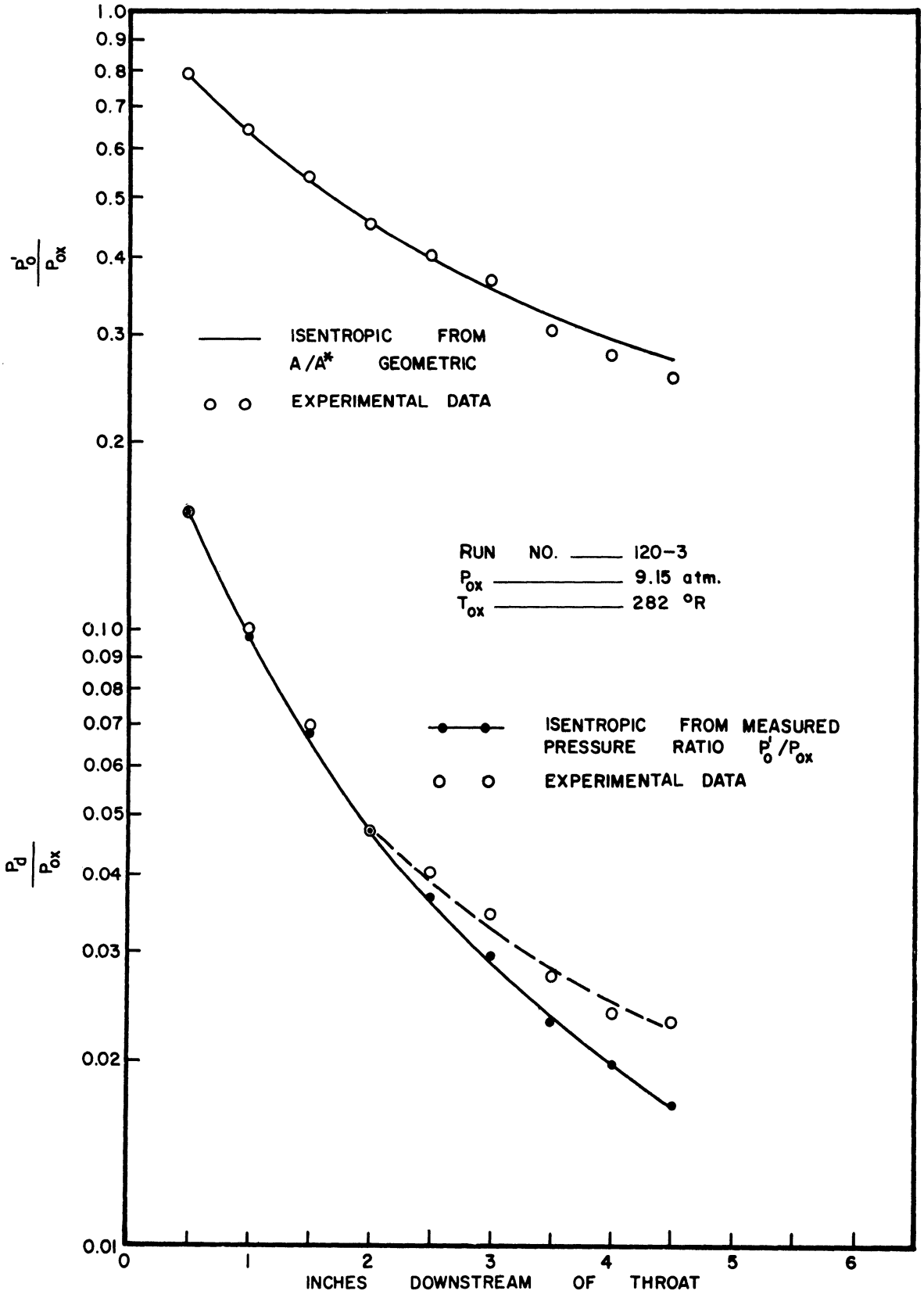

Figure 4-6. Comparison of Experimentally Measured Pressure Ratios Along Nozzle with Isentropic.

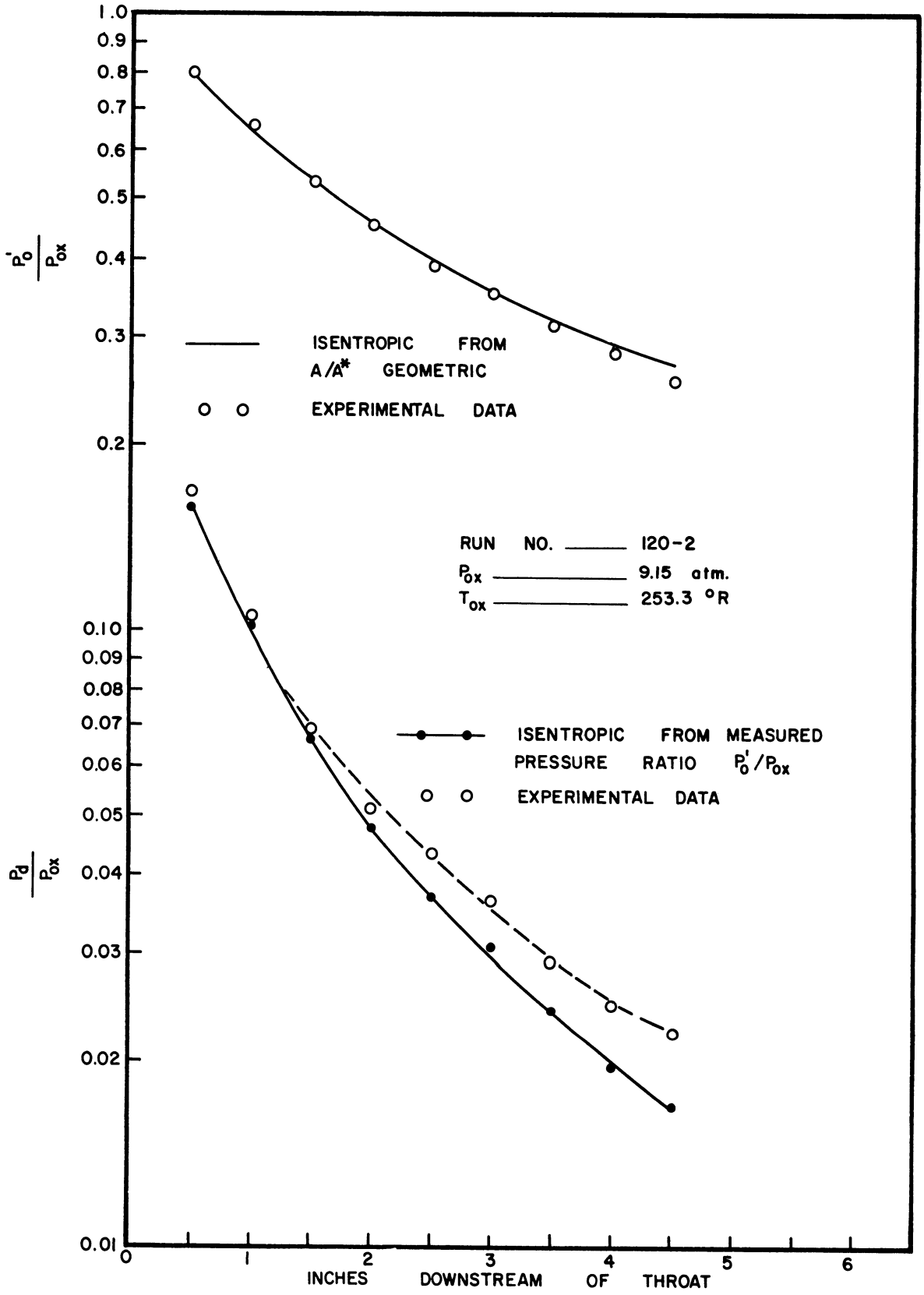

Figure 4-7. Comparison of Experimentally Measured Pressure Ratios Along Nozzle with Isentropic.

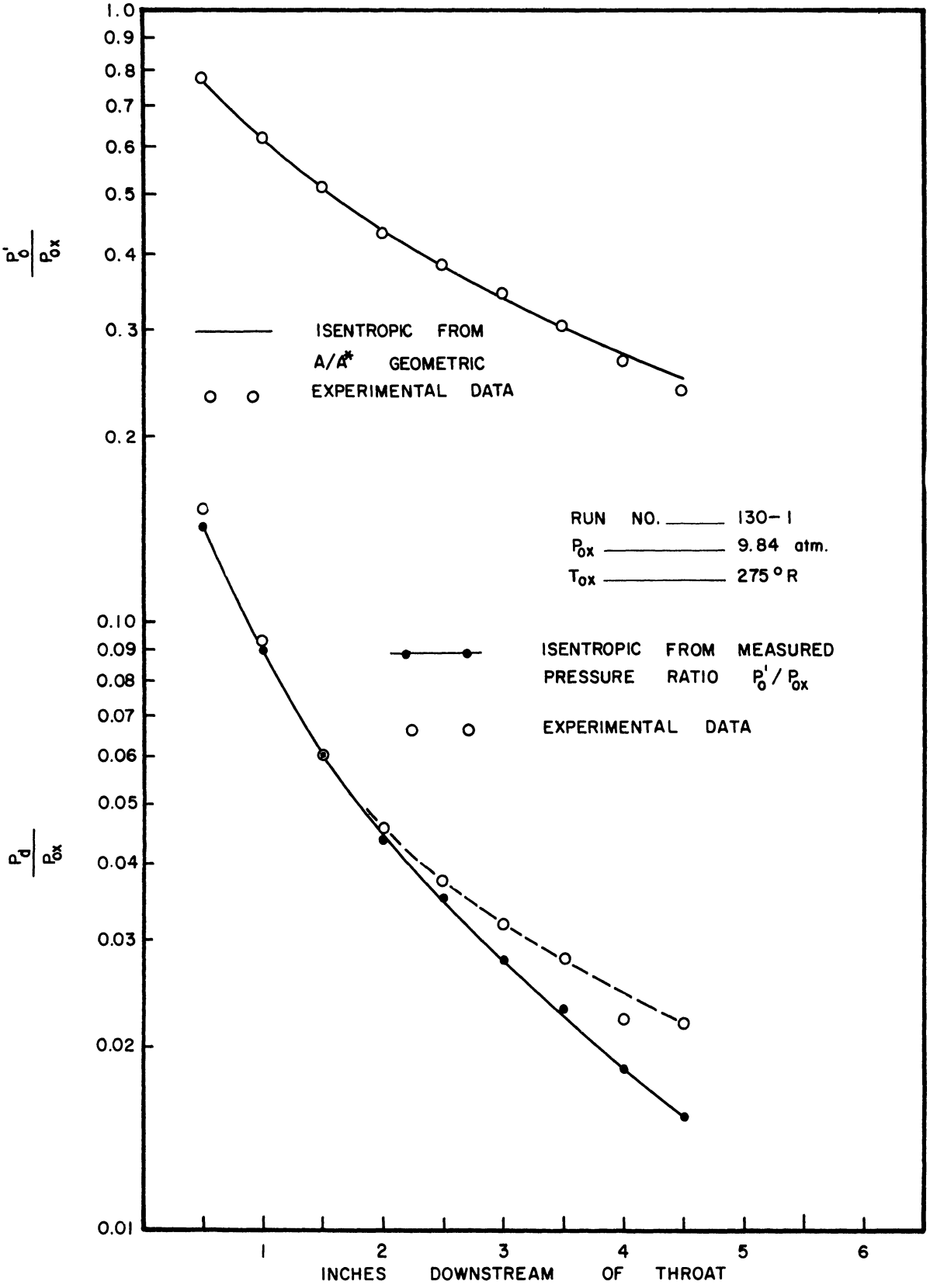

Figure 4-8. Comparison of Experimentally Measured Pressure Ratios Along Nozzle with Isentropic.

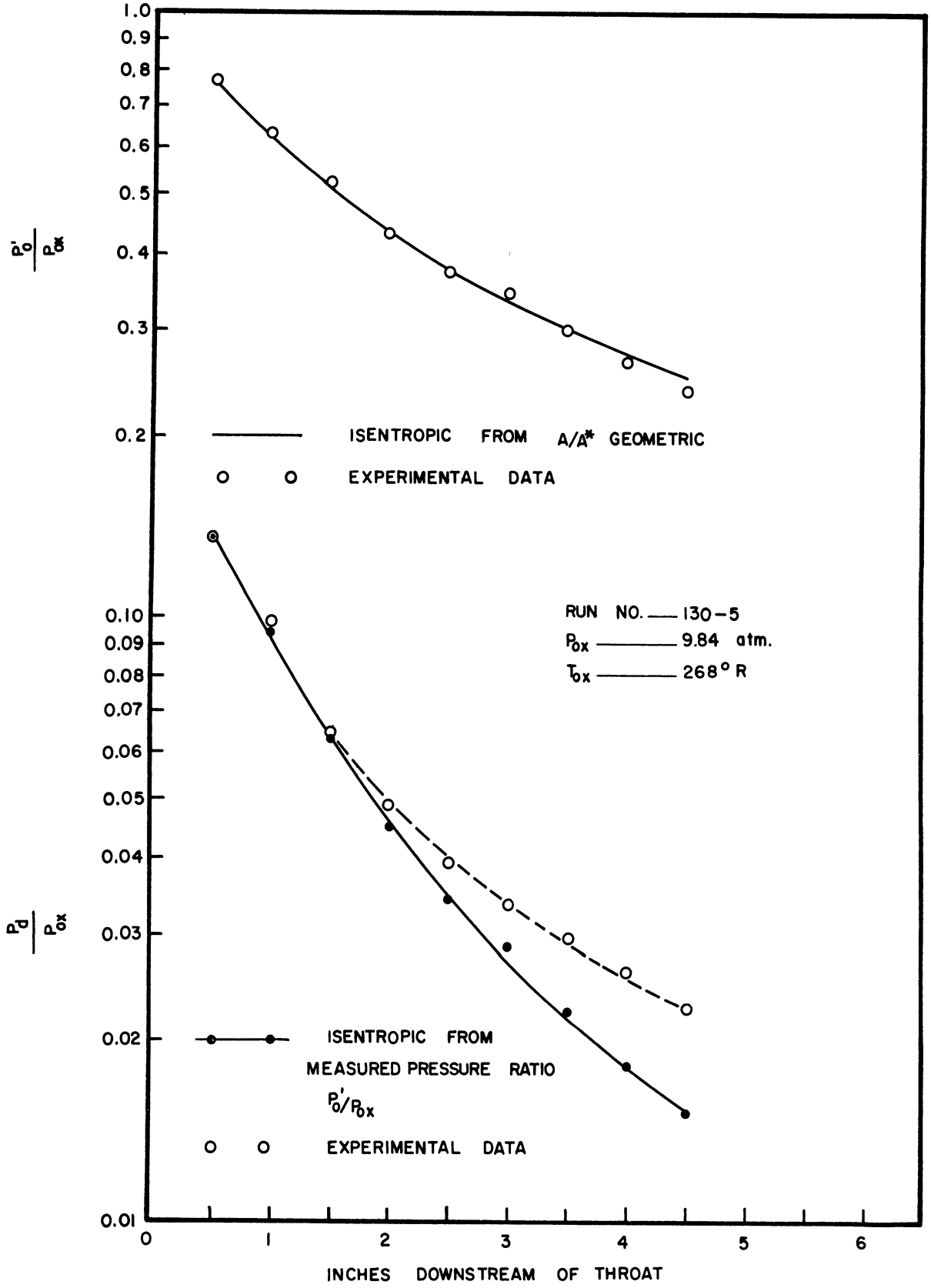

Figure 4-9. Comparison of Experimentally Measured Pressure Ratios Along Nozzle with Isentropic.

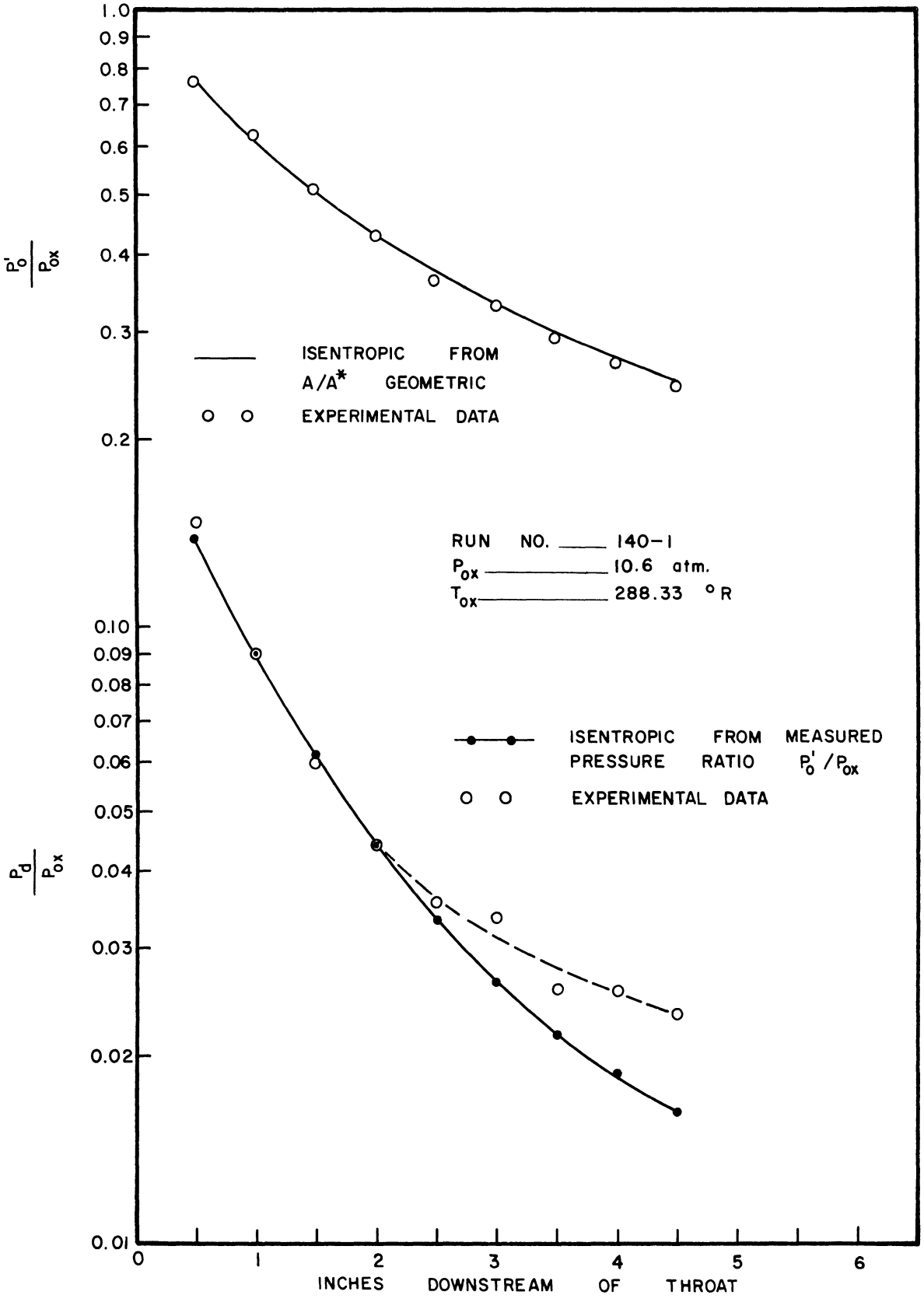

Figure 4-10. Comparison of Experimentally Measured Pressure Ratios Along Nozzle with Isentropic.

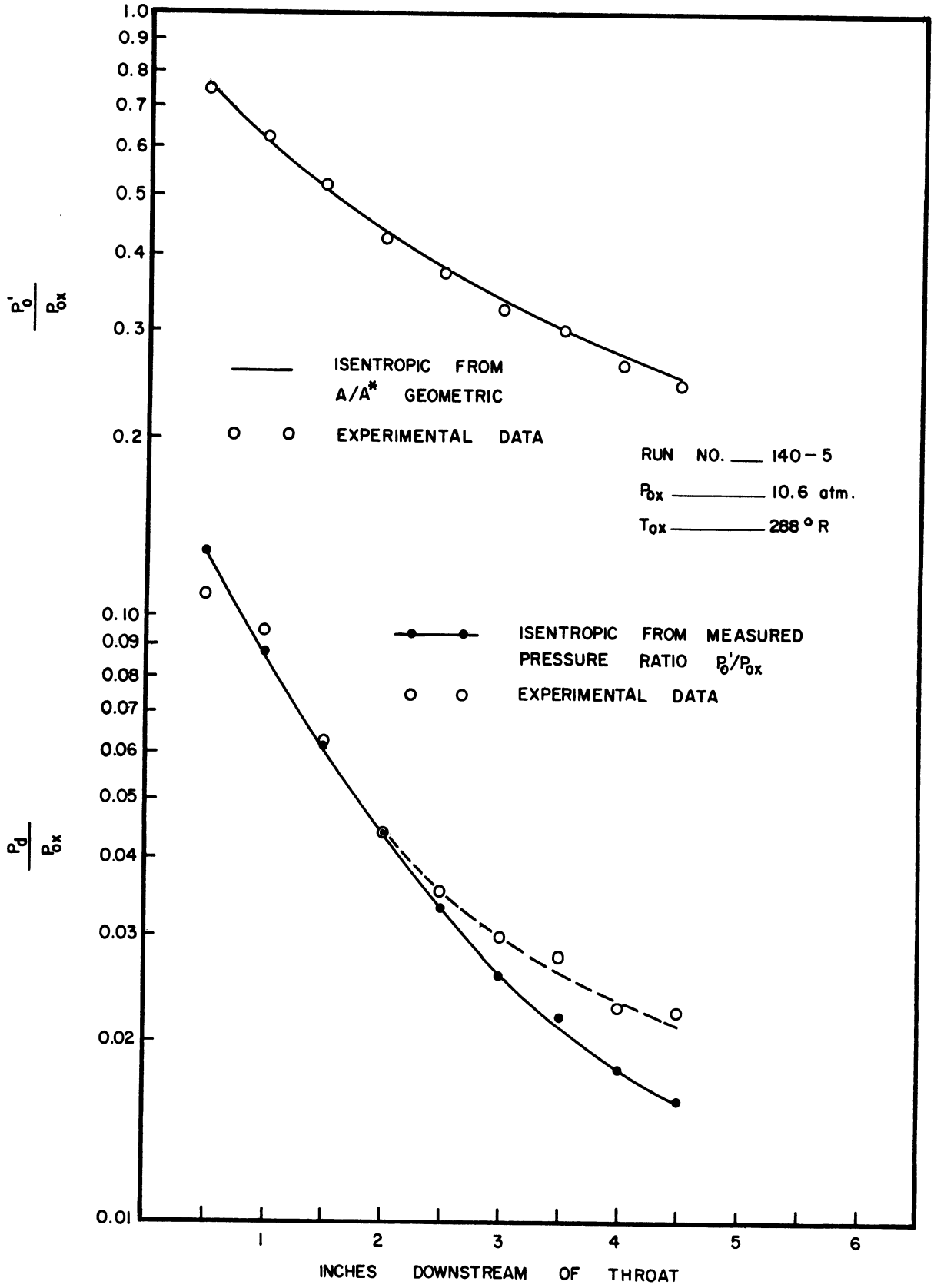

Figure 4-11. Comparison of Experimentally Measured Pressure Ratios Along Nozzle with Isentropic.

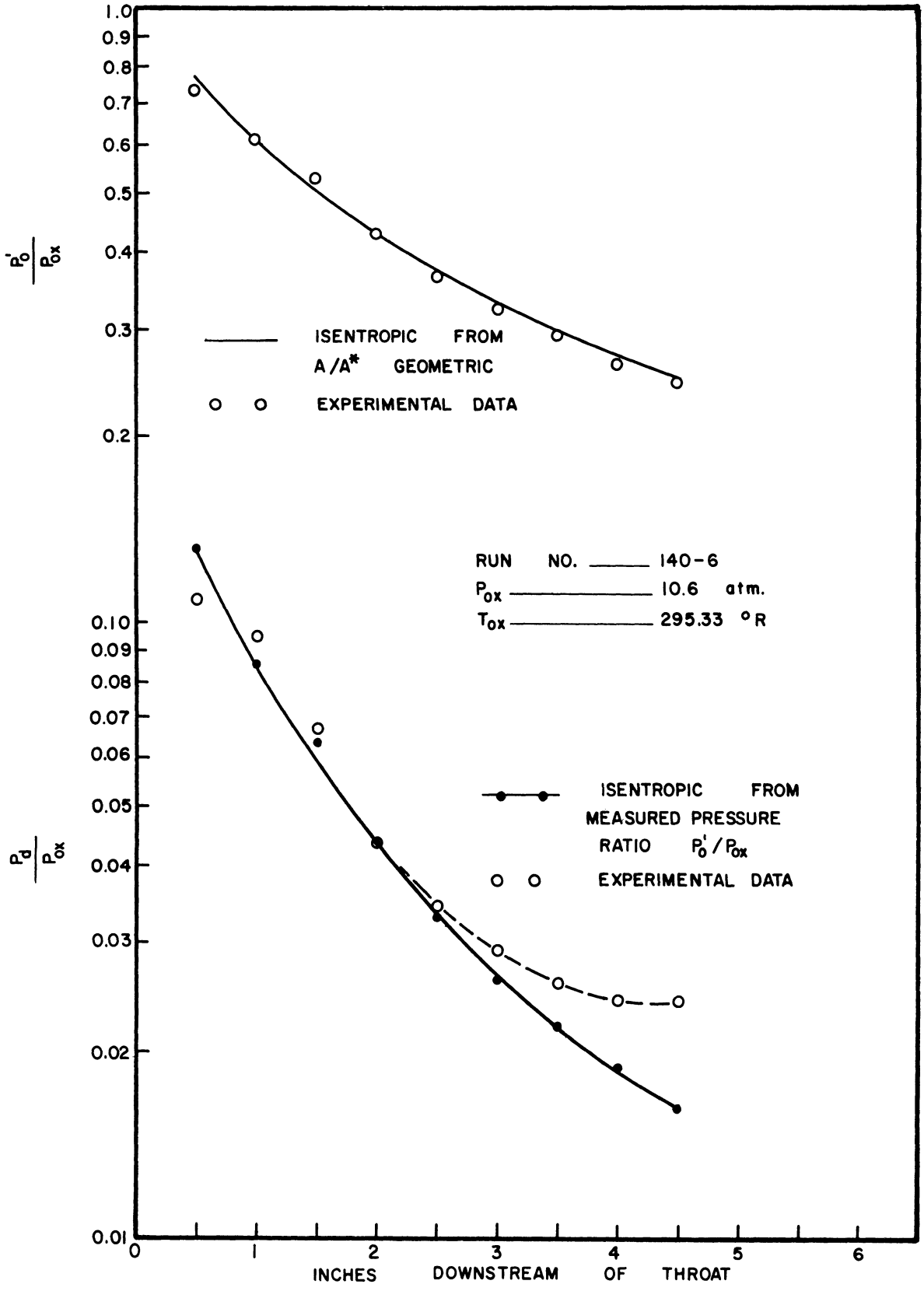

Figure 4-12. Comparison of Experimentally Measured Pressure Ratios Along Nozzle with Isentropic.

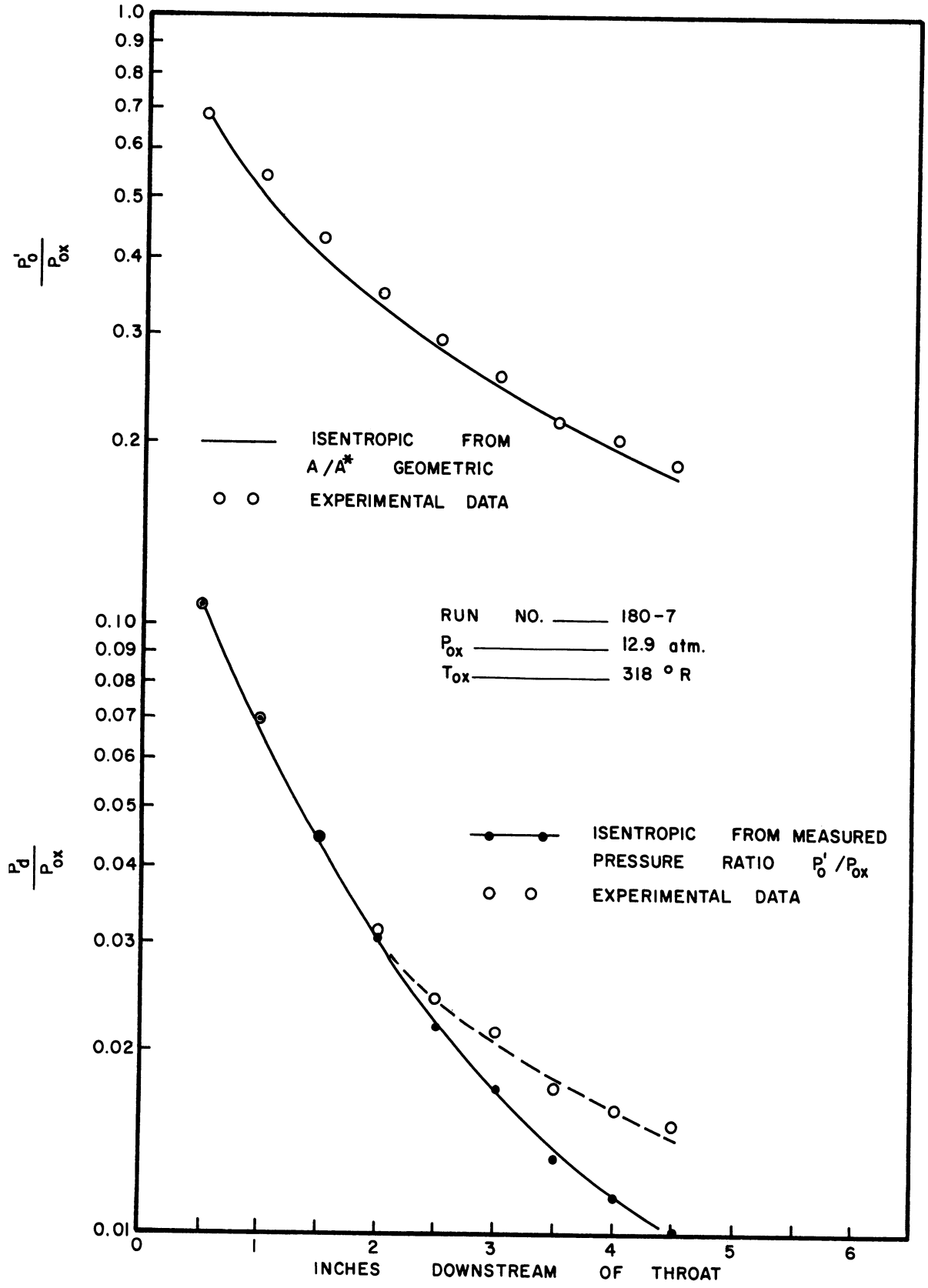

Figure 4-13. Comparison of Experimentally Measured Pressure Ratios Along Nozzle with Isentropic.

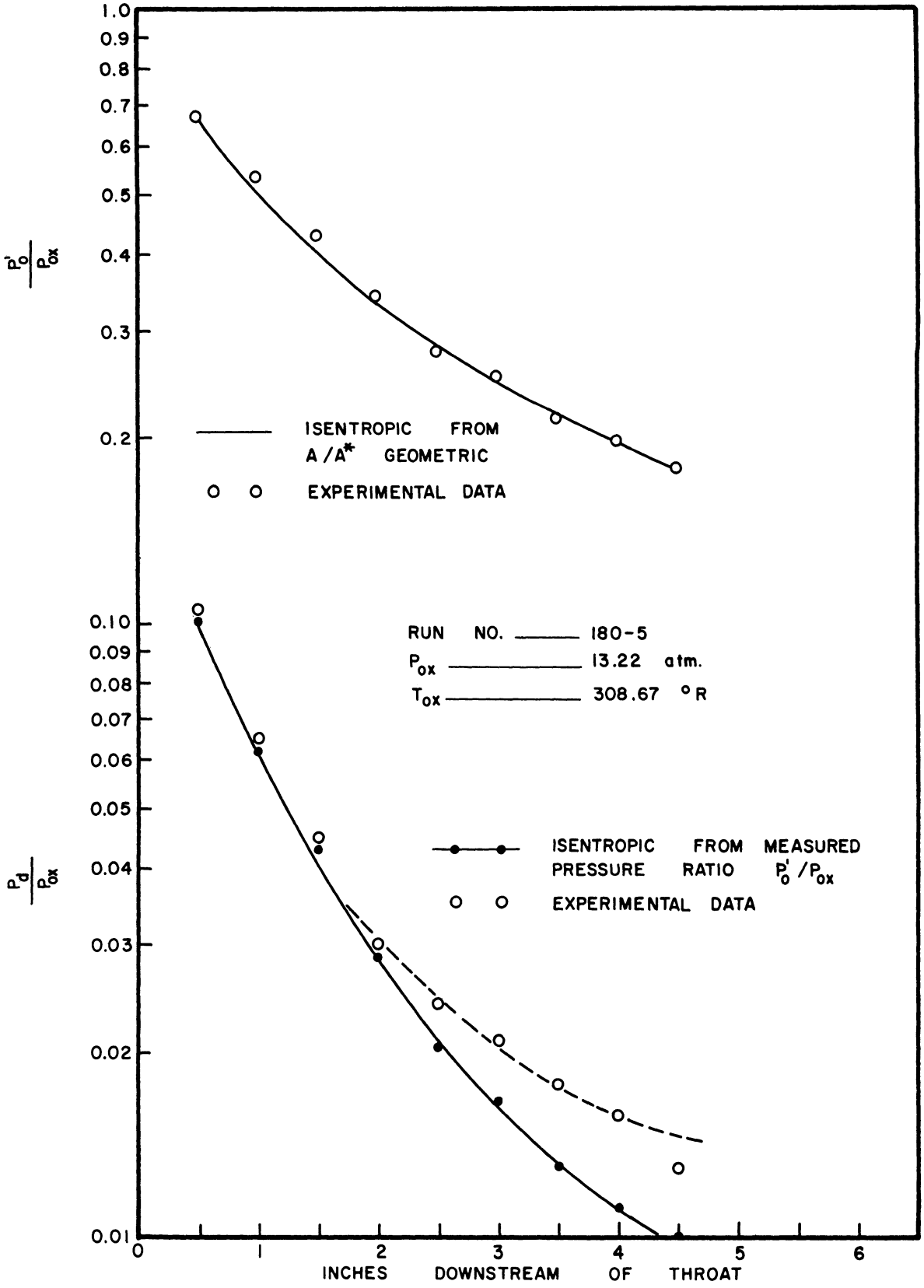

Figure 4-14. Comparison of Experimentally Measured Pressure Ratios Along Nozzle with Isentropic.

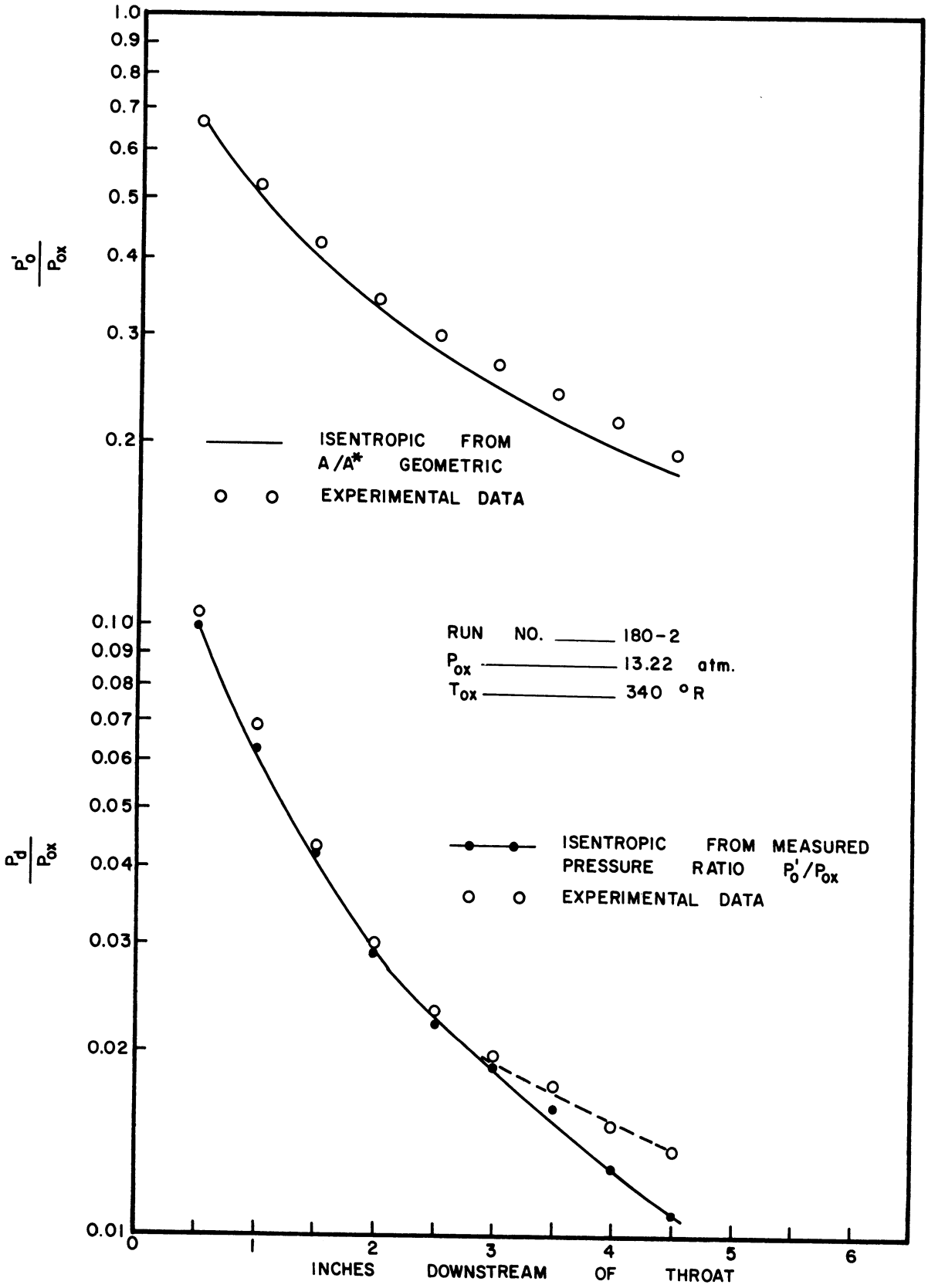

Figure 4-15. Comparison of Experimentally Measured Pressure Ratios Along Nozzle with Isentropic.

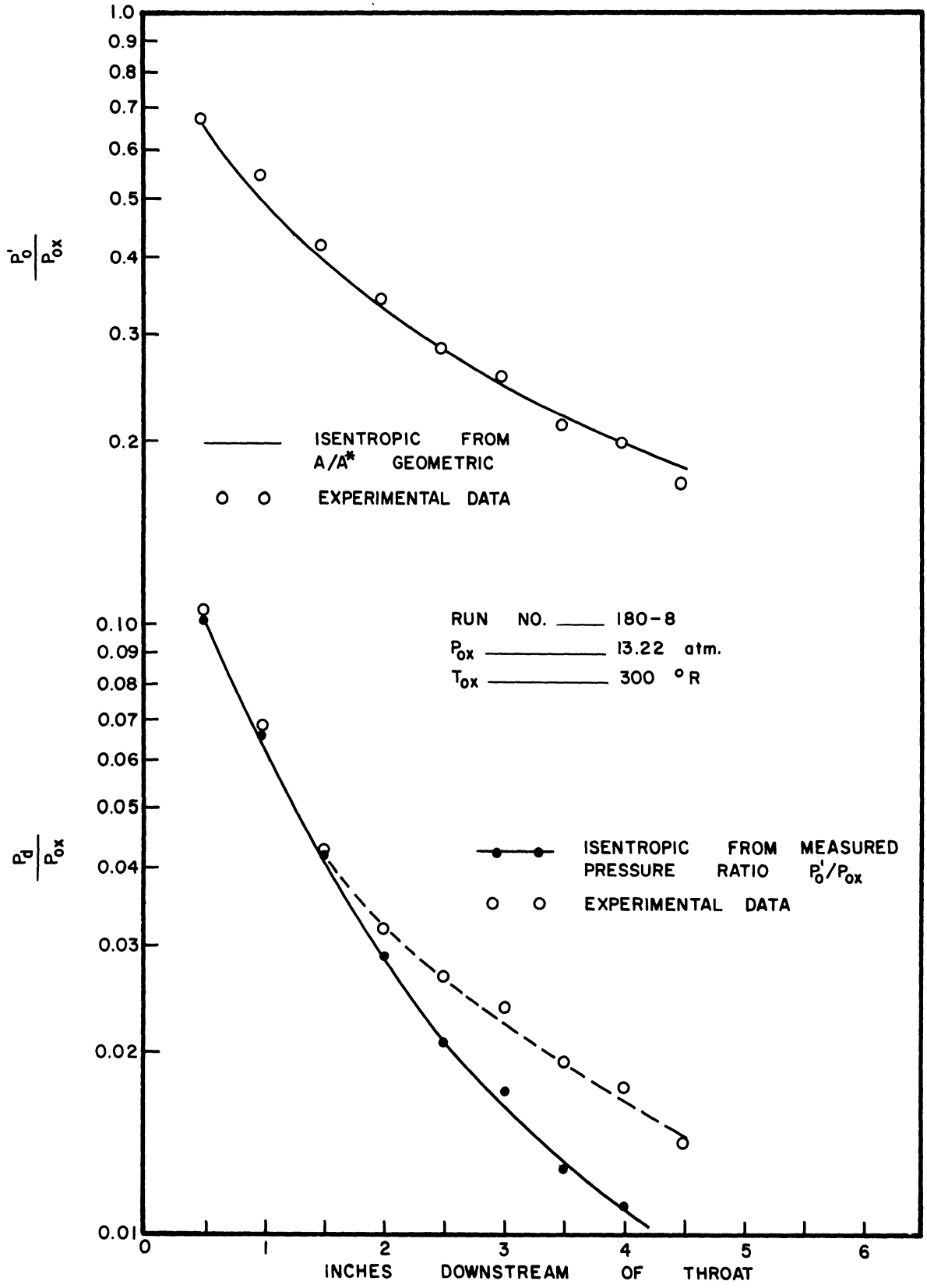

Figure 4-16. Comparison of Experimentally Measured Pressure Ratios Along Nozzle with Isentropic.

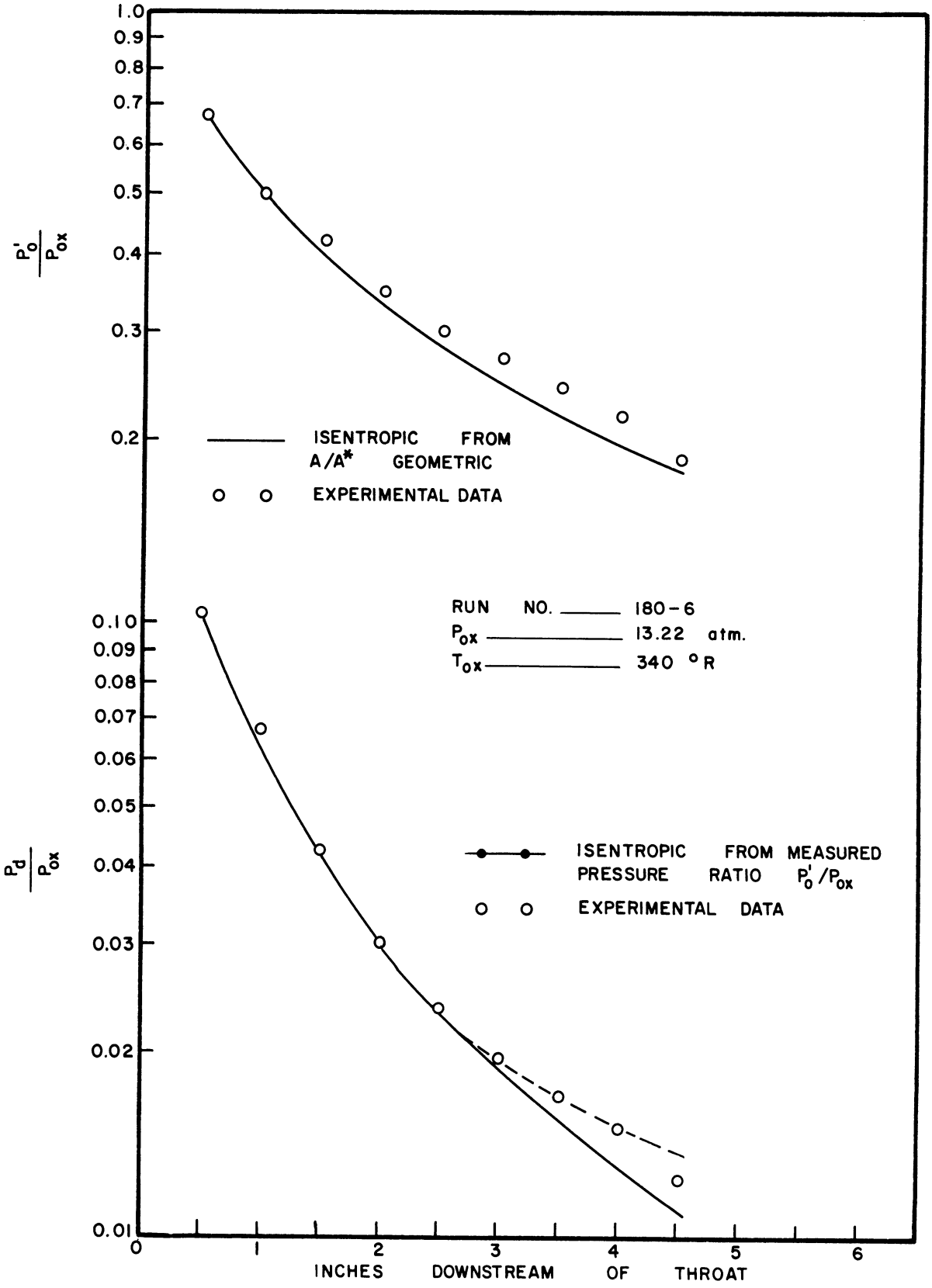

Figure 4-17. Comparison of Experimentally Measured Pressure Ratios Along Nozzle with Isentropic.

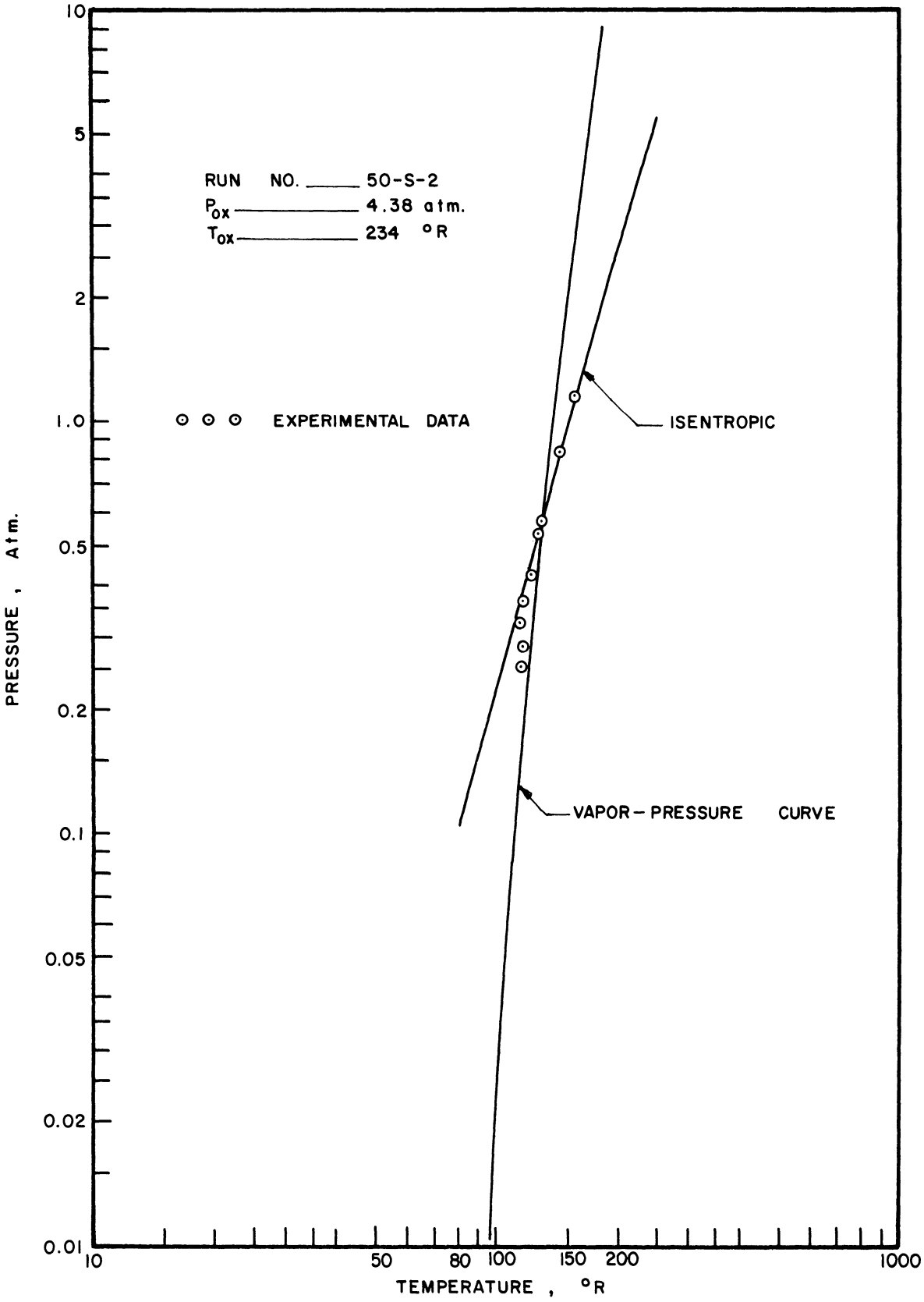

Figure 5-1. Measured Pressure vs. Computed Temperature.

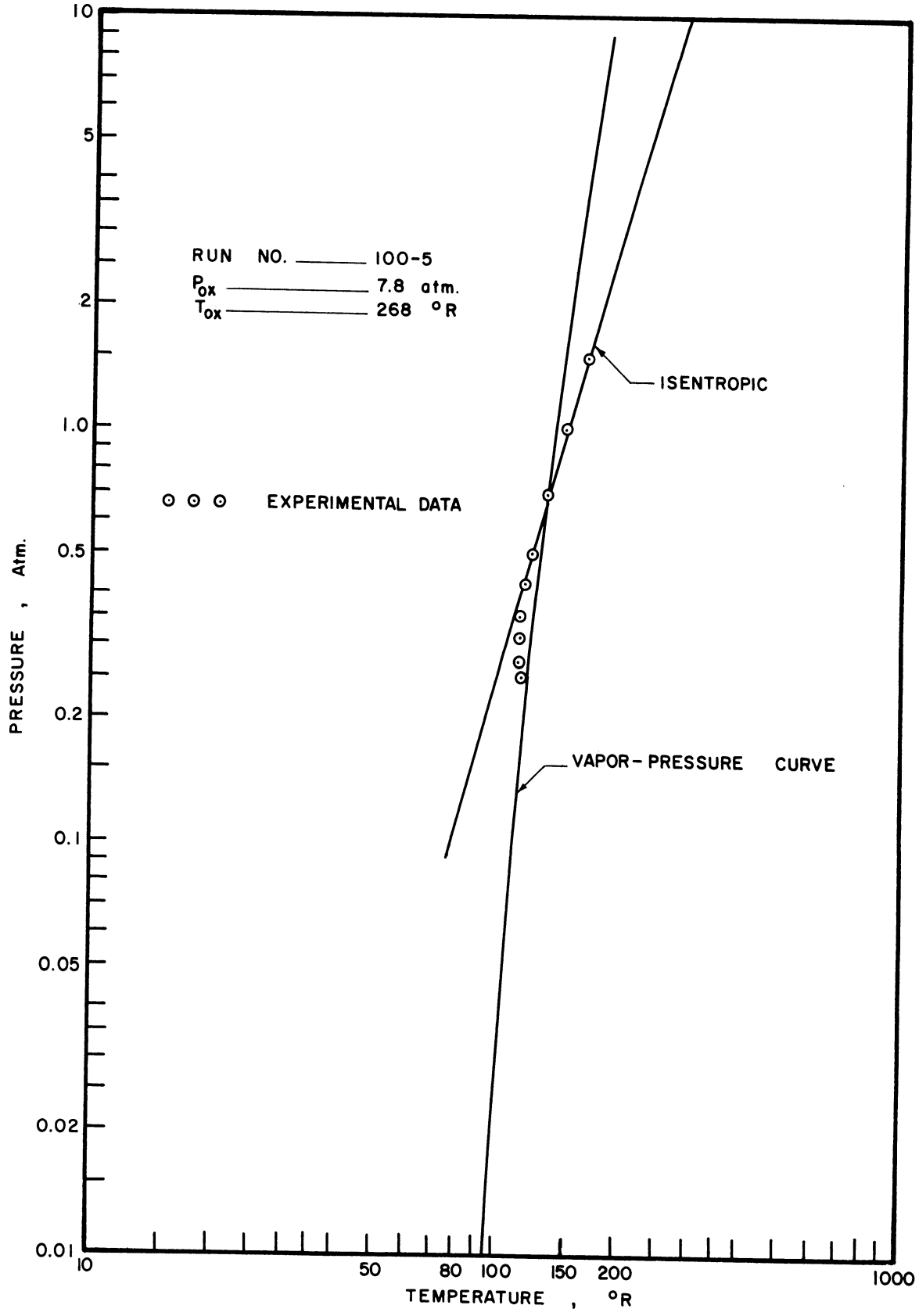

Figure 5-2. Measured Pressure vs. Computed Temperature.

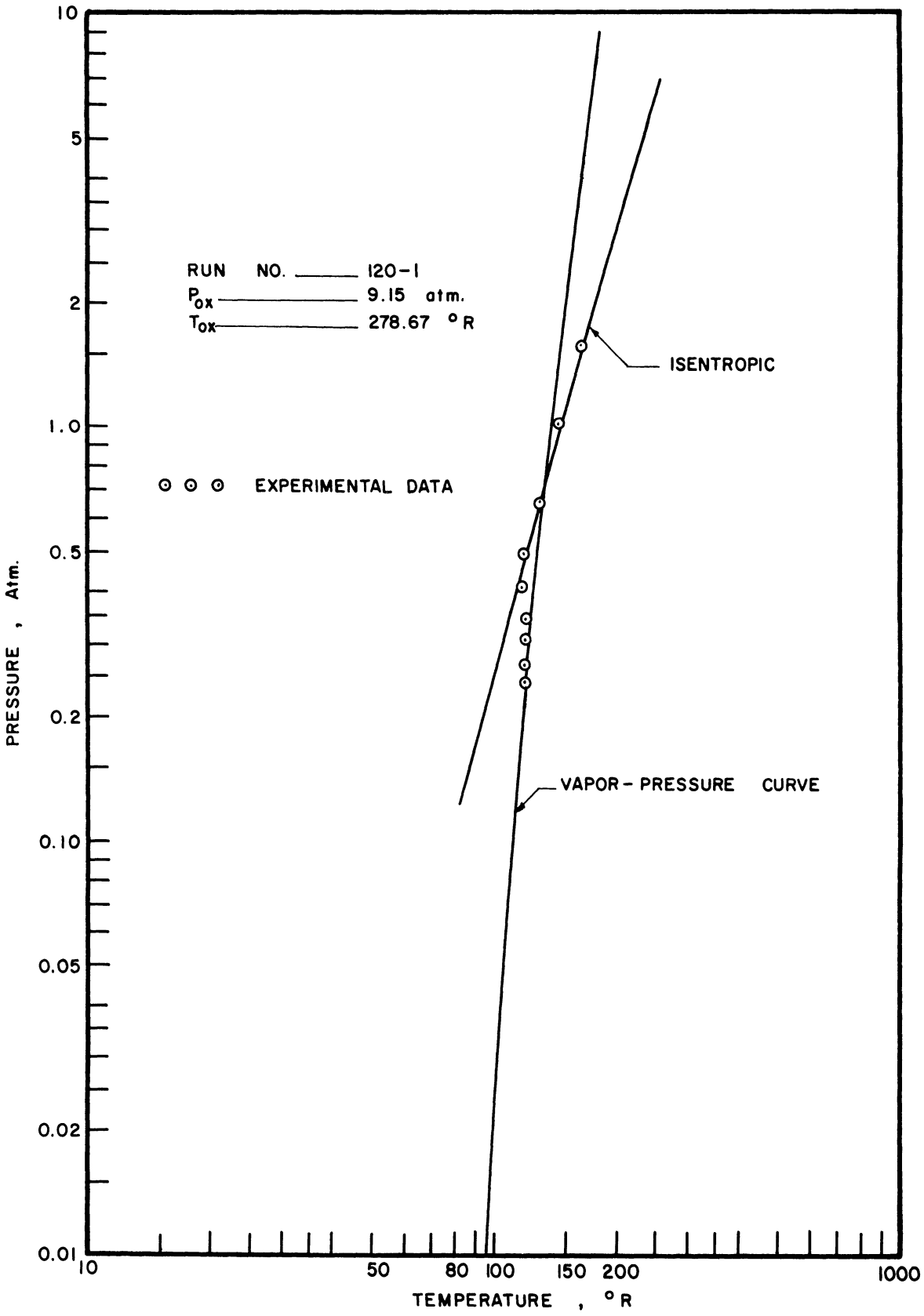

Figure 5-3. Measured Pressure vs. Computed Temperature.

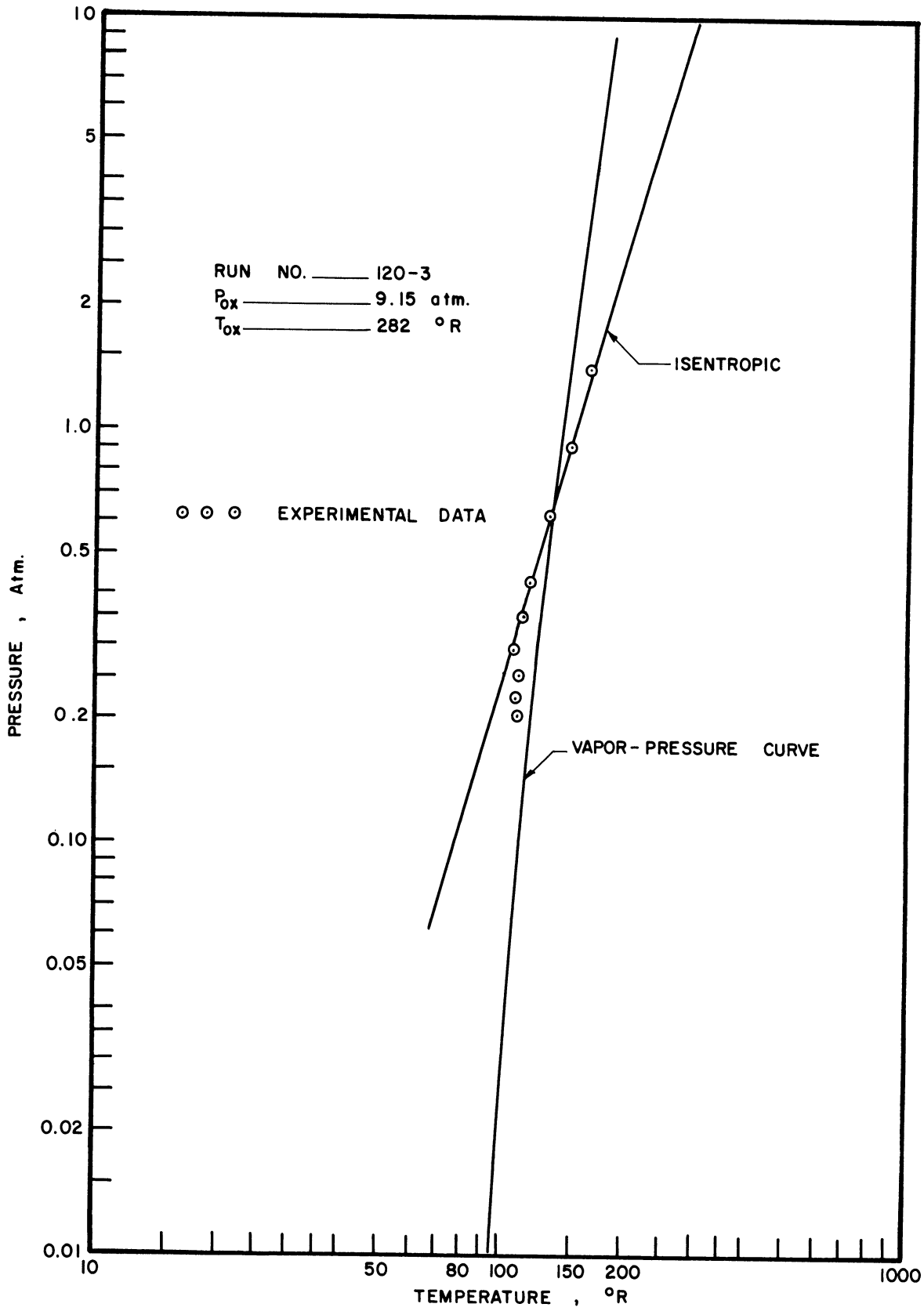

Figure 5-4. Measured Pressure vs. Computed Temperature.

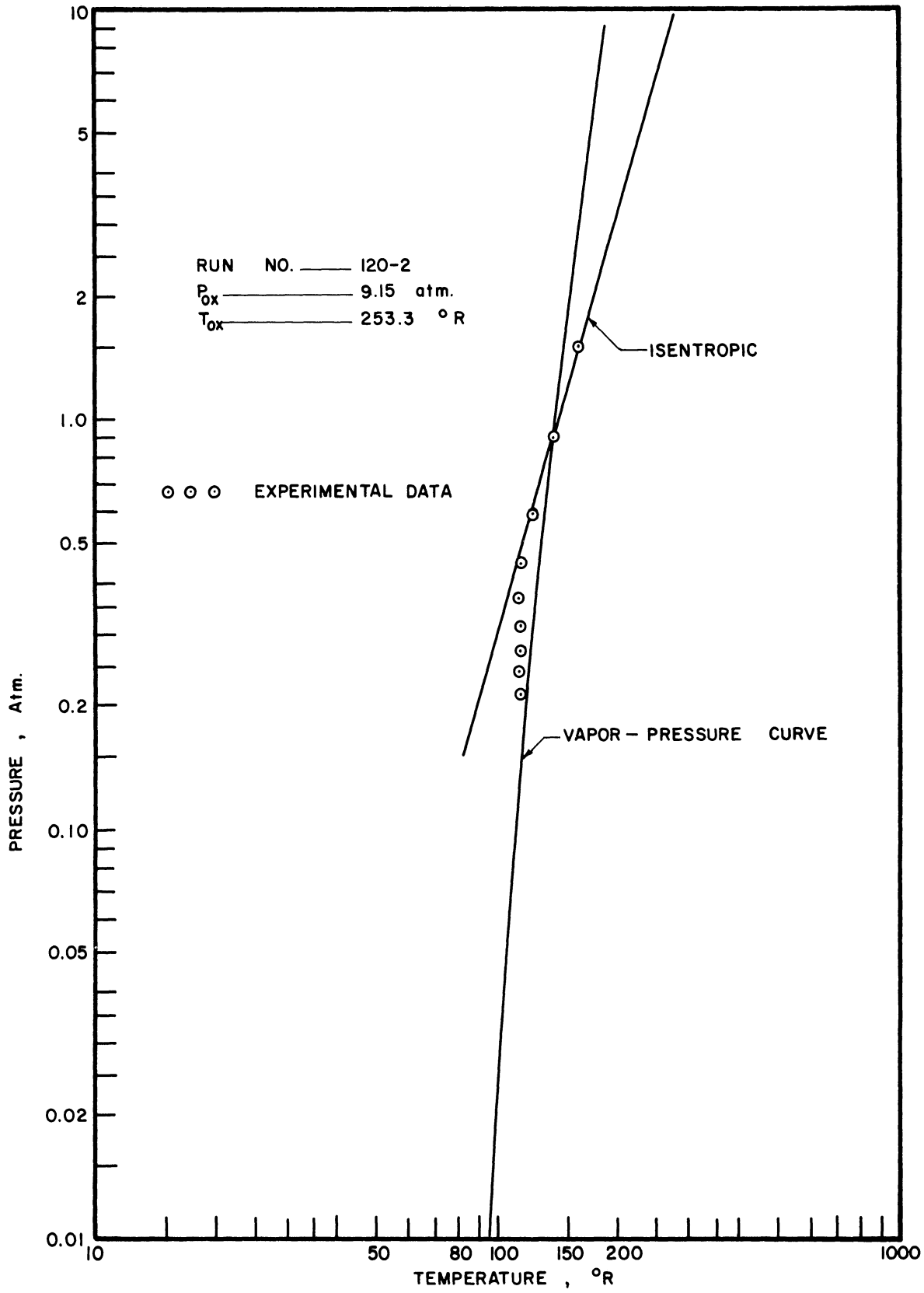

Figure 5-5. Measured Pressure vs. Computed Temperature.

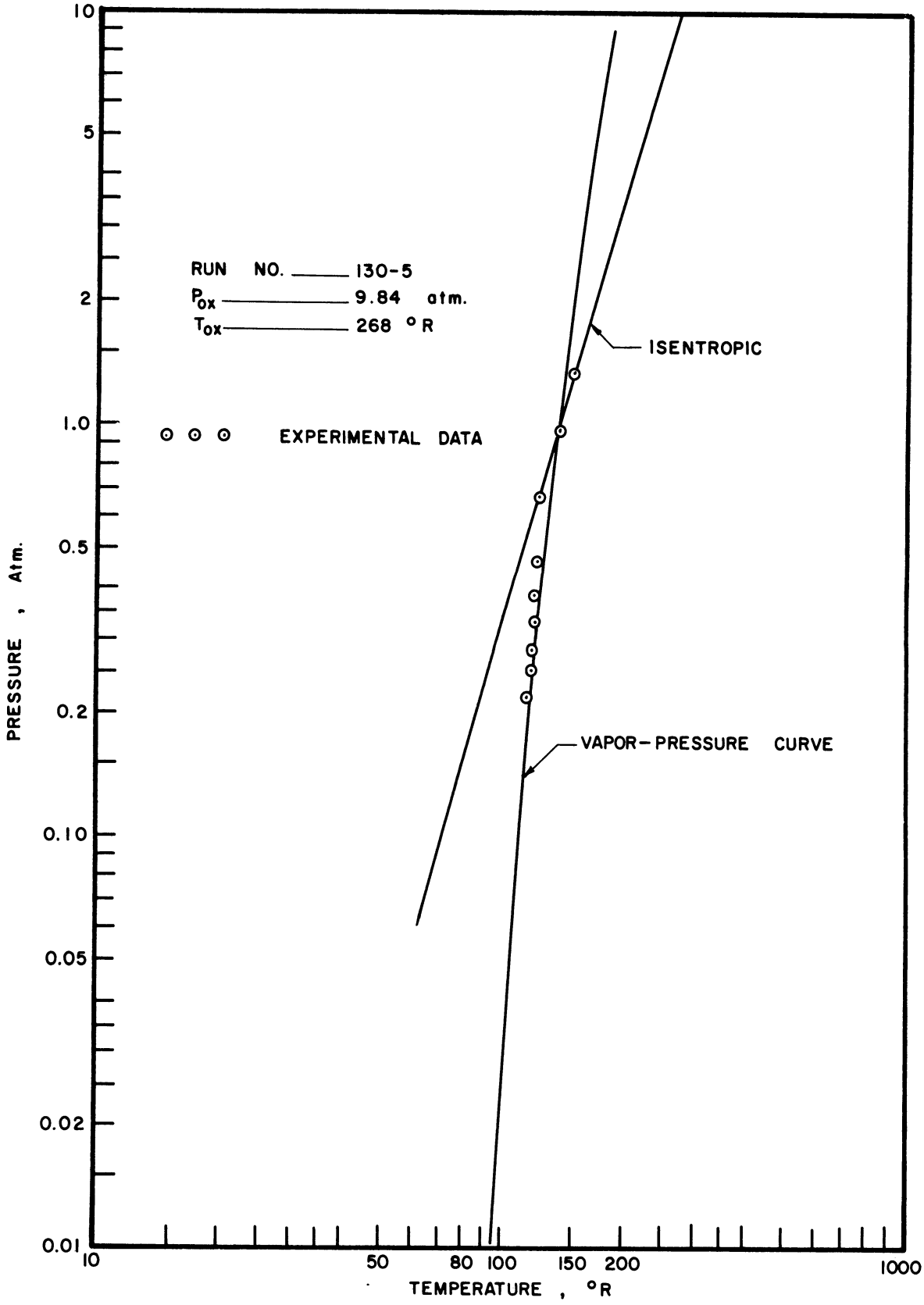

Figure 5-6. Measured Pressure vs. Computed Temperature.

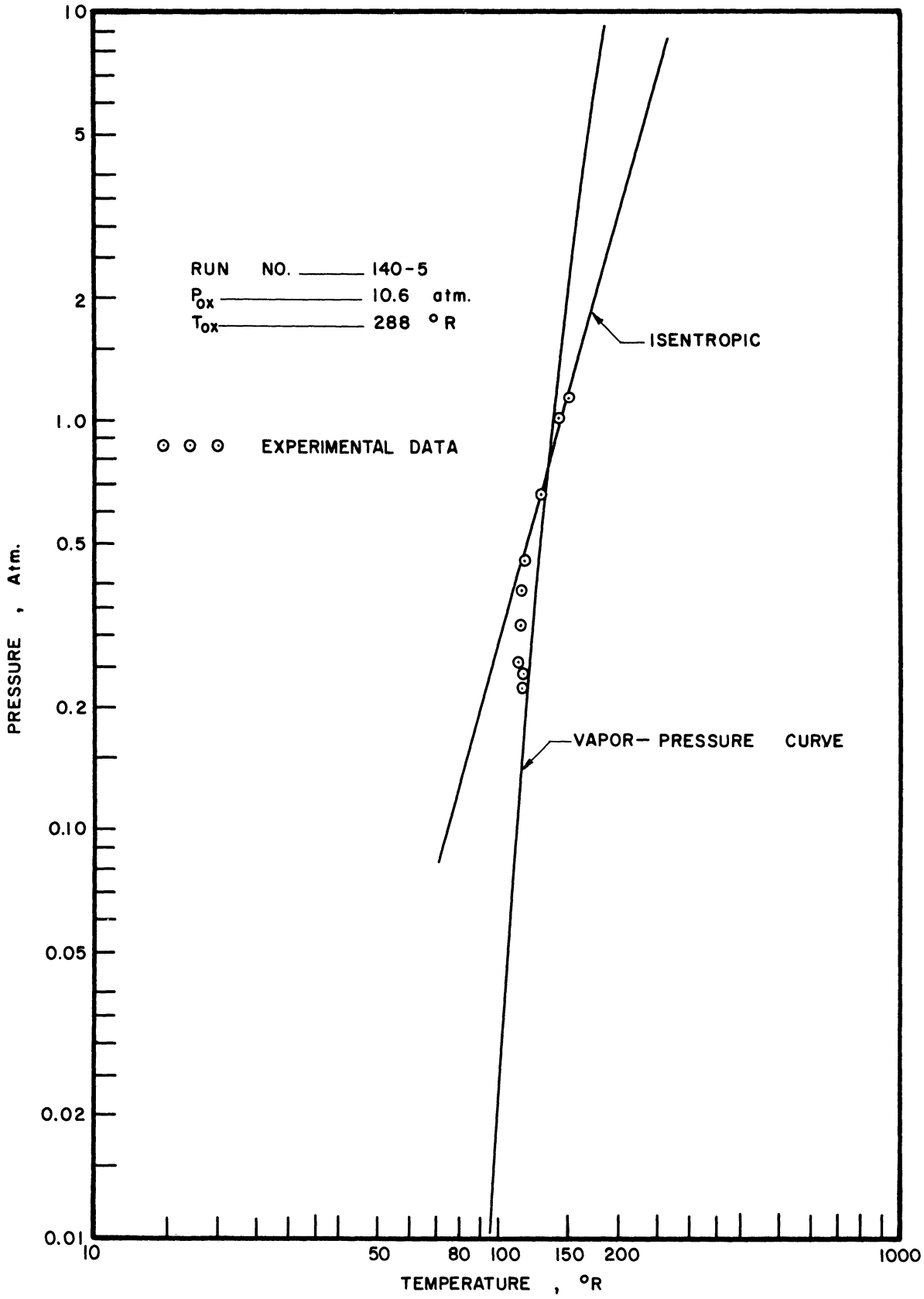

Figure 5-7. Measured Pressure vs. Computed Temperature.

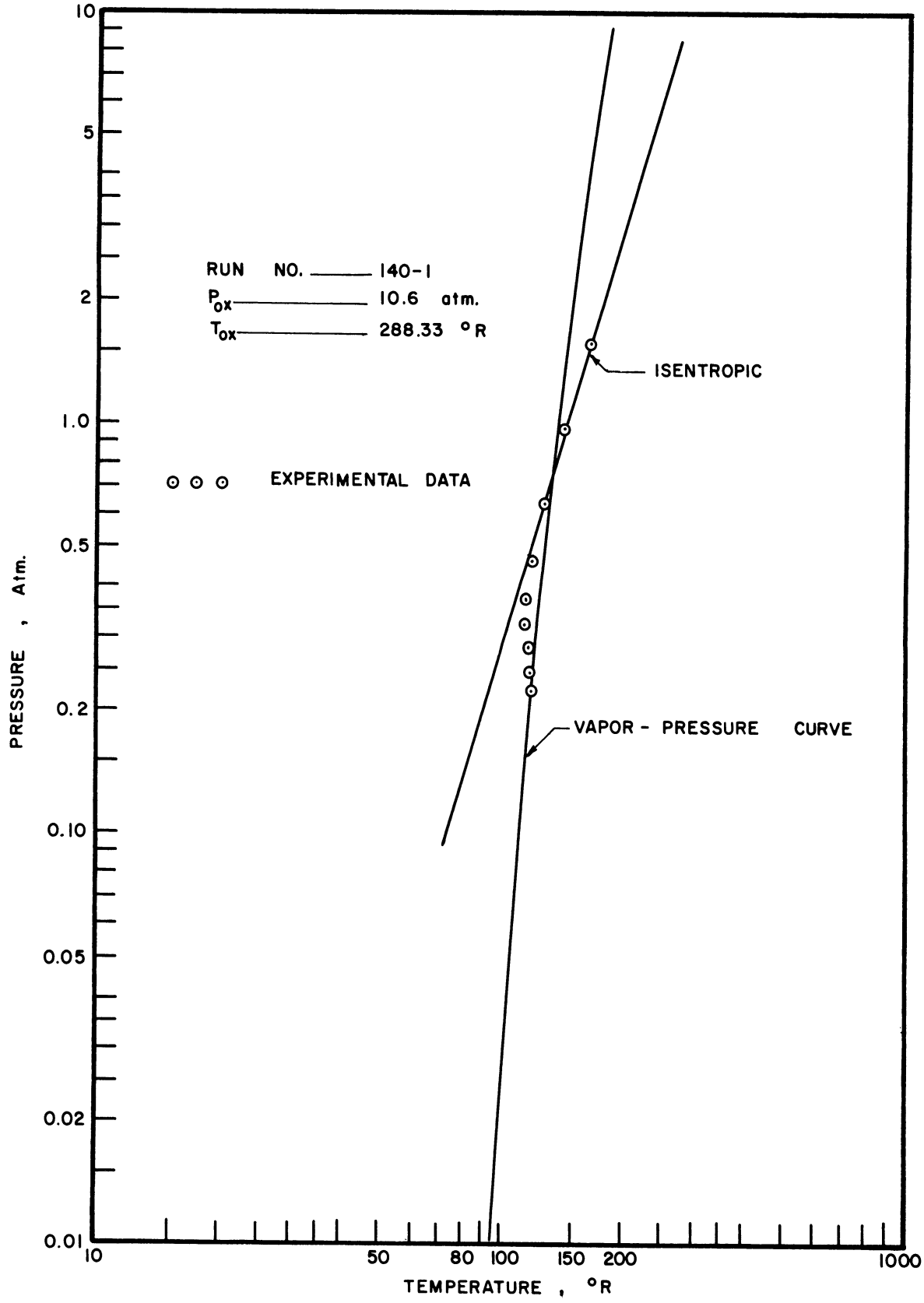

Figure 5-8. Measured Pressure vs. Computed Temperature.

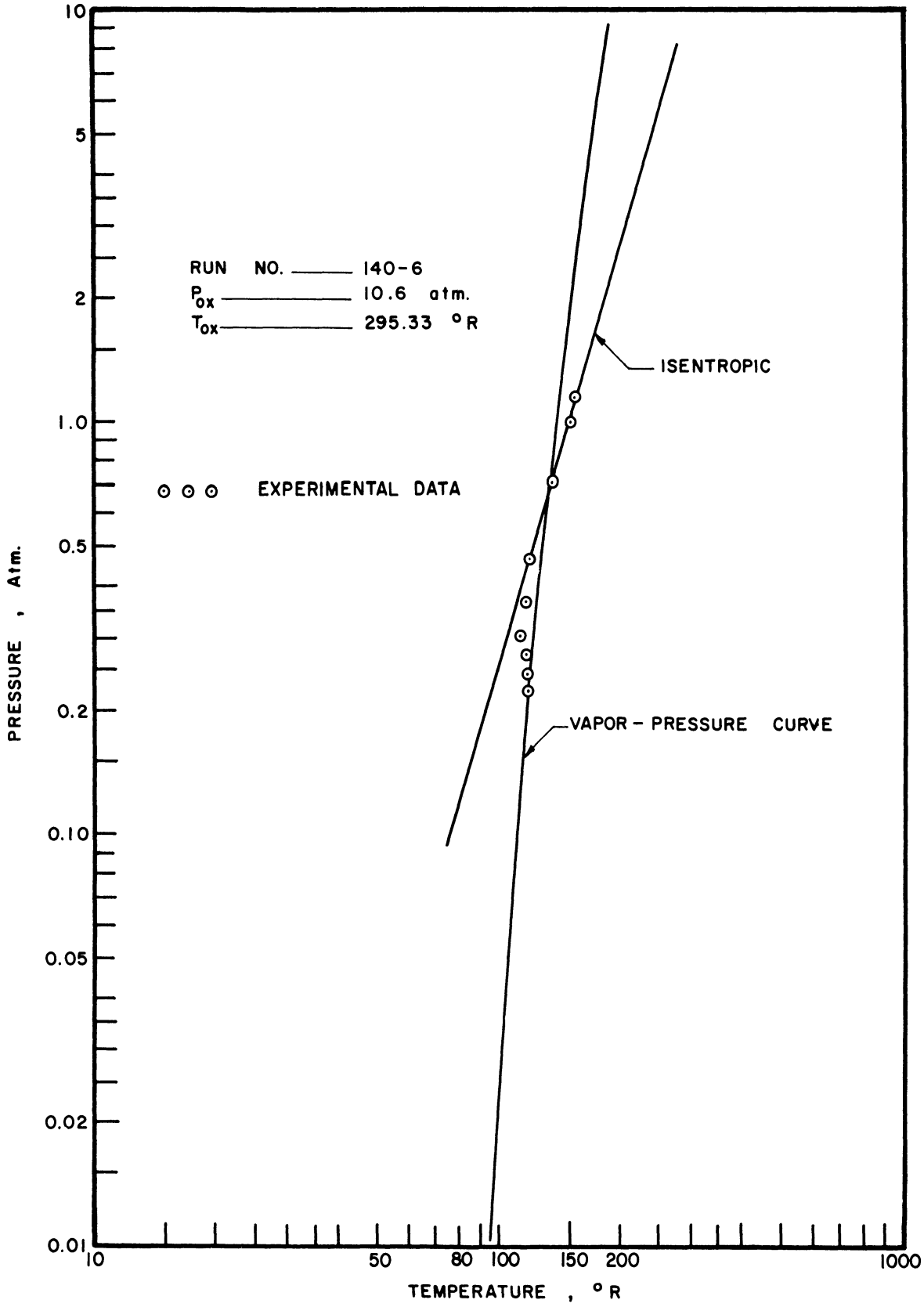

Figure 5-9. Measured Pressure vs. Computed Temperature.

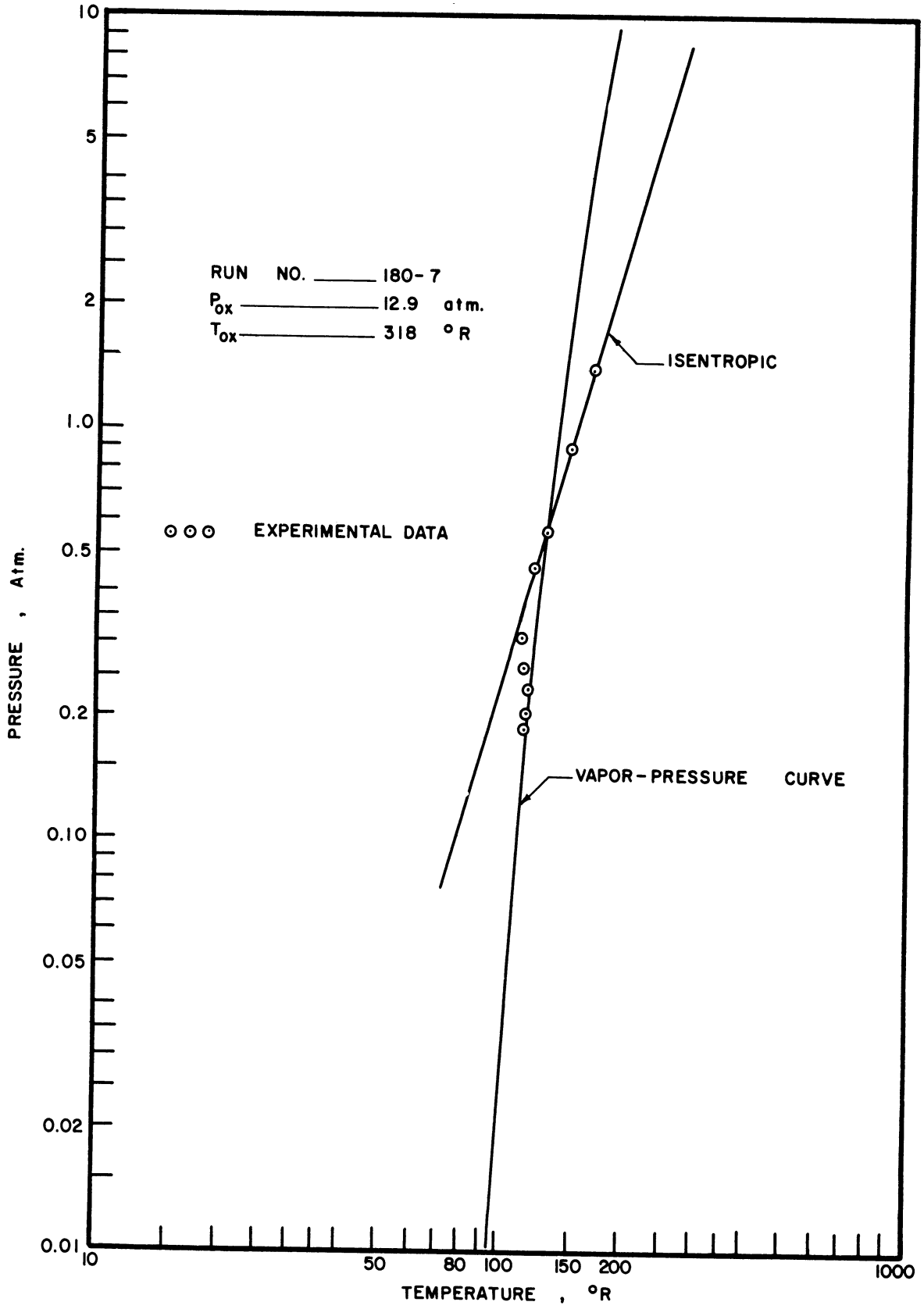

Figure 5-10. Measured Pressure vs. Computed Temperature.

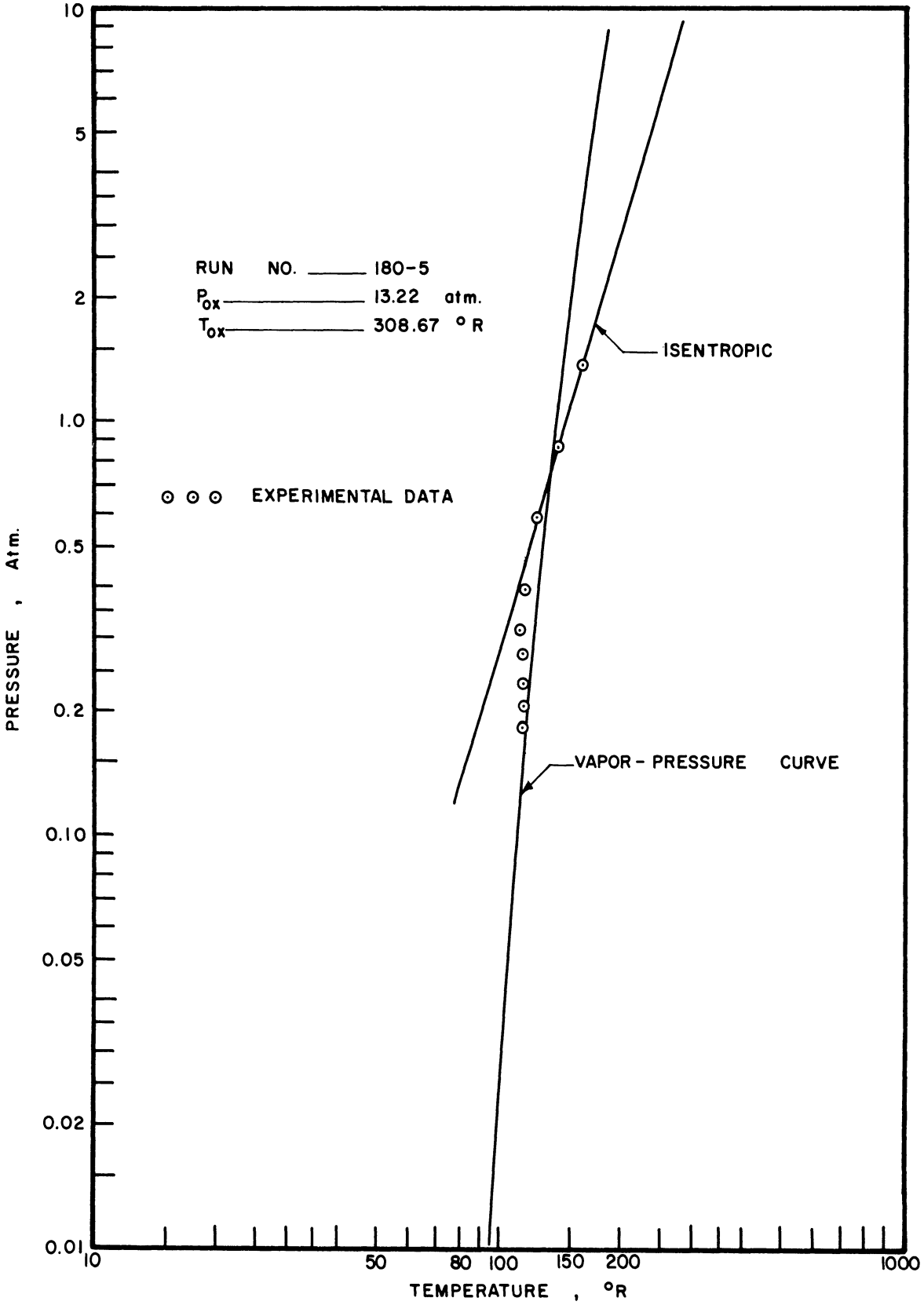

Figure 5-11. Measured Pressure vs. Computed Temperature.

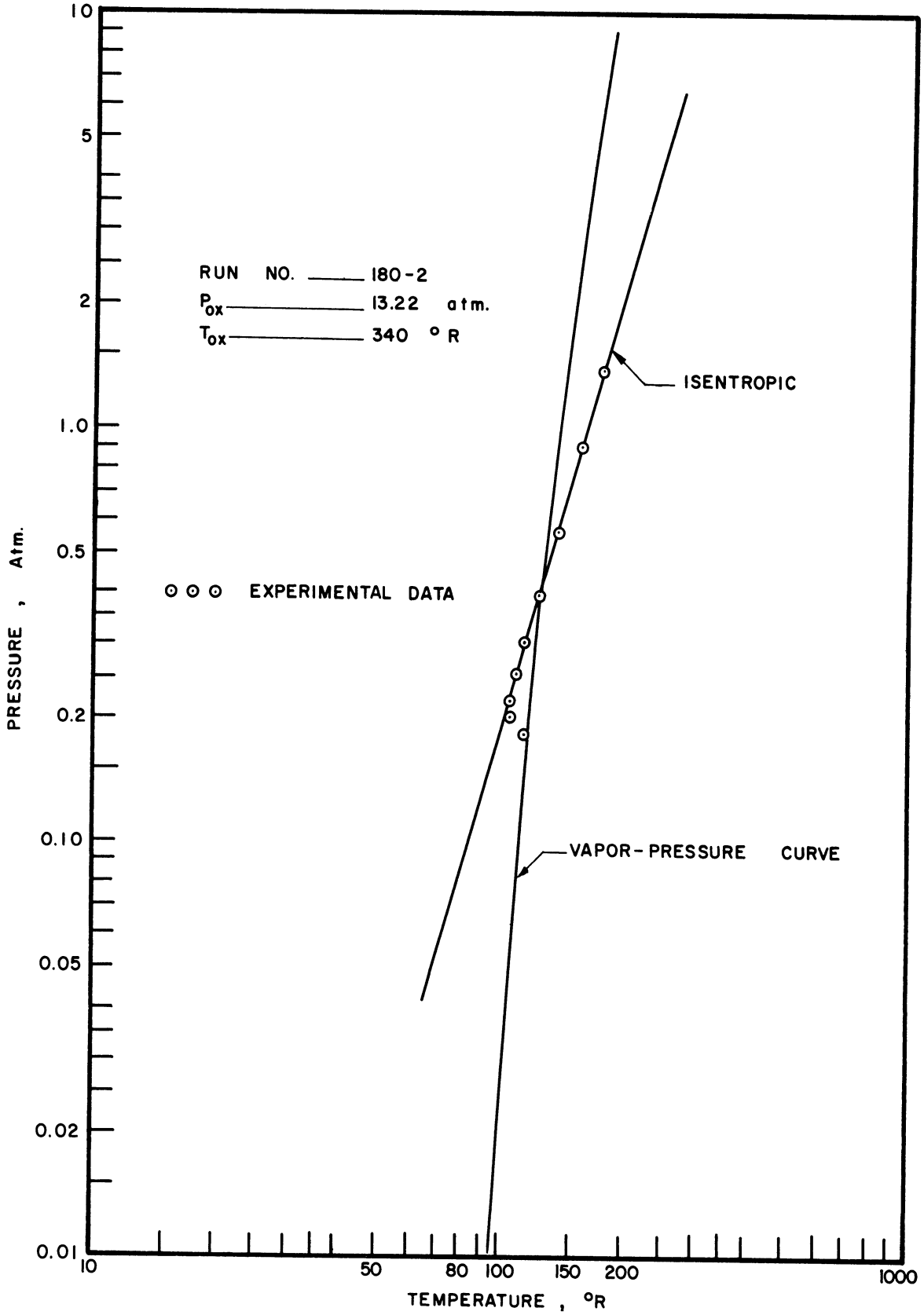

Figure 5-12. Measured Pressure vs. Computed Temperature.

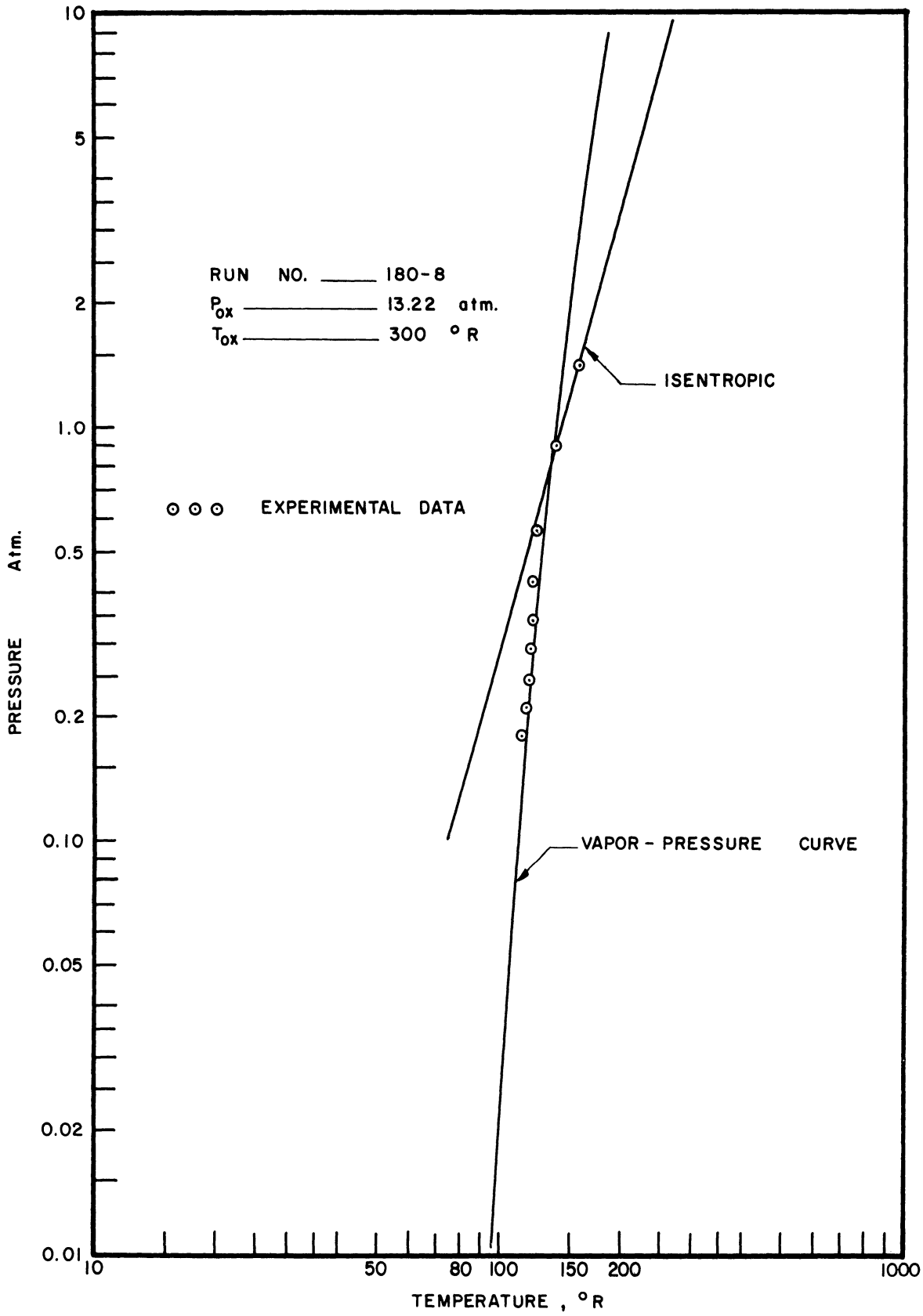

Figure 5-13. Measured Pressure vs. Computed Temperature.

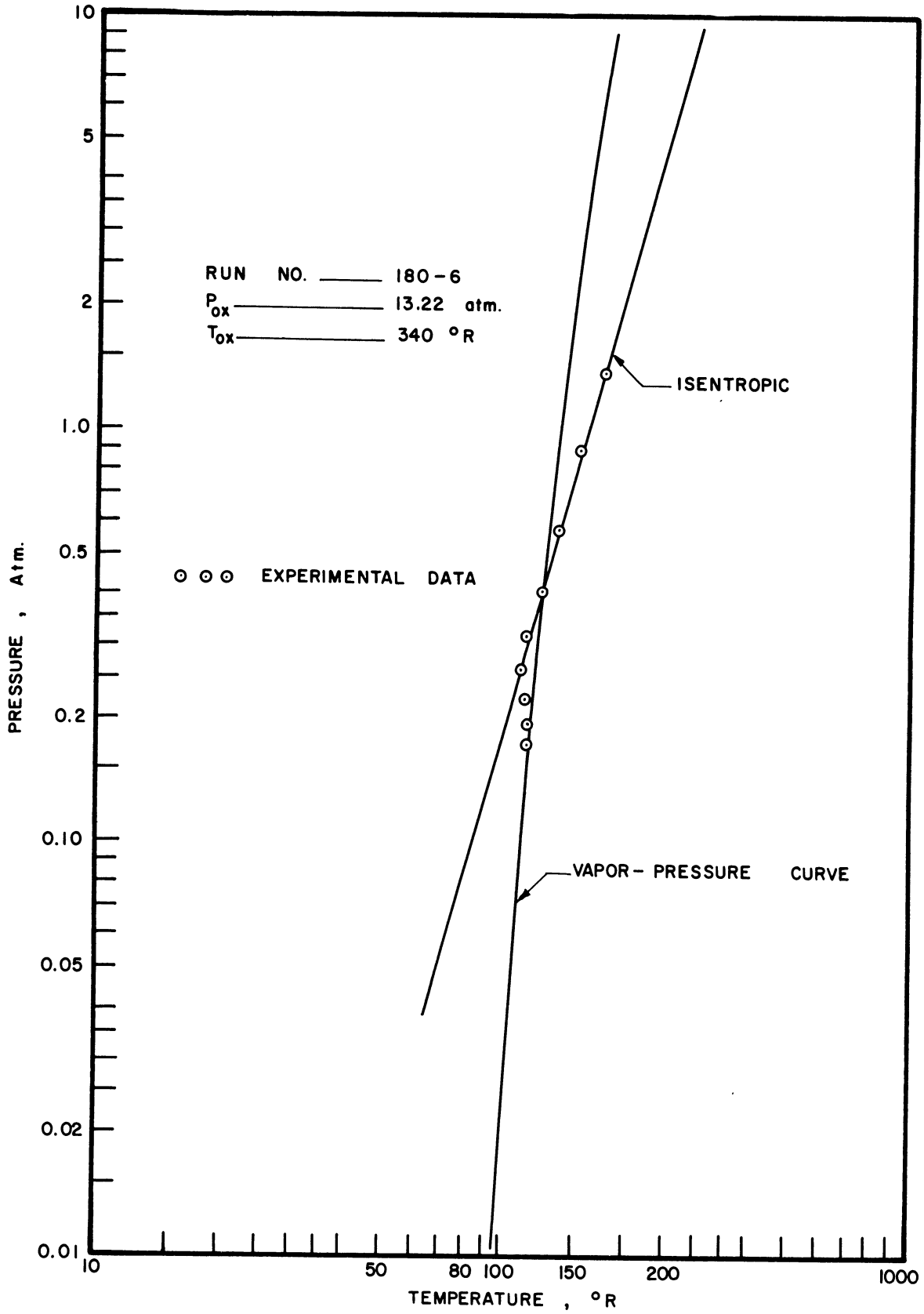

Figure 5-14. Measured Pressure vs. Computed Temperature.

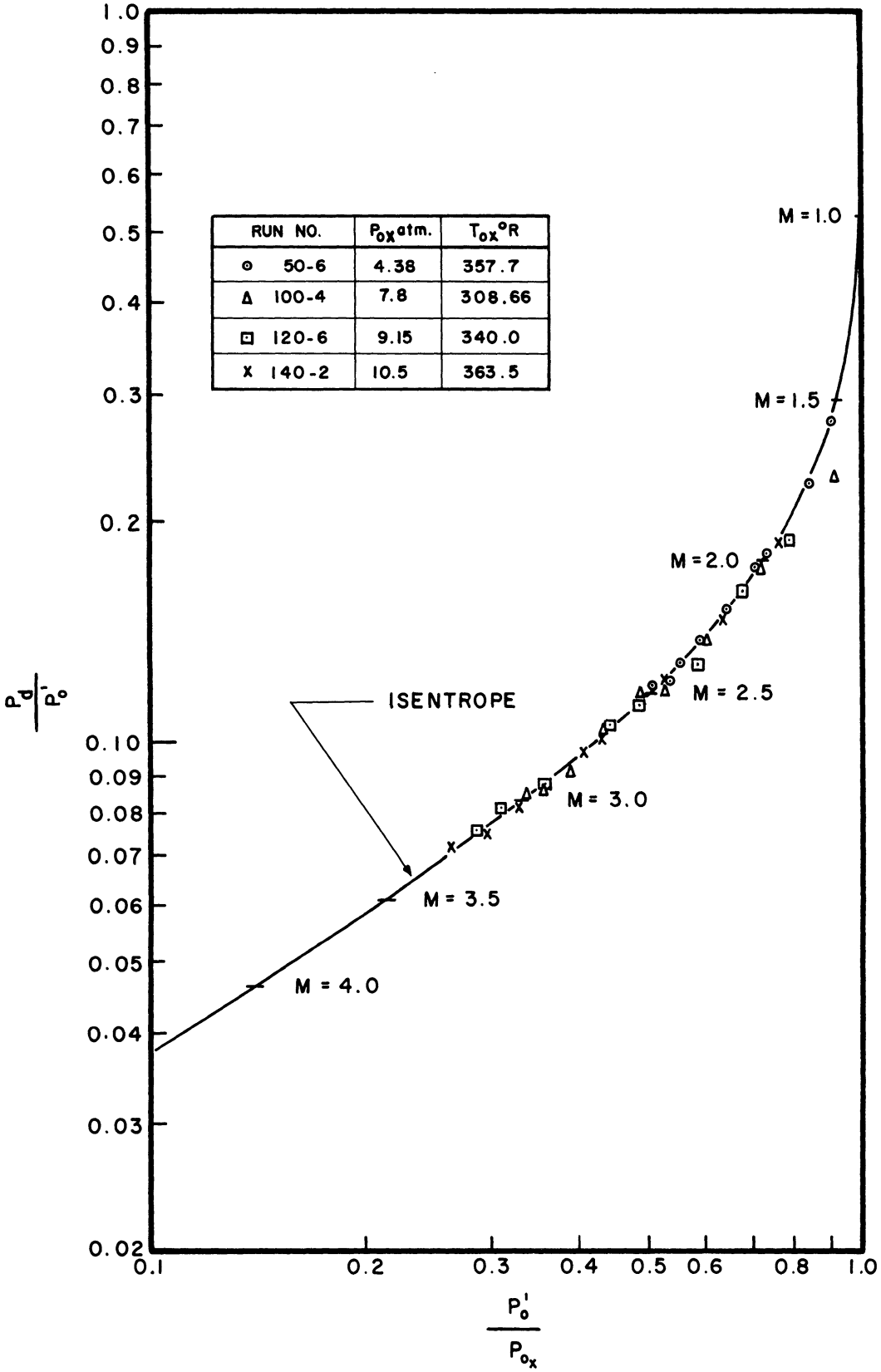

Figure 6. Comparison of Actual Expansion with Isentropic p_o'/p_{ox} vs. p_d/p_o' Runs Without Condensation.

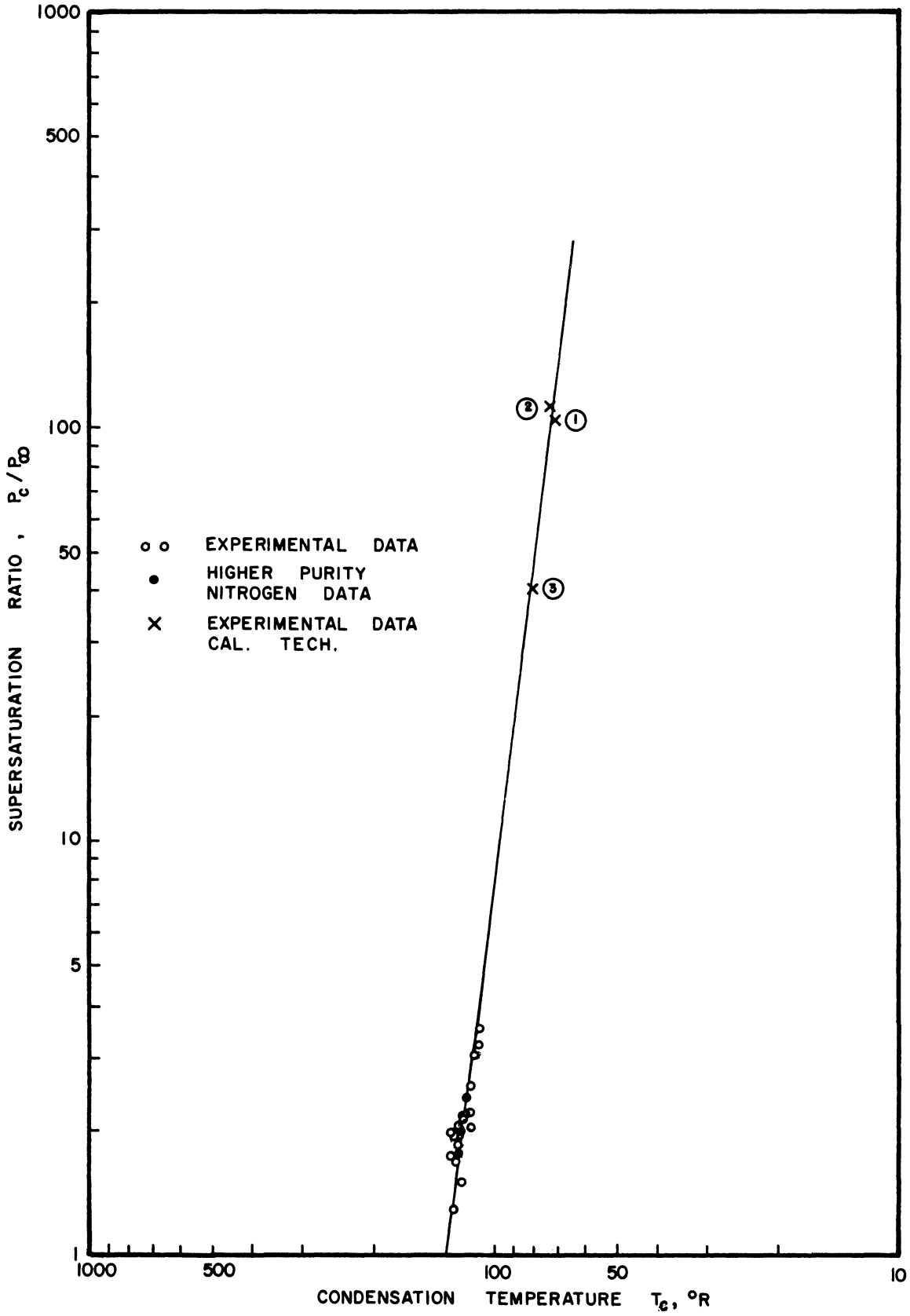

Figure 7. Supersaturation Ratio vs. Condensation Temperature.

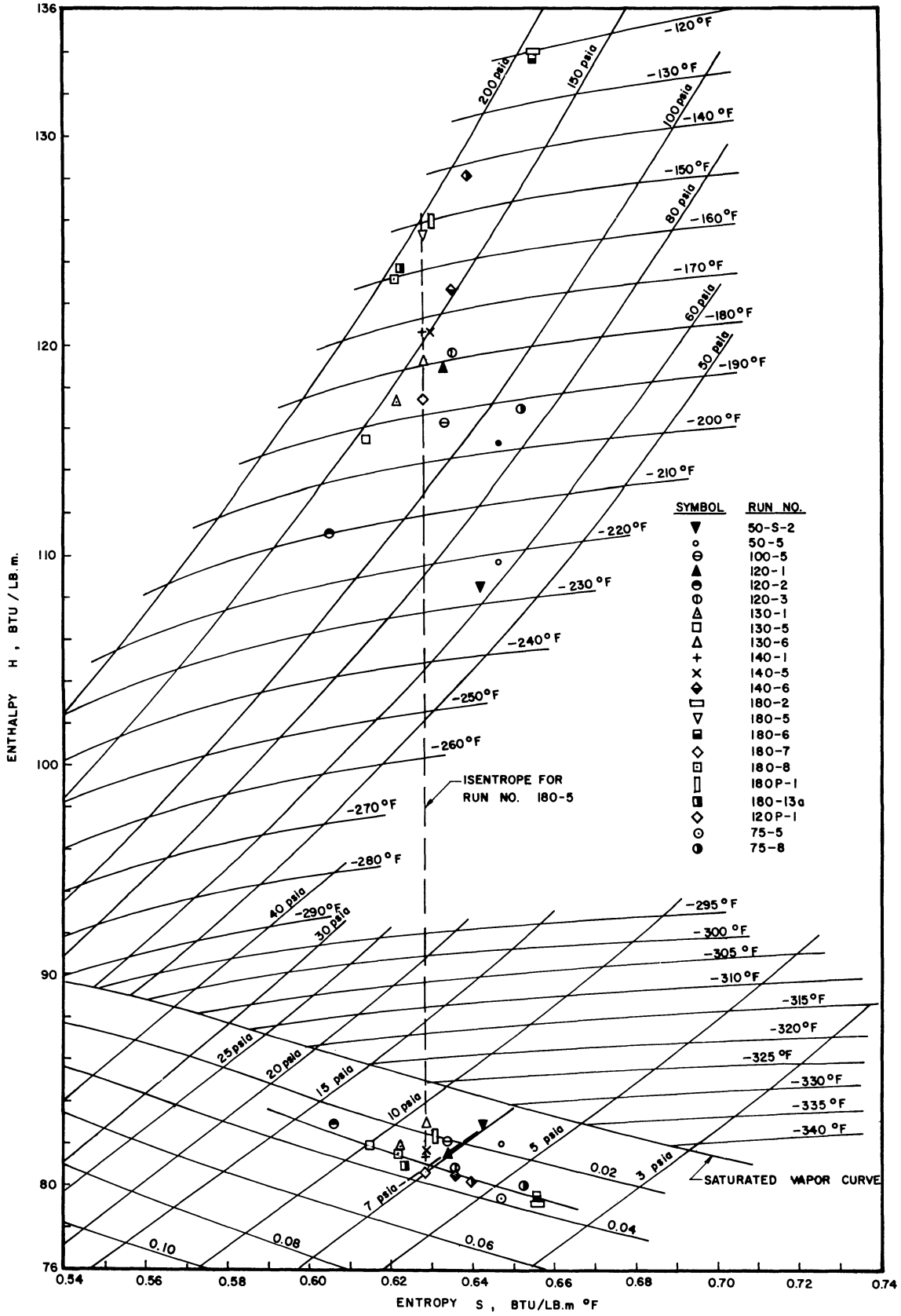

Figure 8. Modified Mollier Diagram with Limit Line of Supersaturation.

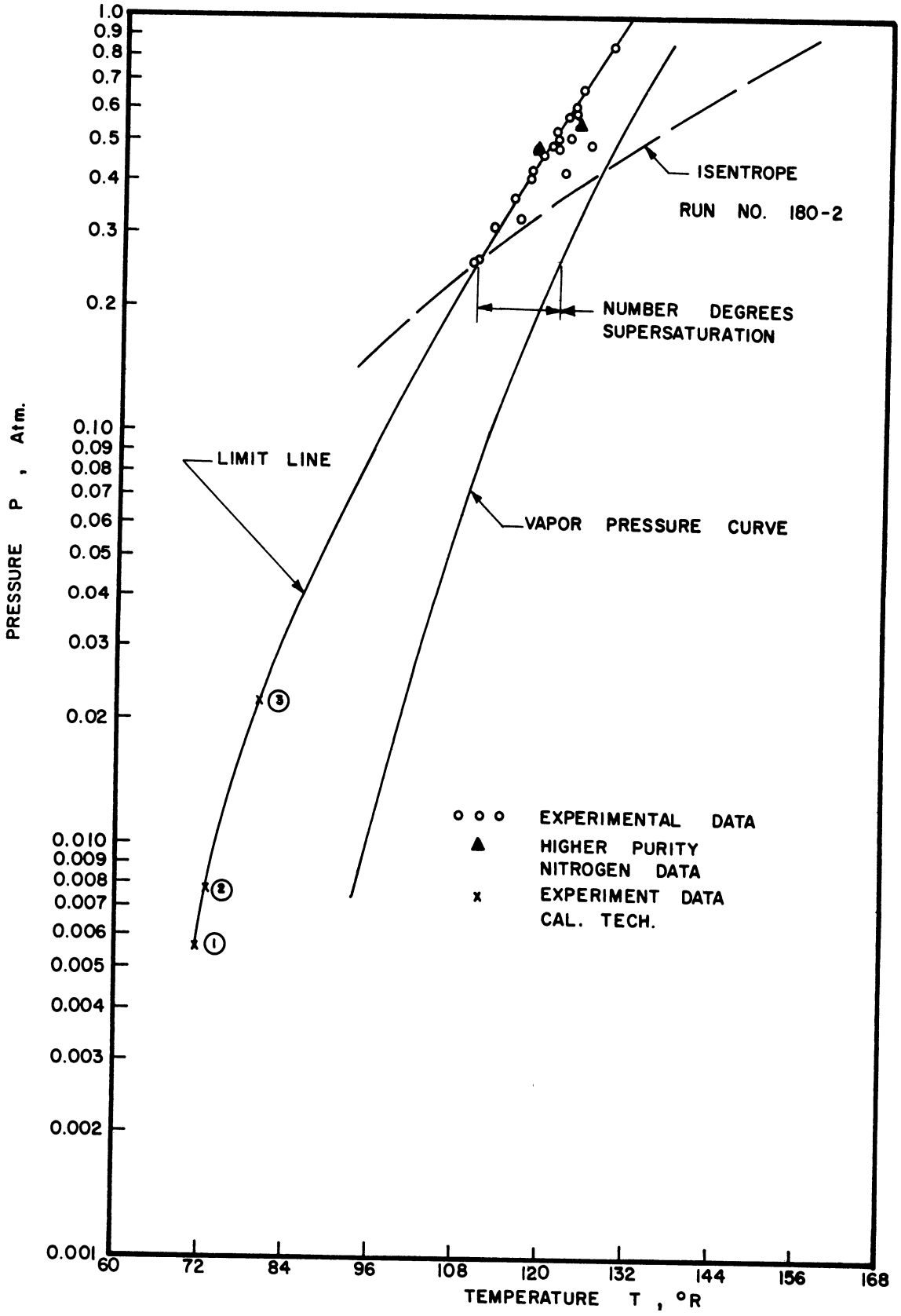

Figure 9. Supersaturation Limit Line Curve for Nitrogen.

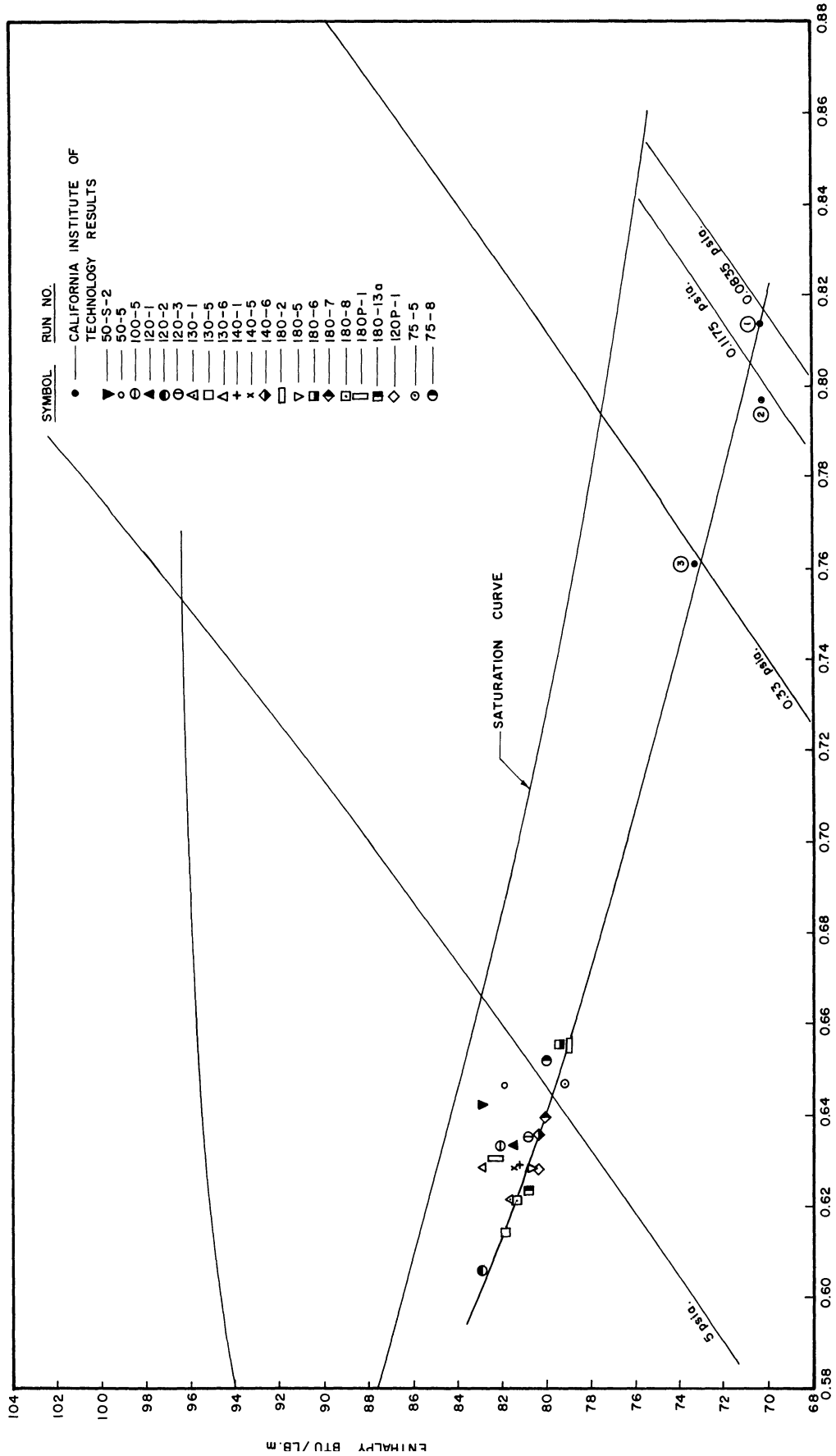

Figure 10. Section of Mollier Diagram Showing Comparison with Results of Previous Investigations.

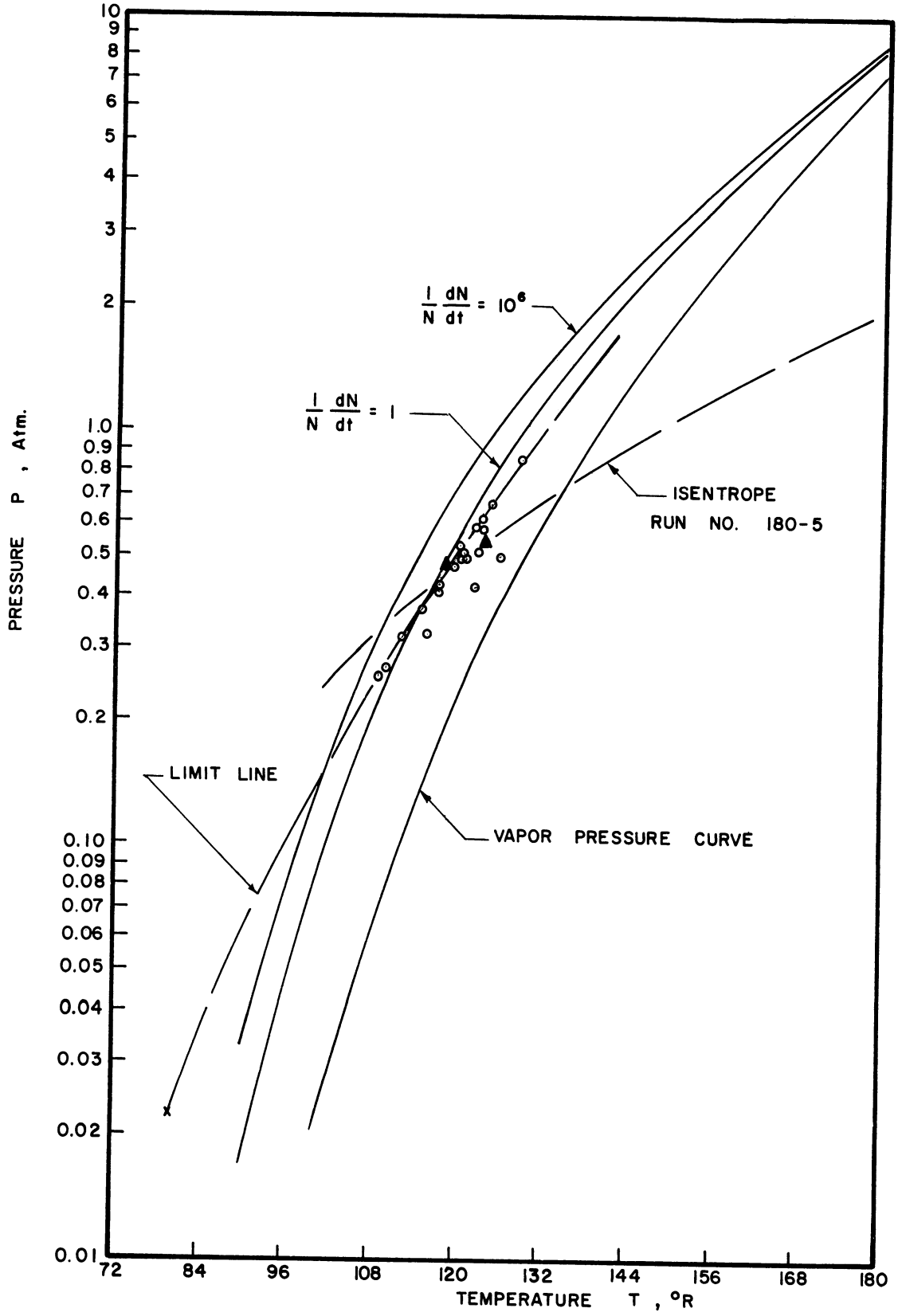

Figure 11. Comparison of Results with Stever-Rathbun Theory.

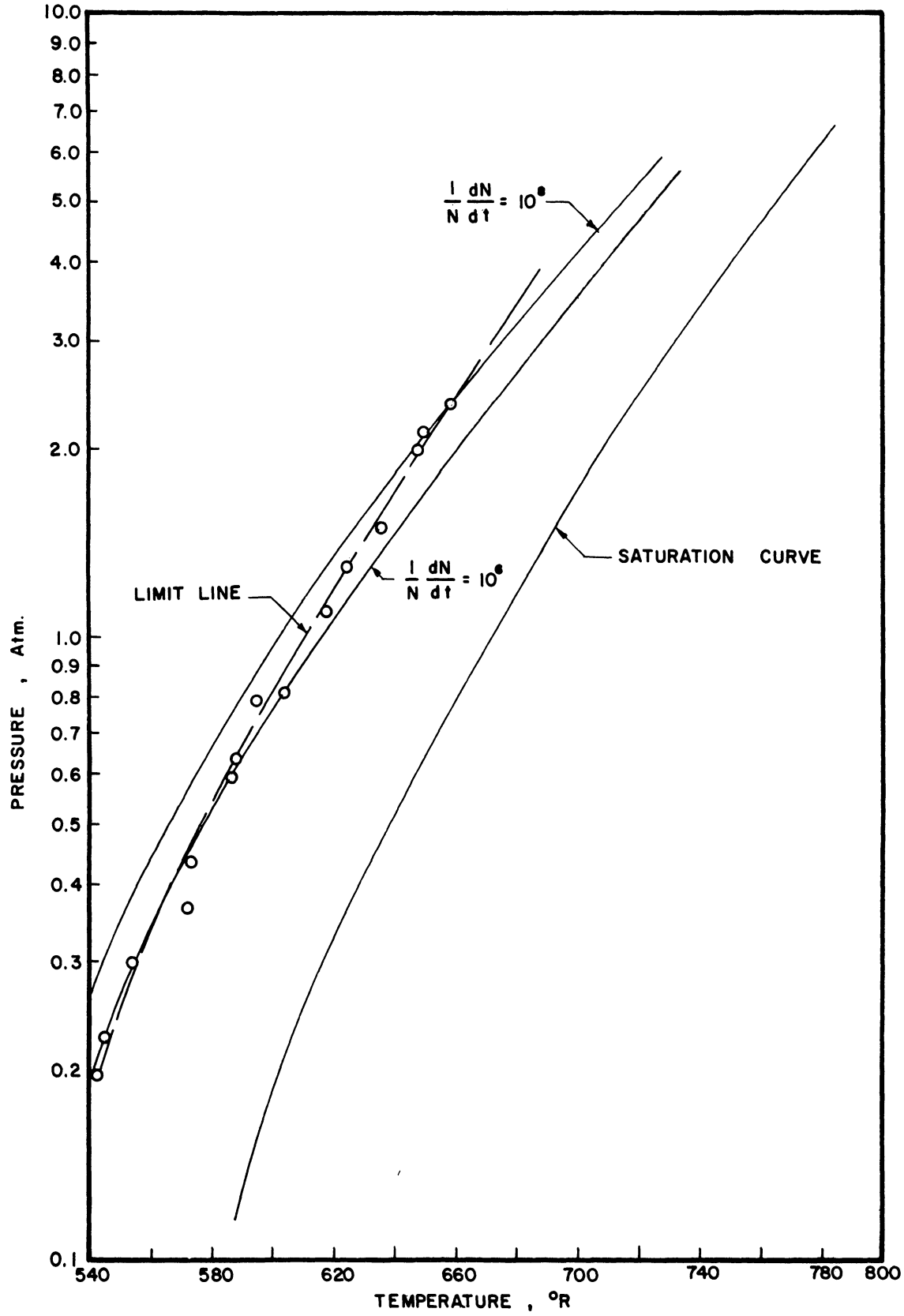

Figure 12. Comparison of Yellott's Experimental Results for Steam with Stever-Rathbun Theory.

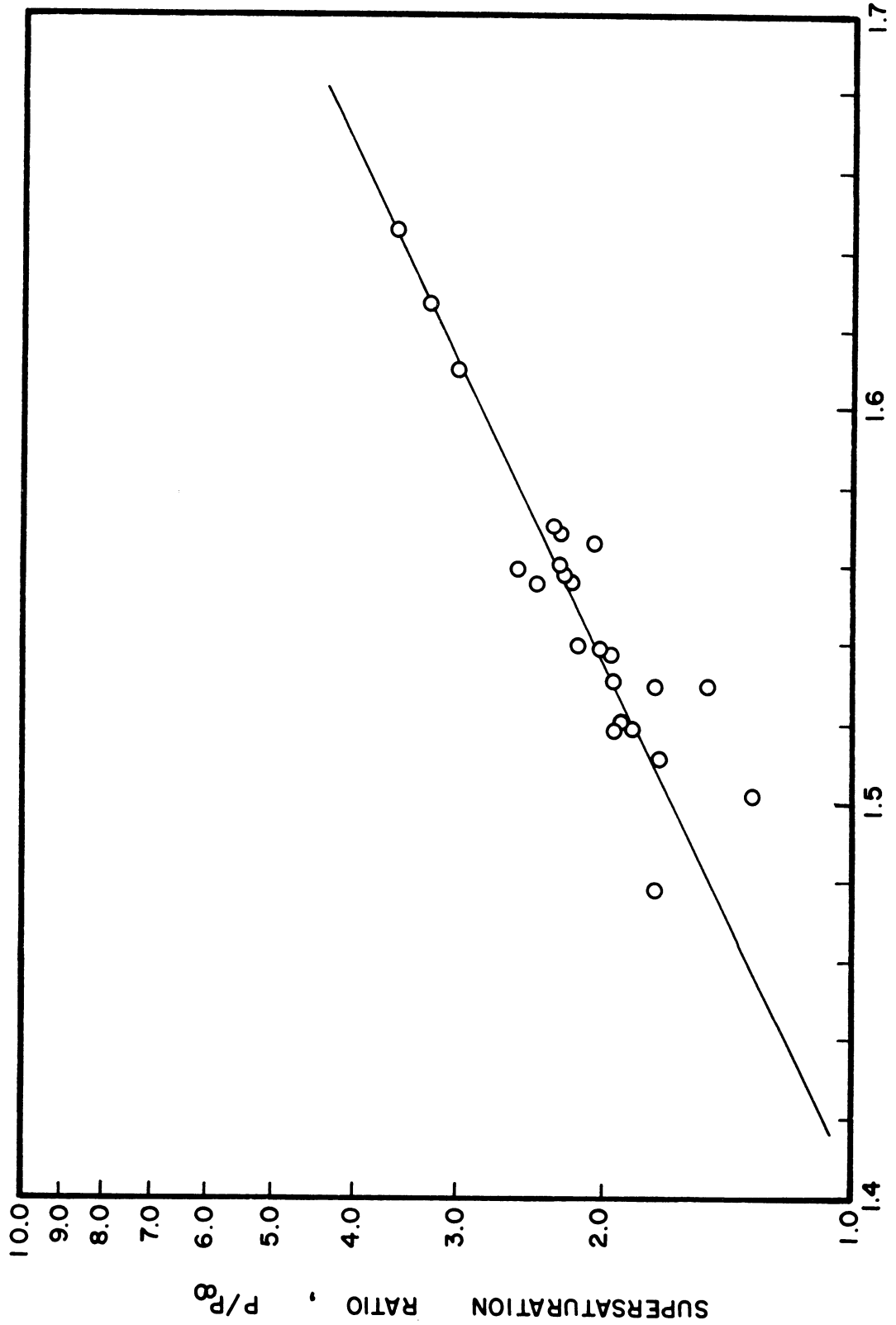

Figure 13. Supersaturation Ratio Versus $1/\rho_{\ell} T_c$.

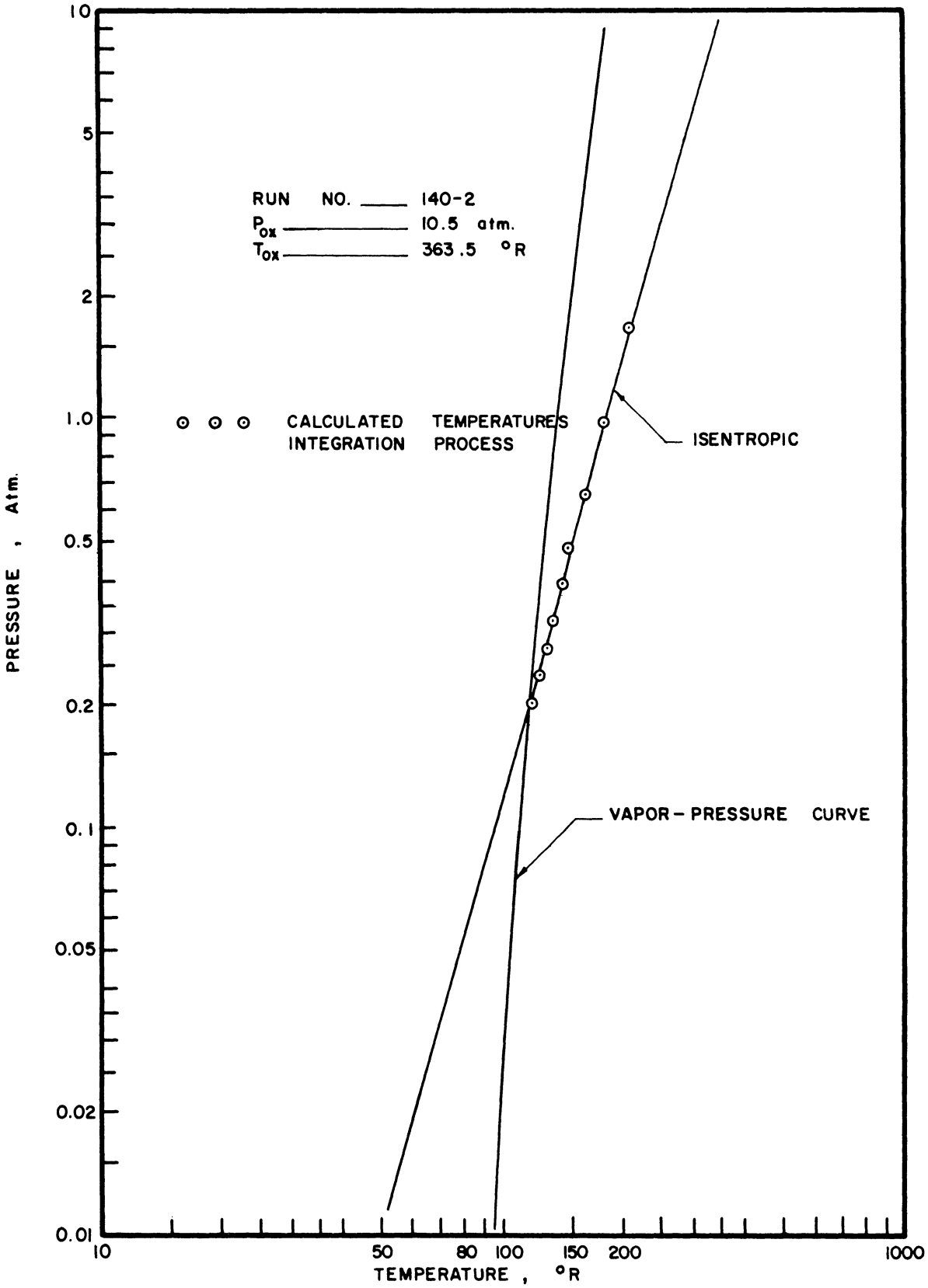

Figure 14. Measured Pressure vs. Calculated Temperature Run Without Condensation.

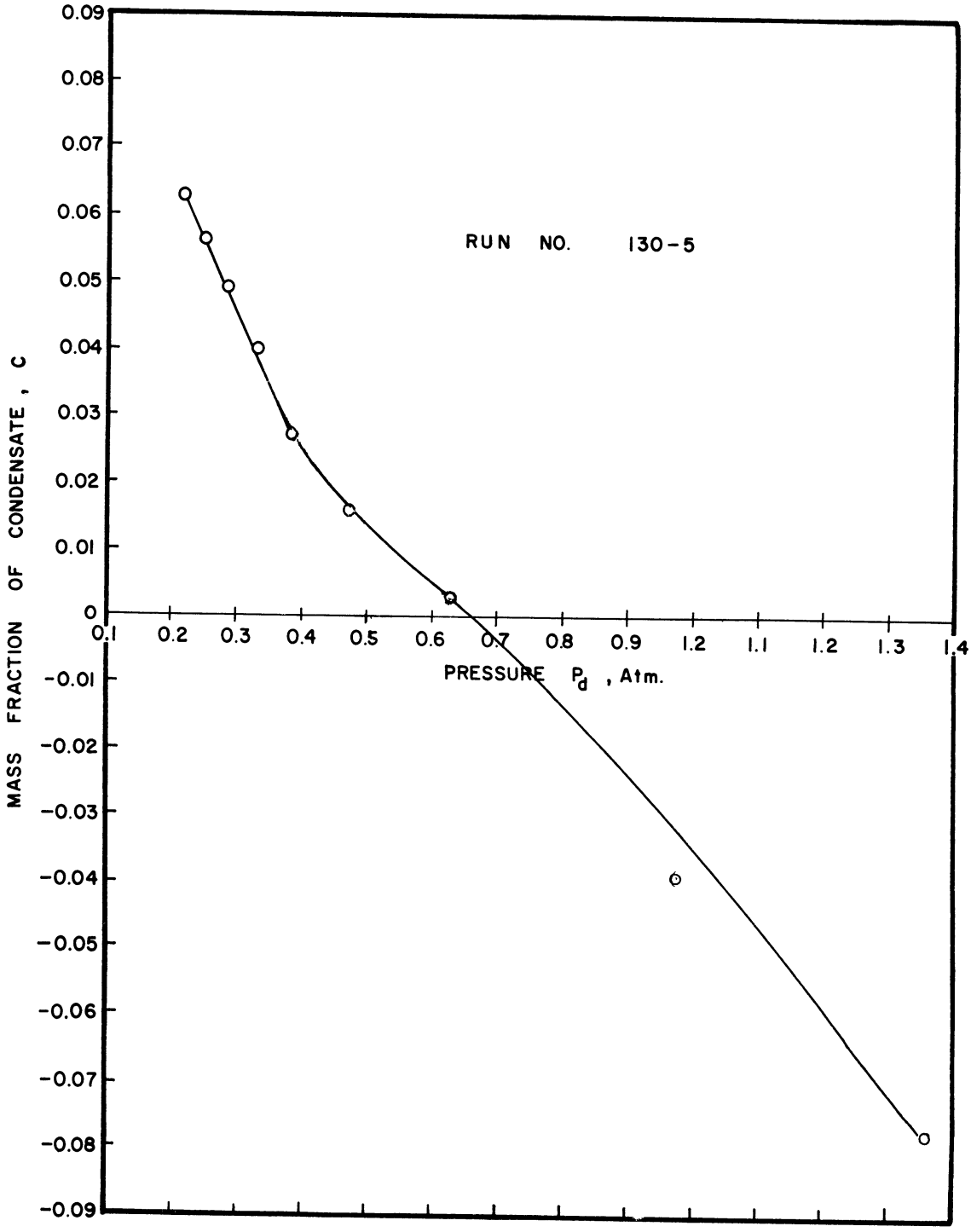

Figure 15. Mass Fraction of Condensate (Calculated) vs. Static Pressure (Measured).

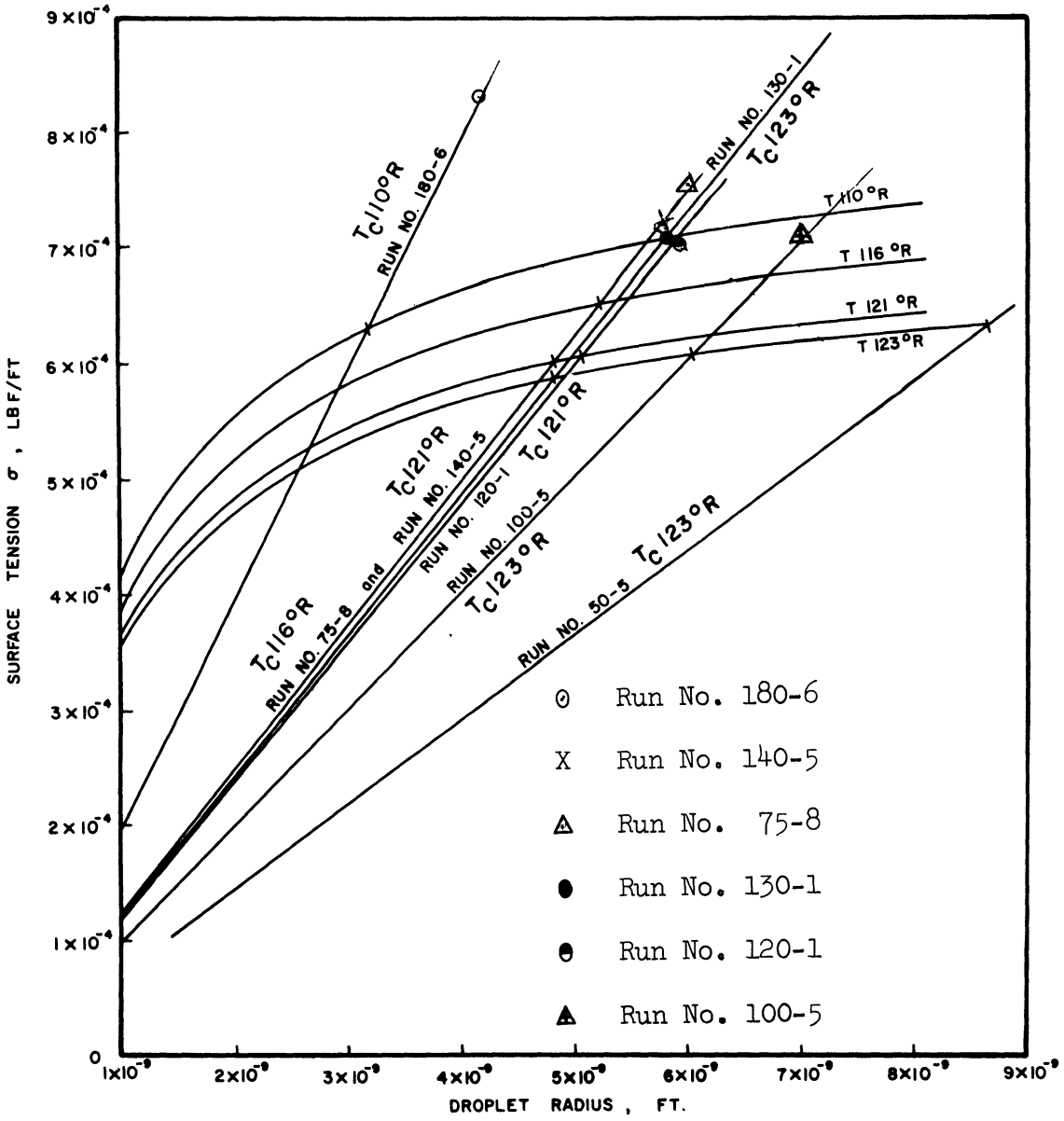

Figure 16. Surface Tension vs. Droplet Radius.

DISCUSSION OF RESULTS

Since the primary purpose of this investigation was to determine experimentally the limit line of supersaturation the method of detection of the onset of condensation was of paramount importance. The pressure measurement method for locating the onset of condensation was chosen because of its accuracy as well as its simplicity.

As mentioned previously the results of the pressure measurements appear in Figures 3, 4, and 5. A comparison of the measured pressures with those calculated theoretically for isentropic-perfect gas flow is shown in Figures 3. The divergence of the static pressure ratio from that predicted by the measured stagnation pressure ratio p_o'/p_{ox} and the isentropic-perfect gas relations after the onset of condensation can be seen in Figures 4. Figures 5 show the temperature computed by the integration process and the measured pressures for the various axial stations in the nozzle. As is apparent from Figures 3 and 4 there was experienced a gradual rise in static pressure to values above those predicted for an isentropic flow.

To ascertain that this deviation of the static pressure as observed was caused by condensation and not by flow breakdown or separation several runs were made at elevated stagnation temperatures for given reservoir pressures. The results plotted in Figure 6 show the flow to be isentropic throughout the nozzle. This indicates therefore that the departures observed for the lower temperature runs were due to condensation, because if the departures were the result of other conditions, the occurrence of these deviations would still have been experienced. Thus the

static pressure departure from the isentropic was taken as the criterion of condensation and the tangential point of departure considered as the onset of condensation.

Figures 3-17, 4-14, and 5-11 which represent run number 180-5 were used to show the existing correlation between the methods of determining the onset of condensation. All three methods of determining this onset were in agreement within the experimental accuracy of the measurements. Each method indicated that the onset of condensation had occurred at a Mach number of approximately 2.81. With this correspondence having been established, the divergence of the actual expansion curve (obtained from the experimentally determined pressure ratios, p_o'/p_{ox} and p_d/p_o') from the isentropic curve for non-condensing flow was used to detect the onset of condensation for all other runs reported.

The experimental results show evidence that the nitrogen supersaturated during the expansion process. By referring to Figures 5 it can be seen that the temperature and pressure of the expanding fluid decreased isentropically to values beyond the intersection of the isentrope and the saturation curve. For equilibrium conditions of flow the condensed phase would begin to appear at this intersection. These curves reveal also that as the expansion continued there was a collapse of the supersaturated state as indicated by the departure of the fluid state from the isentrope. Following the phase change there appears a subsequent approach of the temperature and pressure to the saturation line for the liquid-vapor equilibrium curve. In general it seems that the temperature and pressure values after the collapse of the supersaturated state reach equilibrium values which parallel the saturation curve.

The calculated values of the supersaturation pressure ratios p_c/p_∞ as obtained from the measured condensation pressure p_c at the onset of condensation have been plotted against the calculated condensation temperatures T_c. As seen in Figure 7 these values can be represented by a straight line. This plot reveals that the supersaturation ratio increases as the condensation temperature is decreased. That this should be the case can be seen from the Von Helmholtz equation. Substitute into Equation (T-1) the linear expressions in terms of absolute temperature for both surface tension and density, and consider the surface tension as being independent of the droplet radius, then for a given size of droplet the supersaturation ratio is a function of absolute temperature only. The differentiation of the logarithm of the supersaturation ratio with respect to temperature can then be shown equal to a negative value. Thus for a decrease in absolute temperature the supersaturation ratio must increase. It is also observed from Equation (T-1) that since the surface tension decreases with increasing temperature and finally vanishes at the critical condition then there can be no supersaturation at the critical condition. This particular presentation provides an excellent means for showing the results of this investigation with the results of previous investigators. The points designated as 1, 2, and 3 on this plot represent the results of three tests conducted at California Institute of Technology[18] where the investigation was concerned with bottled nitrogen gas at room temperature expanding to hypersonic flows. As observed their results could also be represented by the same straight line representing this study.

The size of the droplet at the onset of condensation was calculated from the experimental results by use of the Von Helmholtz equation and the values tabulated in Table IV. To check the order of magnitude of the droplet size, the experimentally measured supersaturation ratio was plotted against the ratio $1/\rho_\ell T_c$, where ρ_ℓ is the density of the liquid and T_c the absolute temperature at the onset of condensation. These results as plotted in Figure 13 can be represented by a straight line. Selection of any point on this straight line, as $p/p_\infty = 2$, and assuming the surface tension to vary only with temperature, and with an estimated temperature, as 121°R, the droplet radius can be determined and for this example it is found to be 5.75×10^{-9} ft. In so-doing the size of the droplet agrees well with the values of Table IV. From Table IV at a condensation temperature of 121°R the radius of the droplet is seen to be 5.79×10^{-9}ft which compares well with the value of 5.75×10^{-9} ft.

A limit of supersaturation curve Figure 9 results when the experimentally measured condensation pressure p_c is plotted against the calculated condensation temperature T_c. With reference to this figure it can be observed that the results from the hypersonic tests, mentioned before, when included in the plot appear to be an extension of the limit line to lower condensation temperatures. If this limit line were extrapolated to higher temperatures the trend of curvature is such that it appears as though that at critical conditions supersaturation ceases to exist. This condition is also predicted by the Von Helmholtz equation. The experimental results as plotted in Figure 9 also reveal that for an

increased number of degrees of superheat the number of degrees of supersaturation is increased and the onset of condensation will occur farther downstream in the nozzle.

This limit of supersaturation curve can also be used to predict the onset of condensation as well as the number of degrees of supersaturation for given initial stagnation conditions. An isentropic expansion intersects this limit line and this intersection indicates the temperature and pressure at which condensation should be expected. Then with these values the remaining properties at condensation can be determined. Since the flow up to the onset of condensation as shown by this investigation is isentropic, the Mach number at the onset can be obtained from the definition of the stagnation temperature

$$M_c = \sqrt{\frac{2}{k-1}\left(\frac{T_{ox}}{T_c} - 1\right)}$$

where M_c and T_c are respectively the Mach number and absolute temperature at the onset. With this calculated Mach number the position in the nozzle at which the condensation occurs can be found from the area relationship

$$A_c/A^* = \frac{1}{M_c}\left[\left(\frac{2}{k+1}\right)\left(1 + \left(\frac{k-1}{2}\right)M_c^2\right)\right]^{\frac{k+1}{2(k-1)}}$$

where A_c and A^* are respectively the cross-sectional areas at the onset of condensation and at the throat. This procedure is useful to the designer in determining the maximum Mach number that could be attained without condensation for given initial conditions. The number of degrees of supersaturation is obtained by measurement on the temperature scale of the horizontal distance from the intersection of the isentropic with the limit line to the saturation curve.

The expansion up to the onset of condensation for all experimental runs are shown on the modified Mollier diagram Figure 8. The curve best fitted to points representing the onset of condensation is again the limit line of supersaturation. Similiar observations can be made from this plot as were made from Figure 9. For given initial reservoir conditions the number of degrees of supersaturation obtained from both Figures 8 and 9 are in good agreement. Figure 10 is the modified Mollier diagram extrapolated to include the hypersonic test results. Again these results designated as 1, 2, and 3, appear to fall on an extension of the limit line representing the results of this study.

Analysis by means of a mass spectrometer and an Orsat apparatus indicated between 5 and 10 percent oxygen in the nitrogen. The lower figure being the most likely percentage was used for this study. To observe the effect, if any, that this percent oxygen content had on the number of degrees of supersaturation, two runs using chemically pure nitrogen were conducted. The comparison of these runs 120 P-1 and 180 P-1 with those of the lesser purity nitrogen revealed no appreciable effect on the amount of supersaturation obtainable. As can be observed from Figures 8 and 9 these results are in agreement well within the experimental accuracy of the measurements.

Figure 11 shows the comparison of the experimental results of this study with the Stever-Rathbun theory. As observed from this plot the resulting predictions of condensation rates fit well the experimental results on the assumption that the condensation is initiated by the formation of nuclei of nitrogen. Thus the results of this study appear to favor the acceptability of the Stever-Rathbun theory. Also the evidence

presented by this investigation appears to indicate that the experimentally detected condensation is onto nuclei of nitrogen.

Figure 12 is a similiar comparison where Yellott's experimental results for steam are compared with the Stever-Rathbun theory. This plot reveals the observed condensation occurred at slightly higher condensation rates than predicted by the theory.

Figures 14 and 15 were plotted to check the validity of the integration process used in calculating the temperatures downstream of condensation. Figure 14 for run number 140-2 wherein no condensation was experienced shows the calculated temperatures by the integration process to be in good agreement with those predicted for the isentropic expansion. Figure 15 shows the mass fraction of condensate upstream of the onset of condensation to take on negative values which can be represented by the same curved line extended for the conditions downstream of condensation. Therefore, it appears that the assumptions used in the integration process introduces only small errors in the computed temperatures.

The objective in plotting the surface tension against the droplet radius as shown in Figure 16 was to show what droplet size would be expected from use of the Stever-Rathbun theory and the experimentally measured supersaturation ratio. The family of curves which are for the experimentally computed condensation temperatures represents the effect droplet size has on the surface tension as obtained from Tolman's expression $\sigma = \sigma_\infty \left(1 + \frac{1}{\frac{2\delta}{r}}\right)$. The straight lines again for the same computed condensation temperatures represent the variation of surface tension with droplet radius as determined from use of the Von Helmholtz equation and the experimentally measured supersaturation ratios. The intercepts of

the curves for the same condensation temperatures give the droplet radii that would have been obtained from use of the Stever-Rathbun theory. As found these radii would have magnitudes 10^{-9} feet less than those for surface tension independent of droplet radius.

The experimental results shown in Figure 3 revals that the departure from the isentrope is quite gradual and this gradual departure makes it difficult to locate the exact point of condensation.

CONCLUSIONS

The results of this investigation show that superheated nitrogen vapor becomes supersaturated when expanded in a straight two-dimensional wedge-type nozzle. The number of degrees of supersaturation experienced ranged from approximately 3.5°R for reservoir conditions of 4.38 atmospheres pressure and 234°R temperature to a value of approximately 12.3°R for reservoir conditions of 13.22 atmospheres pressure and 340°R temperature.

The conclusions resulting from this study are separated into two groups. The first group represents those which are in conformity with conclusions advanced by previous investigators, whereas the second group represents conclusions heretofore not previously realized from experimental work.

The conclusions which fall into the first group are as follows:

1. The experimental results indicate conclusively that the condensation of the nitrogen was gradual and that there was no evidence of a condensation shock.

2. The measured stagnation pressure along the centerline of the nozzle is approximately the same as that predicted for isentropic flow.

3. The number of degrees of supersaturation is increased for an increased number of degrees of superheat.

4. Although experimental data from one test run is certainly not an adequate basis for drawing conclusions, it is nevertheless evident from run number 130-6 in which it is

believed there was a high concentration of foreign impurities that the number of degrees of supersaturation is decreased as a result of the presence of such impurities in the flow.

5. It can be observed from Figure 5 that the temperature and pressure, after the collapse of the supersaturated state, appear to reach equilibrium values which parallel the saturation curve for a plane surface of nitrogen.

Those conclusions which fall into the second group are as follows:

1. As observed from the comparison of the principal experimental results with those conducted with chemically pure nitrogen, no appreciable effect on the amount of supersaturation was revealed. This is as would be expected for nitrogen with up to five percent oxygen content. For if the number of degrees of supersaturation had been calculated by considering the nitrogen to have expanded from its own initial partial pressure, the values obtained would be approximately four percent less than those in Table IV. Therefore the oxygen content did not act as a nucleus for condensation and thus a limit of supersaturation was observed.

2. The evidence presented by the experimental results appears to indicate that the nitrogen may have condensed due to self-nucleation.

3. A limit line curve resulted as shown in Figure 9. This plot enables one to predict the position in the nozzle wherein condensation would be expected to commence and also

to predict the number of degrees of supersaturation for given initial reservoir conditions.

5. The results of this study appear to favor the acceptability of the Stever-Rathbun theory.

APPENDICES

APPENDIX A

DERIVATION OF EQUATIONS USED IN CALCULATION OF PROPERTIES OF TWO-PHASE FLUID

The equations used in computation of temperature following the onset of condensation are here developed in accord with the procedure outlined by Buhler.[14]

The equations of continuity and momentum in a condensing flow were assumed to remain unchanged and therefore they may be written directly as

$$m = \rho A V \tag{A-1}$$

and

$$V dV + \frac{dp}{\rho} = 0 \quad . \tag{A-2}$$

The equation of state however, was based on the assumption that the pressure exerted by the mixture of the droplets and vapors was due only to the vapor phase. Thus if c represents the fraction by mass of the condensed phase the equation of state is then

$$p = (1-c)\rho R T \quad . \tag{A-3}$$

In the development of the conservation of energy thermal and dynamic equilbrium were assumed. That is to say the droplets of the liquid phase were in thermal equilbrium with the vapor and the velocity of the liquid droplet was assumed to be that of the vapor. Considering the conditions downstream of the onset of condensation the stagnation enthalpy is a constant. Hence for the two phase fluid, its value is

$$H_o = \omega_v \left(\frac{V_v^2}{2} + h_v \right) + \omega_L \left(\frac{V_L^2}{2} + h_L \right)$$

Assuming $V_L = V_V$ then with W_V and W_L the respective masses of vapor and liquid the stagnation enthalpy is

$$H_o = (W_V + W_L)\frac{V^2}{2g_o} + W_V h_V + W_L h_L$$

or

$$\frac{V^2}{2g_o} + \left(\frac{W_V}{W_L + W_V}\right) h_V + \left(\frac{W_L}{W_V + W_L}\right) h_L = \text{constant}$$

but $c = \frac{W_L}{W_V + W_L}$, and also $(1-c) = \frac{W_V}{W_L + W_V}$, then $dc = d\frac{W_L}{W_L + W_V}$

and since $dW_L = -dW_V$ the expression rewritten is

$$\frac{V^2}{2g_o} + (1-c) h_V + c\, h_L = \text{constant} \quad .$$

In differential form the above becomes

$$V dV - (h_V - h_L)\, dc + dh_V - c\, dh_V + c\, dh_L = 0 \quad .$$

However, $h_V - h_L = h_{fg}$ and neglecting the products $c\,dh_V$, and $c\,dh_L$ as they are small, the conservation of energy is then

$$V dV - h_{fg}\, dc + dh_V = 0 \quad . \qquad \text{(A-4)}$$

Since the pressure and nozzle area are known from experimental data the equations of continuity and momentum may be solved for the velocity at any section downstream of condensation. Multiplying Equation (A-2) by the integrating factor ρA and substituting Equation (A-1) into this result dV becomes

$$dV = -\frac{A}{m}\, dp \quad .$$

Integrating the above from the throat section designated with an asterik to any section downstream of the throat the velocity is given by

$$V(x) = V^* - \frac{1}{m}\int_{x^*}^{x} A(x)\, \frac{dp(x)}{dx}\, dx \quad .$$

The pressure gradient dp(x)/dx is discontinuous at the onset of condensation and therefore a more accurate result will be had if this equation is integrated by parts.

$$V(x) = V^* - \frac{1}{m}\left[\{A(x)\, p(x)\}_{x^*}^{x} - \int_{x^*}^{x} p(x)\, \frac{dA(x)}{dx}\, dx\right]$$

Rewritting the above in dimensionless form and realizing that m = ρ*A*V* the velocity ratio obtained is

$$\frac{V(x)}{V^*} = 1 + \frac{p^*}{\rho^*(V^*)^2} - \frac{1}{\rho^*(V^*)^2}\left[\frac{A(x)}{A^*}p(x) - \int_{x^*}^{x} p(x)\,\frac{d\left(\frac{A(x)}{A^*}\right)}{dx}\,dx\right] .$$

But $\rho^*(V^*)^2 = p^* k (M^*)^2$ and since $M^* = 1$ then $\rho^*(V^*)^2 = p^* k$

hence, the velocity ratio becomes

$$\frac{V(x)}{V^*} = \frac{k+1}{k} - \frac{1}{p^* k}\left[\frac{A(x)}{A^*}p(x) - \int_{x^*}^{x} p(x)\,\frac{d\left(\frac{A(x)}{A^*}\right)}{dx}\,dx\right] .$$

However there exists an isentropic expansion from the throat to the onset on condensation and in addition from the definition of stagnation pressure the pressure at the throat is expressed as

$$p^* = p_o \Big/ \left(\frac{k+1}{2}\right)^{\frac{k}{k-1}} .$$

From this it follows that the velocity ratio is given by

$$\frac{V(x)}{V^*} = \frac{k+1}{k} - \frac{1}{k}\left(\frac{k+1}{2}\right)^{\frac{k}{k-1}}\left[\left(\frac{A(x)}{A^*}\frac{p(x)}{p_o}\right) - \int_{x^*}^{x}\frac{p(x)}{p_o}\,\frac{d\left(\frac{A(x)}{A^*}\right)}{dx}\,dx\right] .$$

In evaluation of the velocity ratio with this expression the nozzle area and pressure near the throat as measured experimentally are needed. These values near the throat are very difficult tc measure experimentally and would introduce a large error. To eliminate this difficulty consider a section x_1 downstream of the throat yet upstream of the onset of condensation. The expression then becomes

$$\frac{V(x)}{V^*} = \frac{k+1}{k} - \frac{1}{k}\left(\frac{k+1}{2}\right)^{\frac{k}{k-1}}\left[\left(\frac{A(x)}{A^*}\frac{p(x)}{p_o}\right) - \left\{\int_{x^*}^{x_1}\frac{p(x)}{p_o}\,\frac{d\left(\frac{A(x)}{A^*}\right)}{dx}\,dx + \int_{x_1}^{x}\frac{p(x)}{p_o}\,\frac{d\left(\frac{A(x)}{A^*}\right)}{dx}\,dx\right\}\right] .$$

At this section x_1 the Mach number can be determined from the pitot formula and neglecting heat transfer effects the velocity at x_1 may be obtained.

In this manner the integral from x* to x_1 can be given by

$$\int_{x^*}^{x_1} \frac{p(x)}{p_o} \frac{d\left(\frac{A(x)}{A^*}\right)}{dx} dx = \left(\frac{V(x_1)}{V^*} - \frac{K+1}{K}\right) \Big/ \frac{1}{K}\left(\frac{K+1}{2}\right)^{\frac{K}{K-1}} + \frac{A(x_1)}{A^*}\frac{p(x_1)}{p_o} = C_1 .$$

Thus the velocity ratio becomes

$$\frac{V(x)}{V^*} = \frac{K+1}{K} - \frac{1}{K}\left(\frac{K+1}{2}\right)^{\frac{K}{K-1}} \left[\frac{A(x)}{A^*}\frac{p(x)}{p_o} - C_1 - \int_{x_1}^{x} \frac{p(x)}{p_o} \frac{d\left(\frac{A(x)}{A^*}\right)}{dx} dx \right] . \qquad \text{(A-5)}$$

This computed velocity ratio and the measured effective area ratio with the aid of the continuity equation gives the following expression for the density ratio

$$\frac{\rho(x)}{\rho^*} = 1 \Big/ \left(\frac{A(x)}{A^*}\frac{V(x)}{V^*}\right) . \qquad \text{(A-6)}$$

With the density ratio known the temperature ratio may then be determined from the equation of state since

$$R = \frac{p(x)}{(1-c)\rho_x T_x} \qquad \text{and} \quad R = \frac{p^*}{\rho^* T^*} \quad \text{where} \quad c^* = 0$$

results in the following expression

$$\frac{T(x)}{T^*} = \left(\frac{p(x)}{p^*}\right) \Big/ (1-c)\left(\frac{\rho(x)}{\rho^*}\right) . \qquad \text{(A-7)}$$

The conservation of energy may now be used to develop an expression for the percent condensed phase.

From Equation (A-4) it is seen that

$$dc = \frac{V\,dV}{h_{fg}} + \frac{KR}{(K-1)h_{fg}}\,dT$$

and

$$\int_{x^*}^{x} dc = \frac{(V(x))^2}{2h_{fg}} - \frac{(V^*)^2}{2h_{fg}} + \frac{KR}{(K-1)h_{fg}} T_x - \frac{KR}{(K-1)h_{fg}} T^* .$$

The fraction of condensed phase can therefore be expressed as

$$c = \frac{(V^*)^2}{2h_{fg}} \left\{ \left(\frac{V(x)}{V^*} \right)^2 - 1 \right\} + \frac{k}{k-1} R T^* \left\{ \frac{T(x)}{T^*} - 1 \right\}$$

since $c^* = 0$.

But $(V^*)^2$ is kRT^*, hence c(x) becomes

$$c(x) = \frac{\left(\frac{k-1}{2}\right)\left(\frac{V(x)}{V^*}\right)^2 + \frac{T(x)}{T^*} - \frac{k+1}{2}}{\frac{k-1}{k}\left(\frac{h_{fg}}{RT^*}\right)} \quad . \qquad \text{(A-8)}$$

APPENDIX B

EXTRAPOLATION OF THE MOLLIER CHART

Plotting of the limit line of supersaturation on the Mollier chart necessitated its extension to pressures below 10 psia. In so doing the enthalpy and entropy values at pressures below 10 psia were calculated along the saturation curve. The equation of state for nitrogen was obtained from Illinois Institute of Gas Technology Bulletin No. 18 and the transport properties from the National Bureau of Standards Circular No. 564.

The equation of state used was

$$p = RT\rho + C_1\rho^2 + C_2\rho^3 + C_3\rho^6$$

and when the constants were properly evaluated it became

$$pv = 0.08206T - 2.28569\left(\frac{1}{v}\right) + 0.12711\left(\frac{1}{v^2}\right) .$$

For the range of interest the last term could be neglected. The enthalpy and entropy values were calculated from a known reference point of 10 psia and -326.8°F. The changes in these properties were determined from the following equations:

$$dh = c_p\,dT + \left\{v - T\left(\frac{\partial v}{\partial T}\right)_p\right\} dp$$

and

$$ds = c_p\frac{dT}{T} - \left\{\frac{\partial v}{\partial T}\right\}_p dp .$$

In their integrated forms over the range in question these equations become

$$h_2 - h_1 = 6.93(T_2 - T_1) + \sqrt{(0.082T)^2 - 9.16p_2} - \sqrt{(0.082T)^2 - 9.16p_1}$$

and

$$s_2 - s_1 = c_p \ln \frac{T_2}{T_1} - \left\{ 0.041 \ln \frac{p_2}{p_1} + 0.041 \ln \frac{\sqrt{(0.082T)^2 - 9.16p_2} - 0.082T}{\sqrt{(0.082T)^2 - 9.16p_2} + 0.082T} \cdot \frac{\sqrt{(0.082T)^2 - 9.16p_1} - 0.082T}{\sqrt{(0.082T)^2 - 9.16p_1} + 0.082T} \right\}$$

where T was used as the average temperature over the range under consideration.

The constant pressure lines for an infinite extent of plane surface were then constructed parallel to the existing ones through these calculated points.

APPENDIX C

SAMPLE CALCULATIONS FOR RUN NUMBER 130-5

The isentropic values calculated from the measured stagnation pressure ratios p_o'/p_{ox} along the nozzle centerline were determined as follows:

At the station 1/2 inch downstream from the throat the experimentally measured stagnation pressure ratio p_o'/p_{ox} was found to be equal to 0.757. The Mach number at this station was then calculated from Equation (R-7) and found to be 1.924.

From the definition of the stagnation pressure ratio, Equation (R-2), the isentropic static pressure ratio was then determined and found to be 0.1435. The static pressure ratios at other stations were determined in a similar manner.

The properties at the onset of condensation were calculated as follows:

At the tangential departure point of Figure 3-11, the value of p_c/p_o' and p_o'/p_{ox} equal to 0.0684. Thus the condensation pressure p_c was found to be 0.669 atmospheres. Since the flow up to the condensation point was shown experimentally to be isentropic the Mach number at condensation was found from Equation (R-2) equal to 2.4. The definition of stagnation temperature $T_{ox}/T = 1 + (\frac{K-1}{2})M^2$ gave the condensation temperature of 124.9°R.

The number of degrees supersaturation 8.43°R was determined by subtracting the condensation temperature 124.9°R from the saturation temperature 133.33°R corresponding to the condensation pressure 0.669 atmospheres.

The supersaturation ratio 1.92 was calculated by dividing the condensation pressure 0.669 atmospheres by the saturation pressure 0.348 atmospheres which corresponded to the condensation temperature 124.9°R.

The droplet size 5.8×10^{-9} feet at the condensation point was found by use of the Von Helmholtz equation, Equation (T-1). Here both the density 53.1 lb_m/ft^3 and the surface tension 6.9×10^{-4} lb_f/ft were obtained at the condensation temperature 124.9°R. The droplet radius found from Equation (T-1) was:

$$r = \frac{2(6.9 \times 10^{-4})}{(53.1)(55.1)(124.9)(0.655)}$$

$$r = 5.8 \times 10^{-9} \text{ feet} .$$

Similiarly the radii for other runs were calculated.

The properties downstream of the onset of condensation were calculated as follows:

At the station two inches downstream of the throat the measured static pressure was 0.476 atmospheres. Equations (A-5), (A-6), (A-7), and (A-8) of Appendix A were then used to determine the other properties at this station.

From Equation (A-5) the velocity ratio is found.

$$\frac{V(x)}{V^*} = \frac{K+1}{K} - \frac{1}{K}\left(\frac{K+1}{2}\right)^{\frac{K}{K-1}}\left[\frac{A(x)}{A^*}\frac{p(x)}{p_{ox}} - C_1 - \int_{X_1}^{X}\frac{p(x)}{p_{ox}}\frac{d\left(\frac{A(x)}{A^*}\right)}{dx}dx\right]$$

where

K is 1.4

$\frac{A(x)}{A^*}$ is 3.08 the ratio of area at this station to the area at the throat.

$\frac{p(x)}{p_{ox}}$ is 0.0484 the measured static pressure ratio.

C_1 is 0.230 and found from

$$C_1 = \frac{\frac{V(x)}{V^*} - \frac{K+1}{K}}{\frac{1}{K}\left(\frac{K+1}{2}\right)^{\frac{K}{K-1}}} + \left(\frac{A(x)}{A^*}\right)\left(\frac{p(x)}{p_{ox}}\right)$$

here x_1 is a station just upstream of the condensation point and equal to 1.45 inches, $V(x_1)/V^*$ and $p(x_1)/p_{ox}$ are respectively 1.795 and 0.0681 found from isentropic relations.

$\frac{d(\frac{A(x)}{A^*})}{dx}$ is 1.04 the slopt of the area ratio curve.

$\frac{p(x)}{p_{ox}}$ in the integral is expressed in terms of x and represents the equation of the static pressure ratio curve downstream of condensation. For this run it is $0.0941X^{-0.906}$.

The velocity ratio was then determined and found equal to 1.869. From Equation (A-6), ρ/ρ^* is shown to be 0.174. By Equation (A-7) the temperature ratio is obtained in terms of

the mass fraction of condensate as

$$\frac{T(x)}{T^*} = \frac{0.526}{(1-c)}$$

With Equation (A-8) the mass fraction is calculated and shown to be 0.016, from which the temperature is obtained as 124°R. The properties at the other stations were determined in a similiar manner.

Sample Calculations for Condensation Rate Lines

The condensation rates were determined from the fractional condensation rate equations.

$$\frac{1}{N}\frac{dN}{dt} = \frac{4}{3}r^3\frac{p}{\gamma T}\left\{\sqrt{\frac{2\pi}{w}}\sqrt{\sigma - r\frac{d\sigma}{dr}}\right\} e^{-\frac{8\pi}{\gamma T}\left\{\int_0^r r\sigma\,dr - \frac{1}{3}r^2\sigma\right\}}$$

where

γ is the Boltzman constant 5.65×10^{-24} ft.lbs$_f$/°R

w is the mass of nitrogen molecule 10×10^{-26} lb$_m$

σ is surface tension equal to $\dfrac{\sigma_\infty}{1 + \dfrac{2\delta}{r}}$

where δ is a constant $.5 \times 10^{-9}$, hence

$$\sigma = \frac{r\sigma_\infty}{r + 10^{-9}}$$

$$\frac{d\sigma}{dr} \text{ is } \frac{\sigma_\infty \times 10^{-9}}{(r + 10^{-9})^2}$$

Then for a pressure of 0.3 atmospheres and a temperature of 108°R the droplet radius from the Von Helmholtz equation is 2.18×10^{-9} feet. The fractional condensation rate then is found to be 10^6 per second.

APPENDIX D

DISCUSSION OF PROBABLE ERRORS

Instrument reading and calibration errors:

Manometer tube	$\pm$ 0.3 inches mercury
Manometer reference pressure	$\pm$ 0.1 inches mercury
Reservoir pressure gage	$\pm$ 1.0 psig
Reservoir temperature	$\pm$ 2°F
Measured stagnation pressure	$\pm$ 1 psig

Resultant pressure ratio accuracy using run number 130-5 with reservoir conditions of 9.84 atmospheres pressure and -192°F temperature

$$\text{Percent error for } p_d/p_{ox} = \frac{100(.3)}{21} + \frac{100(1)}{129.6} + \frac{100(.1)}{31.3}$$

$$= \pm 2.5\%$$

Similiarly

$$p'_o/p_{ox} = \pm 3.7\%$$

$$p_d/p'_o = \pm 5.4\%$$

The above values are for the low pressure readings, errors at stations closer the throat are less than these.

At the point of departure from the isentrope, the absolute value of M_c is probably accurate to $\pm$ 0.1. Hence p_c is accurate to $\pm$ 0.005 atmospheres and T_c to $\pm$ 1.5°R. The number of degrees of supersaturation is accurate to about $\pm$ 1.5°R.

BIBLIOGRAPHY

1. Von Helmholtz, R. "Versuche mit einem Dampfstrahl." Annal der Phys., 32, (1887), 1.

2. Yellott, J.I. "Supersaturated Steam." ASME Transactions, 56, No. 6, (June 1934), 411-31.

3. Stodola, A. Steam and Gas Turbines. New York: McGraw-Hill Book Co., 1927.

4. Oswatitsch, K.L. "Condensation Phenomena in Supersonic Nozzles." Z.A.M.M., 22, No. 1, Feb. 1942, or R.T.P. Translation No. 1905, (English).

5. Head, R.M. Investigation of Spontaneous Condensation Phenomena. Thesis, California Institute of Technology, 1949.

6. Becker, J.V. "Results of Recent Hypersonic and Unsteady Flow Research at the Langley Aeronautical Laboratory." Journal Appl. Phys., 21, No. 7, (1950), 619-28.

7. Nagamatsu, H.T. "Results of Recent Hypersonic Flow Research in the Army Ordnance - C.I.T. Hypersonic Wind Tunnel." Phys. Soc. Meeting, Urbana, Illinois, May, 1950.

8. Stever, H. and Rathbun, K. "Theoretical and Experimental Investigation of the Condensation of Air in Hypersonic Wind Tunnels." NACA TN 2559, Oct., 1950.

9. Thompson, Sir William, Lord Kelvin. "On the Equilibrium of Vapor at a Curved Surface of Liquid." Proc. Roy. Soc. (Edinburgh), VII, No. 80, (1870), 63-68; also Phil. Mag., Ser. 4, 42, 1871.

10. Von Helmholtz, R. "Untersuchungen uber Dampfe and Nebel, besonders uber solche von Losungen." Ann. Phys., Bd. 27, Heft 4, (1886), 508-43.

11. Becker, R. and Doring, W. "Kinetische Behandlung der Keimbildung in in Ubersattigen Dampfen." Ann. Phys., Folge 5, Bd. 24, (1936), 719-52.

12. Volmer, M. Kinetik der Phasenliding. Dresden: Theordor Steinkopff, 1939.

13. Charyk, J. and Lees, L. Condensation of the Components of Air in Supersonic Wind Tunnels. Aero. Eng. Lab., Rep. No. 127, Princeton Univ., March 1, 1948.

14. Buhler, R. Recent Results of the Condensation Investigation. Army Ordnance - C.I.T. Hypersonic Wind Tunnel Memoranda, July, 1950 - Aug., 1950.

15. Wegener, P. "N.O.L. Hyperballistics Tunnel No. 4, Results I: Air Liquefaction." NAVOR Rep. No. 1742, Jan., 1951.

16. Bogdonoff, S.M. and Lees, L. Study of the Condensation of the Components of Air in Supersonic Wind Tunnels. Aero. Eng. Lab., Rep. No. 146, Princeton Univ., May, 1949.

17. Nagamatsu, H.T. and Willmarth, W.W. "Condensation of Nitrogen in a Hypersonic Nozzle." Journal of Applied Phys., 23, No. 10, (Oct., 1952), 1089.

18. Arthur, P.D. and Nagamatsu, H.T., Effects of Impurities on the Supersaturation of Nitrogen in a Hypersonic Nozzle. Heat Transfer and Fluid Mechanics Institute, Univ. of Calif., Los Angeles, June, 1952.

19. Faro, I.D., Small, T.R., and Hill, F.K. "Supersaturation of Nitrogen in a Hypersonic Wind Tunnel." Journal of Applied Phys., 23, No. 1, (Jan., 1952), 40.

20. Hoge, H.J. and King. G.J. "The N.B.S. - N.A.C.A. Tables of Thermal Properties of Gases. The Vapor Pressure of Nitrogen." Natl. Bur. Std., Table No. 11.50, July, 1950.

21. National Bureau of Standards Circular 564. "Tables of Thermal Properties of Gases." Nov., 1955.

22. Das Gupta, N.N. and Ghosh, S.K. "A Report on the Wilson Cloud Chamber and Its Application in Physics." Rev. Modern Phys., 18, No. 2, (April, 1946), 225-90.

23. Volmer, M. and Weber, A. "Keimbilding in Ubersattigen Gebilden." Zeitschr. Phys. Chemie, Abschn. A., Bd. 119, Heft 3 and 4, (1926), 277-301.

24. Kaishew, R. and Stranski, I. "Zur Kinetischen Ableitung der Keimbildungsgeschwindigkeit." Zeitschr. Phys. Chemie, Abschn. B, Bd. 26, Heft. 4 and 5, (1934), 317-26.

25. Farkas, L. "Keimbildungsgeschwindigkeit in Ubersattigen Dampfen." Zeitscher Phys. Chemie, Abschn. A, Bd. 125, Heft. 3 and 4, (1927), 236-42.

26. Zeldovich, Y.B. "Theory of the Formation of a New Phase Cavitation." Journal Exp. and Theoretical Phys. (USSR), 12, (1942), 525-38.

27. Kantrowitz, A. "Nucleation in Very Rapid Expansions." Journal of Chem. Phys., 19, (1951) 1097-1100.

28. Frenkel, J. Kinetic Theory of Liquids. New York: Oxford University Press, 1946.

29. Wegener, P. and Smelt, R. Summary of Naval Ordnance Laboratory Research on Liquefaction Phenomena in Hypersonic Wind Tunnels (N.O.L. 159). Naval Ordnance Laboratory Memorandum 10772, Feb. 15, 1950.

30. Probstein, R.F. "Time Lag in Self-Nucleation of a Supersaturated Vapor." Journal of Chem. Phys., 19, (1951), 619.

31. Tolman, R.C. "Effects of Droplet Size on Surface Tension." Journal Chem. Phys., 17, No. 3, (March, 1949), 333-37.

32. Kirkwood, J.G. and Buff, F.P. "The Statistical Mechanical Theory of Surface Tension." Journal of Chem. Phys., 17, No. 3, (March, 1949), 338-43.

33. Shapiro, A.H. The Dynamics and Thermodynamics of Compressible Fluid Flow. New York: The Ronald Press Co., 1953.